A Contribution to Fire Detection Modelling and Simulation

Der Fakultät für Ingenieurwissenschaften der

Universität Duisburg-Essen

zur Erlangung des akademischen Grades eines

Doktor-Ingenieurs

genehmigte Dissertation

von

Claudia Rexfort

aus

Oberhausen

Referent:	Prof. Dr.-Ing. Heinz Luck
Korreferent:	Prof. Dr.-Ing. Heinz Fissan

Tag der mündlichen Prüfung: 10. März 2004

Vorwort

Die vorliegende Arbeit entstand während meiner Tätigkeit als wissenschaftliche Angestellte im Fachgebiet Nachrichtentechnische Systeme des Instituts für Nachrichten- und Kommunikationstechnik an der Universität Duisburg-Essen
An dieser Stelle gilt mein besonderer Dank dem ehemaligen Leiter des Fachgebiets Herrn Prof. Dr.-Ing. H. Luck für seine Betreuung und fortwährende Unterstützung bei der Erstellung dieser Arbeit.
Darüber hinaus danke ich Herrn Prof. Dr.-Ing. H. Fissan, ehemaliger Leiter des Fachgebiets Aerosolmeßtechnik für die Übernahme des Korreferats.
Ferner danke ich allen Kollegen, die durch ihre konstruktive Kritik und Diskussionsbereitschaft zum Gelingen der Arbeit beigetragen haben.
Further I thank Dr. McGrattan and Mr. Cleary for their support during my visit at the National Institute of Standards and Technology.
Nicht zuletzt danke ich meinen Eltern für Ihre Unterstützung während meines Studiums und meiner Promotion.

Duisburg, im März 2004

A contribution to fire detection modeling and simulation

Computer simulations become more and more important in various fields. They help to understand and optimize different kinds of processes. Also in the fire detection simulations are an important tool. Simulations give a better and more detailed understanding of the physics and chemistry of combustion. Fire sensor models and models of fire sensor signals help to optimize the automatic fire detection. The development of any kind of computer model requires a detailed knownledge about the underlying processes. This aspect makes computer models very interesting from a scientific point of view.

Different models for different parts of the automaitc fire detection exist. Target of this PhD is to build up an interface between a fire model and a smoke sensor model. For the fire simulation the Fire Dynamics Simulator of the National Institute of Standards and Technology is used, for the sensor simulation a sensor model developed by Frank Gockel at the Institute Communication Systems is used. In the first step it will be investigated which of the input signals of the sensor model can be provided by the fire model. With respect to the smoke development during a fire the fire model provides the smoke mass density, while the sensor model needs the parameters of the size distribution of the smoke particles. Simulation results show, that also the mechanism of coagulation and the removal of particles from the aerosol has to be implemented in the model to get suitable simulation results. To implement the coagulation a solution of the general dynamic equation (GDE) is used. Different approaches to solve the GDE are implemented and by comparing and the suitable approach is chosen. For the implementation of the removal of particles also the GDE is used. For the evaluation of the model three smoke sensor types have been simulated two optical ones, a scattered light sensor and an extinction light sensor and an ionization chamber and the simulation restlts are compared to measurements.

Contents

Index of important Symbols and Notations

Notation:

- vectors are marked as bold small letters, e.g. $\mathbf{x}$
- matrices are marked as bold capital letters, e.g. $\mathbf{X}$
- references to equations are alway written in brackets, e.g. (2.5)
- complex values are underlined, e.g. $\underline{m}$
- units are given in square brackets, e.g. [m]
- weighted signals are marked by a hat, e.g. $\hat{\sigma}_{\mathrm{ext}}$

Nomenclature:

a	distance between the scattering particle and the light source (Chap 2.2.1)
c_{p}	specific heat by constant pressure (Chap 3.1.1)
C	Cunningham correction factor (Chap 4.2)
C_{ext}	extinction cross section (Chap 2.2.1)
d	particle diameter (Chap 2.1)
d_{g}	geometric mean particle diameter (Chap 2.1)
D	diffusion coefficient (Chap 3.1.1)
$\mathbf{f}$	external forces (Chap 3.1.1)
$\mathbf{g}$	gravitational force (Chap 3.1.1)
h	enthalpy (Chap 3.1.1)
ΔH	heat release per unit mass of oxygen consumed (Chap 3.3.1)
i_0	chamber current of ionization chamber without particles (Chap 2.2.2)
i_1 ,i_2	intensity functions (Chap 2.2.1)
i_{c}	chamber current of ionization chamber (Chap 2.2.2)
I_0	intensity of the incoming light (Chap 2.2.1)
I_{e}	intensity of the attenuated light (Chap 2.2.1)
I_{s}	intensity of scattered light (Chap 2.2.1)
I	condensation rate (Chap 4.1.1)
k	Boltzmann constant (Chap 4.2), thermal conductivity (Chap 3.1.1)
K_{c}	collision coefficient (Chap 4.2)

Kn	Knudsen number (Chap 4.2)
Kn_0	initial Knudsen number (Chap 4.2.3)
L	rate of nucleation (Chap 4.1.1)
m	removal coefficient (Chap 4.3)
$\dot{m}_i'''$	mass production rate for i-th species (Chap 3.1.1)
$\dot{m}_{\mathrm{O}}'''$	mass consumption rate of oxygen (Chap 3.3.1)
$\underline{m}$	complex refraction index (Chap 2.1)
$\underline{m}_{\mathrm{C}}$	complex refraction index of carbon(Chap 2.1)
$\underline{m}_{\mathrm{W}}$	complex refraction index of water(Chap 2.1)
M	molecular weight of gas mixture (Chap 3.1.1)
$M_k(t)$	k-th order moment of a distribution (Chap 4.2.1)
n	number of particles (Chap 2.2.1)
n_{d}	particle diameter distribution (Chap 2.1)
n_{v}	particle volume distribution (Chap 4.1)
N	particle number concentration (Chap 2.1)
N_0	initial particle number concentration (Chap 4.2)
p	pressure (Chap 3.1.1)
p_0	background pressure (Chap 3.1.1)
$q1$,$q2$	quality criteria for the simulation results (Chap 4.4.1)
$\dot{q}'''$	heat release rate (Chap 3.3.1)
$\mathbf{q}_r$	radiative heat flux (Chap 3.1.1)
r	particle radius (Chap 4.2)
R_{m}	removal coefficient (Chap 4.3)
$R(v,t)$	removal rate (Chap 4.1.1)
$\mathscr{R}$	universal gas constant (Chap 3.1.1)
$\mathbf{S}$	surface of control volume (Chap 3.1.1)
S_{m}	measured sensor signals (Chap 5)
S_{s}	sensor simulated signals (Chap 5)
S_{o}	over-all simulated signals (Chap 5)
t'	dimensionless time (Chap 4.2.3)
∂t	time step for temporal discretisation (Chap 3.2)
T	temperature (Chap 3.1.1)
$\mathbf{u}$	flow velocity (Chap 3.1.1)
u	x component of flow velocity (Chap 3.2)
v	particle volume (Chap 4.1), y component of flow velocity (Chap 3.2)
v_{g}	geometric mean particle volume (chap 4.1)
$v_{\mathrm{g},0}$	initial geometric mean particle volume (Chap 4.2.1)
V_{part}	total particle volume (App B)

V_{sc}	scattering volume (Chap 2.2.1)
V_m, V_s, V_o	variation coefficient(Chap 6.1)
w	z component of flow velocity (Chap 3.2)
x	travel length of light (Chap 2.2.1)
∂x	length of grid cell in x direction (Chap 3.2)
X	statistic signal part (Chap 6)
y	smoke density (ionization chamber) (Chap 2.2.2)
y_d	deterministic signal part (Chap 6)
∂y	length of grid cell in y direction (Chap 3.2)
Y_i	mass fraction of specie i [kg/kg](Chap 3.1.1)
Y_d	mass fraction of dust [kg/kg](Chap 7)
Y_O	mass fraction of oxygen (Chap 3.3.1)
Y_O^∞	ambient value of mass fraction of oxygen (Chap 3.3.1)
∂z	length of grid cell in z direction (Chap 3.2)
Z	mixture fraction (Chap 3.3.1)
Z_f	stoichiometric mixture fraction (Chap 3.3.1)

Greek letters:

α	ratio of particle diameter to wavelength of light (Chap 2.2.1)
β	coagulation kernel/rate (Chap 4.2)
$\delta(v)$	Dirac's delta distribution (Chap 4.1.1)
η	chamber constant (Chap 2.2.2)
γ	ratio of specific heats (Chap 3.1.1)
κ	fraction of carbon monoxide (Chap 2.1)
λ	mean free path length of gas molecules (Chap 4.2)
λ_l	wavelength of light (Chap 2.2.1)
μ	dynamic fluid viscosity (Chap 4.2)
Ω	control volume (Chap 3.1.1)
ρ	density (Chap 3.1.1)
ρ_{smoke}	smoke mass density [kg/m^3] (App B)
ρ_{part}	specific soot/smoke density [kg/m^3] (App B)
ρ_a	density of air [kg/m^3] (Chap 7)
ρ_d	specific dust density [kg/m^3] (Chap 7)
ρ_{dust}	dust mass density [kg/m^3] (Chap 7)
σ_d	geometric standard deviation of particle diameter distribution (Chap 2.1)
$\ln \sigma_r$	geometric standard deviation of particle volume distribution (Chap 4.1)

$\ln \sigma_{r,0}$	initial geometric standard deviation of particle volume distribution (Chap 4.2.1)
σ_{ext}	extinction coefficient (Chap 2.2.1)
τ	stress tensor (Chap 3.1.1)
τ_{spd}	time to reach self preserving distribution (Chap 4.2.2)
Θ	scattering angle (Chap 2.2.1)

Abbreviations:

CFD	Computational Fluid Dynamics (Chap 3)
DNS	Dynamic Numerical Simulation (Chap 3.3)
FDS	Fire Dynamics Simulator (Chap 3)
LES	Large Eddy Simulation (Chap 3)
GDE	General Dynamic Equation (Chap 4.1.1)
NIST	National Institute of Standards and Technology (Chap 3)
MIC	Measurement Ionization Chamber (Chap 5.3)

1 Introduction

Computer simulations are becoming more and more important in various fields. They help to understand and optimize different kinds of processes. They are also an important tool in fire detection simulations. Simulations give a better and more detailed understanding of the physics and chemistry of combustion. Fire sensor models and models of fire sensor signals help to optimize the automatic fire detection. The development of any kind of computer model requires a detailed knownledge of the underlying processes. This aspect makes computer models very interesting from a scientific point of view. The principle of an over-all modelling in automatic fire detection was stated by Luck [39]. The idea of this over-all modelling is to simulate the process of automatic fire detection from the beginning of the fire up to the alarm decision at the output of the fire detector. Figure 1.1 shows the structure of this

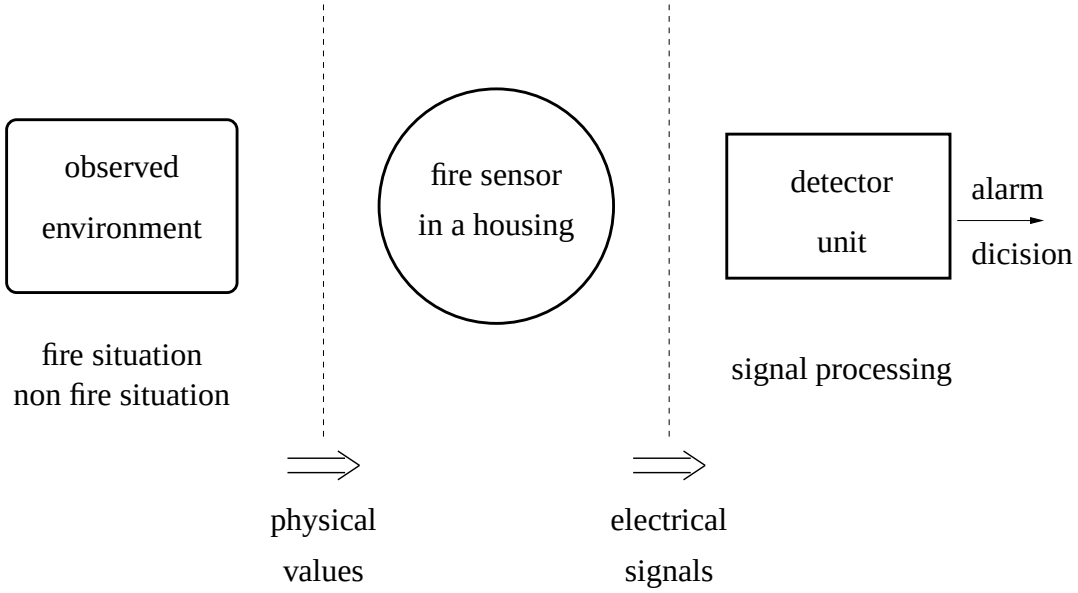

Figure 1.1: Over-all model for automatic fire detection

over-all model, which mainly consists of three parts. The first part on the left hand side of the figure is the observed environment where a fire or a non fire situation exists. The second part of the model represents the fire sensor including its housing, where the conversion from the physical properties observed in the environment to electrical signals takes place. The third part is the detector unit where the sensor signal is processed and the alarm decision is made. For the three parts there exist different separate realizations (e.g. [17], [22], [30]), but

the interfaces between the different model parts are still missing. The realization of these interfaces is a next step to develop an over-all model for automatic fire detection.
One field of application for such an over-all model arises from the investigation of the analog output signals of scattered light sensors [30], [49], [60]. These signals contain impulsive parts which have an amplitude much higher than the signal. For signal processing these impulses are treated in different ways. In Klose's [30] approach of analyzing and simulating the

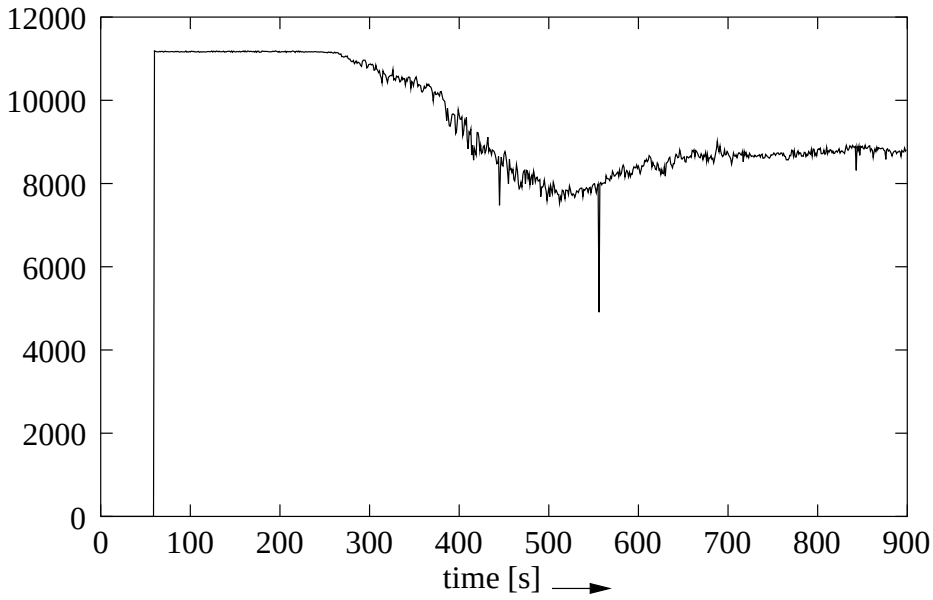

Figure 1.2: Analog output signal of scattered light sensor

signals of scattered light sensors the impulses are treated as additive noise and they are filtered out as a first step of the signal processing. By simulating the signals of the sensor they are implemented again just by adding them to the simulated signal. In another approach [60] the impulses are considered to be a part of the signal, and they are modelled by using an autoregressive model with an impulsive input signal. In both of the mentioned approaches the origin of the impulses is not clear, whether they are caused by the electronic of the sensor or the measurement principle or the smoke properties. In the last case they could be used as an additional quantity for the smoke detection. An over-all model would be a helpful instrument to investigate this effect in more detail.

2 A Model of Smoke Sensors

At the institute of communication systems at the University Duisburg-Essen, a general model of a fire sensor in its housing has been developed by Frank Gockel [22]. The model output provides the sensor response to a given fire or non fire situation. This chapter describes the physical background of the sensor model, with reference to three selected smoke sensor models. The fire situation is defined by the input parameters of the model. With this simulated sensor signal the detector unit can decide whether there is a fire situation or not. The sensor model is a deterministic model. Different types of sensors can be simulated with the sensor model, e.g. different types of smoke sensors, heat sensors and some gas sensors. Figure 2.1 shows the structure of the sensor model. The sensor model consists of four parts

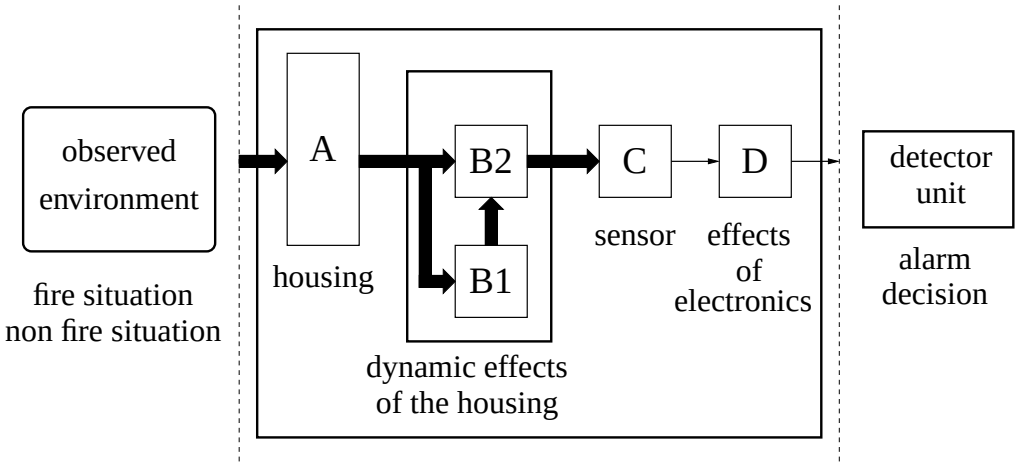

Figure 2.1: Model of a fire sensor in its housing [22]

named A, B, C and D. These parts represent different physical parts and/or properties of the sensor. The model part A is a memoryless system which represents the housing of the sensor and its time invariant properties, which are realized by multiplying the input signal with constant transformation factors. Part B represents the dynamic effects of the housing and of the sensor. These effects can vary with time and can be non linear. Part B is divided into two submodels. In order to account for the dynamic effects part B2 is a linear time invariant system which convolutes the different properties transferred by part A with an impulse response. This impulse response is provided by the part B1 and can change over time to consider the possible time variance of the system. Part C is a realization of the sensor characteristics, i.e. the conversion from the measured values to the sensor signal. Part D represents possible

effects of the electronics at the output side of the sensor. The modular structure of the model gives the opportunity to expand the model to other sensor types without having to develop a completely new model. Between the four different parts of the described sensor model exist interfaces, which define the structure of the parameters that have to be transferred from one model part to another. Up to this point the model parts are independent of each other. To expand the model for a new type of smoke sensor, e.g. a scattered light sensor with two scattering angles, only part C of the model has to be modified for the new sensor type, considering the interfaces to the other model parts. A new type of housing can be considered by the parameters for model part A and model part B.

2.1 Smoke Model

Gockel's models of smoke sensors are based on a simple smoke model, which is described by two main properties of the smoke [22].
Next to combustion products like heat, gases and water one of the products of most combustions of hydrocarbon fuel is smoke. The smoke emerges due to an undersupply of oxygen during the combustion. Therefore the combustion is incomplete and next to the combustion products of a complete combustion, like carbon dioxide and water, also smoke and carbon monoxide emerge.
Smoke is a condensation aerosol [57] and it consists of a mixture of different products which are released during combustion [10]. These are soot particles, water vapor, smoke gases and heated air [25]. This mixture is carried by the heated air which raises from the fire.
One main property of the smoke is the size distribution of the smoke particles. In a first approximation the smoke particles are considered as spherical. This assumption is maintainable at least for small particles and its failure to account for larger particles is negligible as long as the particle number concentration is below 10^7 per cm^3.
As mentioned before smoke is a condensation aerosol and the particle size distribution $n_\mathrm{d}(d)$ of this kind of aerosol is given by the logarithmic normal distribution [24, chap 4.4]

$$n_\mathrm{d}(d) = \frac{N}{\sqrt{2\pi}\sigma_d d} \exp\left(-\frac{1}{2}\frac{\ln^2(\frac{d}{d_\mathrm{g}})}{\sigma_\mathrm{d}^2}\right), \tag{2.1}$$

where d is the particle diameter, d_g is the geometric mean particle diameter, N the particle number concentration and σ_d is the standard deviation of the distribution, whereby all values are standardized. Another characteristic property of the smoke is its absorption of light. To include this property of smoke in his model Gockel assumes that the smoke particles only consist of carbon in its pure or in bounded form, e.g. CO_2, CO and water. With this approximation the degree of absorption of light by the smoke can be defined by the carbon fraction, whereby carbon is the only material emerging from a fire that absorbs visible

or infrared light at a high degree [8]. The larger the carbon fraction is the larger is, the absorption of light. Consequently the carbon fraction is a necessary parameter to model optical procedures of smoke measurement.
Using this smoke model the smoke is described by four parameters. The particle number concentration N, the geometric mean particle diameter d_g and the variance of the particle size distribution σ_d^2 denote the particle size distribution. The fourth parameter is the carbon fraction κ respectively the refractive index $\underline{m}$ of the smoke particles, which describe the optical properties of the particulate matter in the smoke. The complex refractive index can be obtained from the carbon fraction in the following way

$$\underline{m} = \kappa \underline{m}_C + (1-\kappa)\underline{m}_W, \tag{2.2}$$

with $\underline{m}_C$ the complex refractive index of carbon and $\underline{m}_W$ the complex refractive index of water [22].

2.2 Smoke Sensors

In this chapter the physical basics of optical smoke sensors and of sensors using the principle of the ionization chamber implemented in Gockel's model are described.

2.2.1 Optical Smoke Sensors

Optical smoke sensors use the effect of scattering and absorption of light by smoke particles to measure the amount of smoke. Therefore light is described as an electromagnetic wave. The sensor measures the intensity of the scattered light (scattered light sensors) or the intensity of the scattered and absorbed light (extinction light sensor), when the electromagnetic wave meets a particle. In this case the electric and magnetic fields have to fulfill Maxwell's Law inside the particle and outside the particle as well as the boundary conditions. In a mathematical view a boundary value problem on a sphere has to be solved. The solution of this boundary value problem is based on a calculation done by Mie [48] and is therefore called the "Mie Theory " [29], [8].

Scattered light sensor

Figure 2.2 shows a setup for the measurement of light scattered by a single particle. The intensity I_s of the scattered light depending on the incoming light can be described as follows [22]

$$I_s = I_0 \frac{\lambda_l^2}{8\pi^2 a^2}(i_1(\alpha, \underline{m}, \Theta) + i_2(\alpha, \underline{m}, \Theta)) \tag{2.3}$$

following the Mie Theory. While I_0 is the intensity of the incoming light, λ_l is the wavelength of the incoming light and a the distance between the scattering particle and the light source.

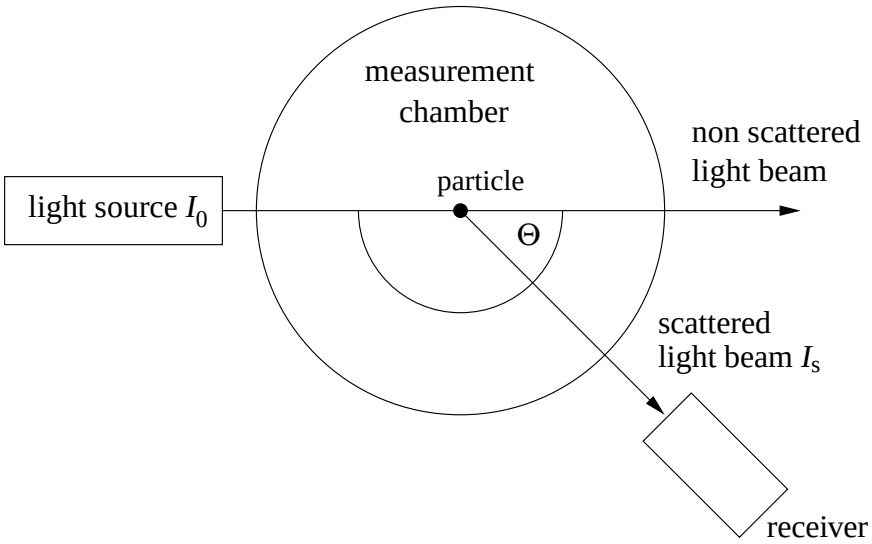

Figure 2.2: Setup for the measurement of scattered light [22]

i_1 and i_2 are two intensity functions which depend on α the ratio between the particle radius and the wavelength of light, on $\underline{m}$ the complex refractive index and on Θ the scattering angle [62]. The complex refractive index is a material property of the particles. The real part of the refractive index describes the scattering of light, the imaginary part describes the absorption of light. If there is no absorption the refractive index is real. With the described smoke model the complex refractive index can be calculated from the carbon fraction and the refractive indices of carbon and water, see equation (2.2).
Considering that the particles are of the same optical properties and the distance between the particles is so large that no multi scattering occurs, all the intensities of the light scattered by the particles can be superimposed. So the intensity of the scattered light is proportional to the number of particles. In general only the number concentration of particles is known. So the intensity of light scattered by one particle has to be multiplied by the number concentration N and the scattering volume V_{sc}. The intensity of light scattered by particles of the same size becomes

$$I_s = I_0 \frac{N \cdot V_{sc} \cdot \lambda_1^2}{8\pi^2 a^2} (i_1(\alpha, \underline{m}, \Theta) + i_2(\alpha, \underline{m}, \Theta)) \tag{2.4}$$

If the particles are different in size and if these differences can be described by the particle size distribution, the scattered intensity has to be integrated over the particle size distribution.

$$I_s = I_0 \int_{d=0}^{\infty} \frac{N \cdot V_{sc} \cdot \lambda_1^2}{8\pi^2 a^2} (i_1(\alpha, \underline{m}, \Theta) + i_2(\alpha, \underline{m}, \Theta) n_d(d) \mathrm{d}d \tag{2.5}$$

From equation (2.5) it can be seen that the scattered intensity depends on the size distribution and the refractive index of the smoke particles. Next to different properties of the sensor itself.

Extinction light sensor

Figure 2.3 shows the setup for the measurement of the extinction of light by particles. The

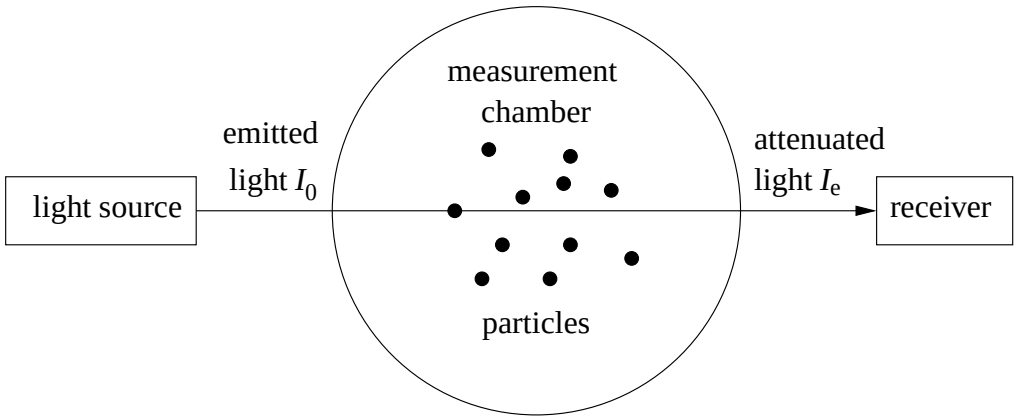

Figure 2.3: Setup for the measurement of the extinction of light [22]

relation between the intensities of the incoming light I_0 and the attenuated light I_e can be described by the extinction coefficient σ_{ext} and the travel length x of the light.

$$I_e = I_0 \exp(-\sigma_{ext} x) \tag{2.6}$$

The extinction coefficient depends on the number of particles n inside the measurement chamber and a proportional factor C_{ext}, which is called extinction cross section. The extinction cross section depends on the size of the particles. Assuming that the particles have all the same size, the extinction coefficient becomes

$$\sigma_{ext} = n \cdot C_{ext}$$

In case of different particles the particle size distribution has to be considered and the extinction coefficient can be calculated as follows

$$\sigma_{ext} = \int_{d=0}^{\infty} C_{ext}(d) n_d(d) \mathrm{d}d. \tag{2.7}$$

With a known distance x the relation between incoming light and measured, attenuated light gives a measure for the extinction cross coefficient.

2.2.2 Ionization Smoke Sensors

Smoke sensors that are based on the fact that ions of air agglomerate on the surfaces of smoke particles [7], [22], are called ionization chambers. Figure 2.4 shows the principle of an ionization chamber. It consists basically of the chamber volume with two electrodes

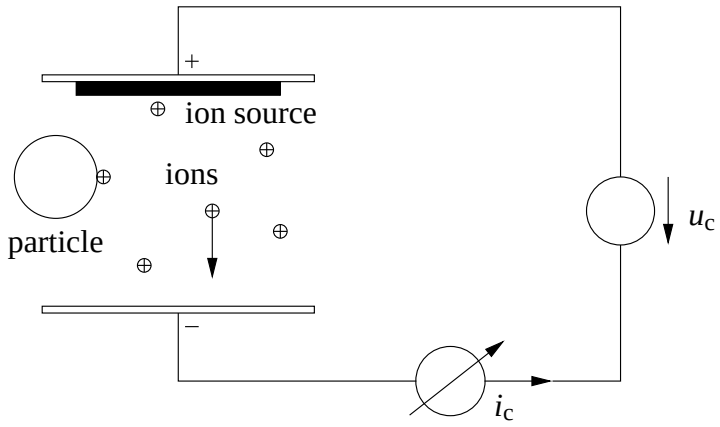

Figure 2.4: Principle of ionization chamber

which form a plate capacitor. At one of these electrodes a radioactive substrate is mounted which emits ions [15],[16] into the space between the electrodes. A dc voltage is applied to the electrode and due to the ions there is a current inside the capacitor. If particles intrude into the chamber volume the ions accumulate on the surfaces of these particles. Due to their adhesion at larger-sized smoke particles the ions are of lower movability and so the current decreases. The decrease of the current, often called chamber current, is a measure for the number of particles inside the plate capacitor.
The chamber current without intruding smoke particles is denoted as i_0. Then the relation between the particle number and size and the chamber current i_c inside the capacitor is [22]

$$d \cdot n = \eta \left(\frac{i_0}{i_c} - \frac{i_c}{i_0} \right), \tag{2.8}$$

for n smoke particles with the diameter d. This equation is called the characteristic chamber equation, with η the chamber constant, which is mainly determined by the geometry of the chamber. A value is defined which gives a measure for the amount of smoke

$$y = \frac{i_0}{i_c} - \frac{i_c}{i_0}. \tag{2.9}$$

This parameter is sometimes called the smoke density [26].
If the particles have different sizes the particle size distribution has to be taken into account in the characteristic chamber equation and equation (2.8) becomes

$$\int_{d=0}^{\infty} dn_d(d)\mathrm{d}d = \eta y \tag{2.10}$$

The integral

$$M_1 = \int_{d=0}^{\infty} dn_d(d)\mathrm{d}d$$

is the first order moment of the distribution and for the log-normal distribution the moment can be written as

$$M_1 = N d_\mathrm{g} \exp\left(\frac{1}{2}\sigma_\mathrm{d}^2\right)$$

and so equation (2.10) becomes

$$N \cdot d_\mathrm{g} \exp\left(\frac{1}{2}\sigma_\mathrm{d}^2\right) = \eta y. \tag{2.11}$$

From equations (2.9) and (2.11) it can be seen that the drop of the chamber current is proportional to the particle number concentration and the particle diameter.

2.3 Input Parameter for Smoke Sensor Models

Several input parameters have to be known for the application of the smoke sensor models described here. All three described models need the particle number concentration, the mean particle diameter and the standard deviation of particle size distribution as input parameters for the simulation. The models for the optical sensors also need a specification of the optical properties of the smoke in form of the carbon fraction or the refractive index of the smoke particles. Additional input parameters are the temperature and the flow velocity of air. For Gockel's investigations of the sensor model [22] the input parameters have been taken from measurements [65], [23] or from literature [17]. Table 2.1 shows the necessary input parameters for the smoke sensor models.

N	particle number concentration
d_g	geometric mean particle diameter
σ_d	geometric standard deviation
$\mathbf{u}$	flow velocity of air
κ or $\underline{m}$	carbon fraction or refractive index (optical smoke sensors)
T	temperature (ionization chamber)

Table 2.1: Input parameters for model of smoke sensors

3 Simulation of Fires

The modelling of a fire in its environment is one part of the over-all model described in chapter 1. The simulation of fires is by no means a trivial problem, due to the complexity of fire scenarios. Hoyt Hottel described this as follows, 'A case be made for fire being, next to life processes, the most complex of phenomena to understand' [27]. Different problems arise concerning the development of tools for fire simulations. On one side there is a huge number of different fires with diverse often unintended reasons and scenarios. On the other side there are a lot of physical and chemical processes in combustion which are not understood in detail and/or cannot be described in a computational way so far. Therefore simplifications for several processes in a fire have to be made [45]. A short history of the development of fire models can be found in the relevant literature [43]. A suitable way is to start with a model of a 'simple' fire situation and to expand this model to more complex problems if it yields satisfactory results. Two types of fire models are of common use in the field of fire simulation. First, there are the zone models, in which the compartment of the fire is separated in two layers, a hot upper layer and a cooler lower layer [54], [28]. The mass and heat transfer between these layers is described by conservation laws. These zone models give reasonable results simulating fire plumes, air flows through different kinds of vents and heat transfer, but they do not give detailed spatial information on the fire environment. For such more detailed information field models, that are based on computational fluid dynamics (CFD), are suitable. In these models the fire compartment is separated into a number of rectangular grid cells by a grid structure. Because of a limited spatial resolution due to grid structures suitable for the calculations the combustion has to be computed in an approximate manner. The turbulent mixture of the fuel, oxygen and the combustion products can be modelled by a large eddy simulation (LES).' The basic idea behind the LES technique is that the eddies that account for most of the mixing are large enough to be calculated with reasonable accuracy from the equations of fluid dynamics ' [45]. The small-scale eddy motion is treated in an approximate manner or it is ignored. In the following chapter a CFD based flow model is described. The model is the basis of the 'Fire Dynamics Simulator' (FDS) [45], [46] a computer software to simulate different fires in different environments. This program was developed at the National Institute of Standards and Technology (NIST) in Gaithersburg, USA, and it is still under development.

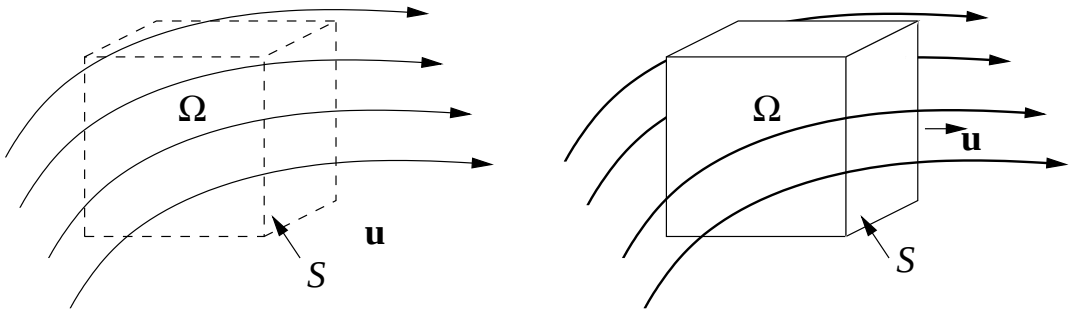

Figure 3.1: left: fixed volume, right: moving fluid volume element [69, chap 2.2]

3.1 Hydrodynamic Model

The basis of the CFD model is the hydrodynamic model, which consists of different conservation laws [45]. For the computational solution a low Mach number approximation is made, which means that waves traveling with velocities close to sonic speed are filtered out. This low Mach number assumption can be made, because the speed of the flow stream in case of a fire driven flow lies far below sonic speed. The assumption has two main advantages. In the first way, only the flow speed is determining for the time step of the algorithm not the sound speed, and in the second way, the number of independent variables in the system of equations, which have to be solved, is reduced.

3.1.1 Conservation Laws

The hydrodynamic model is based on the four conservation equations for a thermally-expandable, multi-component mixture of ideal gases [45]. For the derivation of these equations two approaches exist (figure 3.1). The first one considers a finite control volume Ω that is fixed in space, and the fluid is streaming through the surface S of this volume. The second approach considers a finite volume of fluid which moves with the fluid velocity $\mathbf{u}$. This volume consists of the same material as the surrounding fluid. The amount of fluid inside the volume and thus the mass of the volume is fixed.

Conservation of Mass

Considering the fixed volume approach, where the fluid flows through the volume Ω, the conservation of mass says that the time rate change of mass inside the volume is equal to the flow of mass through the surface of the volume [69]. This can be described as follows

$$-\frac{\partial}{\partial t}\iiint_{\Omega}\rho \mathrm{d}\Omega = \iint_{S}\rho\mathbf{u}\mathrm{d}\mathbf{S}, \tag{3.1}$$

where the term on the left hand side of equation (3.1) describes the time rate change of mass

inside the volume Ω and the term on right hand side describes the mass flow through the surface S with the fluid velocity $\mathbf{u}$. ρ is the density of the fluid. With the Gaussian theorem the conservation equation becomes [69, chap 2.5]

$$\frac{\partial}{\partial t}\iiint_{\Omega}\rho \mathrm{d}\Omega + \iiint_{\Omega}\nabla(\rho\mathbf{u})\mathrm{d}\Omega = 0.$$

For an infinitesimal volume $\Omega \to 0$ it holds

$$\frac{\partial}{\partial t}\rho + \nabla\rho\mathbf{u} = 0,$$

which is the equation for the conservation of mass.

Conservation of Species

The law for the conservation of species can be obtained by applying the law of the conservation of mass to each of species. Species are all products emitted by the combustion process. In addition to the convective mass flow of species through the volume surface determined by the fluid flow, described as $\nabla\rho Y_i\mathbf{u}$, there is a diffusional flow of species due to molecular diffusion $\nabla\rho D_i\nabla Y_i$, with the diffusion coefficient D. Y_i is the mass fraction of i-th species. And there might be a source of specie in the volume due to chemical reaction described by the generation rate $\dot{m}_i'''$ of i-th species per unit time and unit volume. The conservation equation results in [45, chap 2.6]

$$\frac{\partial}{\partial t}(\rho Y_i) + \nabla\rho Y_i\mathbf{u} = \nabla\rho D_i\nabla Y_i + \dot{m}_i''',$$

which is applied for every specie.

Conservation of Momentum

The moving fluid element model from the right hand side of figure 3.1 is taken to derive the equation of the momentum conservation. The conservation of momentum is nothing else than Newton's 2nd law, which says that 'the force on the fluid element equals its mass times the acceleration of the element' [69]. There are body forces like gravitational force and electric and magnetic forces, acting directly on the mass of the volume element as well as forces, acting on the surfaces of the volume element, caused by the pressure distribution and the sheer and stress distributions. The influence of the body forces can be written as follows

$$\mathbf{f}_{\mathrm{m}} = \rho\mathbf{g} + \mathbf{f},$$

where $\rho\mathbf{g}$ is the gravitational force and $\mathbf{f}$ represent other external forces. The influence of the surface forces can be written as follows

$$\mathbf{f}_{\mathrm{s}} = \nabla p - \nabla\cdot\tau,$$

with the pressure p and the viscous stress tensor τ. The conservation of momentum can now be written as follows [69]

$$\rho\left(\frac{\partial \mathbf{u}}{\partial t}+(\mathbf{u}\nabla)\mathbf{u}\right)=\rho\mathbf{g}+\mathbf{f}+\nabla\cdot\tau-\nabla p. \tag{3.2}$$

The term in brackets on the left hand side of equation (3.2) describes the time rate and the spatial change of the velocity field. The terms on the right hand side describe the forces acting on the volume.

Conservation of Energy

Again the model of the moving fluid element is used for the derivation of the energy equation. The conservation of energy is described by the first law of thermodynamics which says, that the rate of change of heat inside such a fluid element equals the flux of heat into this element plus the rate of working done by forces acting on the mass of the element, e.g. gravity force, or on the surfaces of the element , e.g. stress force [69].
The work done by pressure shall be the only work to be considered and it can be written as follows

$$\frac{\partial p}{\partial t}+\mathbf{u}\nabla p.$$

The heat flux into the volume element can have different sources. There might be a heat flux due to convection, which is $\nabla k\nabla T$, where k is the thermal conductivity, a radiative heat flux $\nabla\mathbf{q}_{\mathrm{r}}$, and a heat flux due to molecular diffusion of the different species $\sum_i \nabla h_i \rho D_i \nabla Y_i$, where h_i is the enthalpy of i-th species, the sum goes over all species. $\rho D_i \nabla Y_i$ is the diffusional flow of species.
The change of heat inside the element can be written as follows

$$\frac{\partial}{\partial t}(\rho h)+\nabla\rho h\mathbf{u}.$$

So the conservation equation becomes [69]

$$\frac{\partial}{\partial t}(\rho h)+\nabla\rho h\mathbf{u}=\frac{\partial p}{\partial t}+\mathbf{u}\nabla p-\nabla\mathbf{q}_{\mathrm{r}}+\nabla k\nabla T+\sum_i \nabla h_i \rho D_i \nabla Y_i, \tag{3.3}$$

where the index i denotes the different species.

Divergence of the flow field

The equation of the conservation of energy - never explicitly solved - is used to obtain an equation to describe the divergence of the flow velocity field. Therefore different assumptions are made, considering the low Mach number assumption. It is assumed that the pressure can be replaced by the background pressure p_0 which is described by the equation for

an ideal gas [45] that relates the thermodynamic quantities

$$p_0 = \rho T \mathscr{R} \sum_i \frac{Y_i}{M_i} = \frac{\rho T \mathscr{R}}{M}, \tag{3.4}$$

with M being the molecular weight of the gas mixture and $\mathscr{R}$ the universal gas constant. The pressure can also be described as

$$p_0 = \frac{\gamma - 1}{\gamma} \rho h$$

in the case that the ratio of the specific heats γ is the same for all species [44]. The enthalpy of the different species h_i can be written as [45]

$$h_i(T) = h_i^0 + \int_{T^0}^{T} c_{\mathrm{p},i}(T') \mathrm{d}T',$$

where h_i^0 is the heat of formation of specie i and $c_{\mathrm{p},i}$ is the specific heat by constant pressure. With these assumptions the divergence of the flow field can be calculated from the conservation of mass (3.1), the conservation of energy (3.3) and the state relation (3.4). The divergence becomes

$$\nabla \cdot \mathbf{u} = \frac{1}{\rho c_\mathrm{p} T} \left(\nabla \cdot k \nabla T + \nabla \cdot \sum_i \left(\int c_{\mathrm{p},i} \mathrm{d}T \right) \rho D_i \nabla Y_i - \nabla \mathbf{q}_\mathrm{r} \right) + \left(\frac{1}{\rho c_\mathrm{p} T} - \frac{1}{p_0} \right) \frac{\mathrm{d}p_0}{\mathrm{d}t}. \tag{3.5}$$

The terms in the left brackets on the right hand side of equation (3.5) represent the effect of convective, diffusional and radiative heat flow. The terms in the right brackets represent the effect of time rate changes of the background pressure. The physical meaning of the divergence of the flow field can be exemplified with the moving volume element approach. The mass of this fluid volume is fixed but the surface and the size of the volume element changes due to the different densities at different locations. The divergence of the flow field is now the time rate of change of the size of volume element per unit volume [69, chap 2.4]. Due to the low Mach number approximation changes of the pressure only depend on changes of the temperature (equation (3.4)). It can be seen from equation (3.5) that changes of the divergence solely depend on changes in temperature. For the derivation of the divergence see the technical manual of the fire dynamics simulator [45].
Therefore the hydrodynamics model is based on a system of five equations, the governing equations.

Conservation of Mass

$$\frac{\partial \rho}{\partial t} + \nabla \cdot \rho \mathbf{u} = 0 \tag{3.6}$$

Conservation of Species

$$\frac{\partial}{\partial t}(\rho Y_i) + \nabla \cdot \rho Y_i \mathbf{u} = \nabla \cdot (\rho D)_i \nabla Y_i + \dot{m}_i''' \tag{3.7}$$

Conservation of Momentum

$$\rho\frac{\partial \mathbf{u}}{\partial t}+\rho(\mathbf{u}\cdot\nabla)\mathbf{u}=\rho\mathbf{g}+\mathbf{f}-\nabla p+\nabla\cdot\tau \tag{3.8}$$

Divergence Constrain

$$\nabla\cdot\mathbf{u}=\frac{1}{\rho c_{\mathrm{p}}T}\left(\nabla\cdot k\nabla T+\nabla\cdot\sum_i(\int c_{\mathrm{p},i}\mathrm{d}T)\rho D_i\nabla Y_i-\nabla\mathbf{q}_{\mathrm{r}}\right)+\left(\frac{1}{\rho c_{\mathrm{p}}T}-\frac{1}{p_0}\right)\frac{\mathrm{d}p_0}{\mathrm{d}t} \tag{3.9}$$

Equation of State

$$p_0=\rho T\mathscr{R}\sum_i\frac{Y_i}{M_i}=\frac{\rho T\mathscr{R}}{M} \tag{3.10}$$

3.2 Numerical Solution

This chapter gives a principle description of the numerical solution of the governing equations used by the FDS software. For a more detailed description see the technical manual of the FDS [45, chap 7]. A numerical solution can only be calculated for discrete spatial points and discrete time steps, therefore a temporal as well as a spatial discretization has to be made to solve the governing equations. The spatial discretization is determined by the computational grid. Inside one grid cell all quantities have the same value. For the computation of the spatial derivatives the method of finite differences [69, chap 5] is used. Thereby the spatial derivatives are replaced by second order finite differences [45]. Scalar values like the density or the temperature are referred to the center of a grid cell, while vector quantities like the flow velocity are referred to a surface of the grid cell in consideration of their direction. The temporal discretization is realized with an estimator-corrector scheme. Whereby the different quantities at discrete time step $n+1$ are first estimated by using the known values at the time step n. In a later step these estimated values are corrected to get the final values at the discrete time $n+1$. During the calculation a stability criterion for the size of the time steps has to be fulfilled. The stability criterion says that the time step must be smaller than the minimum quotient between the length of the grid cell in one direction and the velocity in the same direction

$$\partial t<\min\left(\frac{\partial x}{u},\frac{\partial y}{v},\frac{\partial z}{w}\right). \tag{3.11}$$

Considering the moving volume approach on the right side of figure 3.1 this means that a fluid element must be accounted in every grid cell and does not have to skip a grid cell during one time step.

3.3 Combustion Model

The combustion process can principally be modelled in two ways, depending on the size of the computational domain. If the computational domain is small enough the combustion can be modelled using direct numerical simulation (DNS). In a DNS the diffusion of oxygen and fuel during combustion can be modelled directly. This can only be realized for very small fires and in a small domain around the fire, because a very dense grid structure is needed. If the grid structure is not fine enough, a large eddy simulation (LES) is suitable. In a LES the diffusion of fuel and oxygen can be computed by a mixture-fraction based model, where it is assumed that physical processes that occur at small time periods and scale length must be computed in an approximate manner, whereas large scale transport processes, convective as well as radiative, can be modelled directly. In the following, a mixture-fraction combustion model, which is a realisation of the LES, is described.

3.3.1 Mixture Fraction Combustion

The mixture-based combustion model [45], [19] rests upon the assumption, that the combustion is controlled by the mixing of fuel and oxygen. Another assumption is that all chemical reactions are so fast that the reactants never coexist (infinite reaction), which means that fuel and oxygen never exist at one location at the same time. Due to this assumptions it is possible to represent all species relevant for the combustion process by one single parameter. This parameter is the mixture fraction $Z(\mathbf{x},t)$, which depends on the space $\mathbf{x}$ and time t, a linear combination of all species mass fractions. For a given value of Z the relation of the mass fractions of species is always the same. Each of the species can be described as a function of Z. So the conservation of species (equation (3.7)) has to be solved only for the mixture fraction instead of all species. Figure 3.2 shows the relation between the mixture fraction Z and the mass fractions of the different species obtained from a simulation of the combustion of n-Heptane with the FDS, where the amount of CO is so small that it is not visible.
In Figure 3.2 a value for Z can be found where the mass fractions of fuel and oxygen are zero. This value is called the stoichiometric mixture fraction Z_{f}. This area in which Z equals Z_{f} is the reaction zone named as the flame sheet. In this area the energy is released during combustion, it is an infinite thin surface. This area complies roughly the visible flame sheet of the combustion. To calculate the heat release rate of the fire with the mixture based combustion model the following approach is taken. The local heat release rate only depends on the local mass consumption of oxygen, whatever fuel is burned [19]. So it is necessary to describe the mass consumption rate of oxygen as a function of the mixture fraction in order to use the mixture fraction combustion model for the calculation of the heat release rate. The

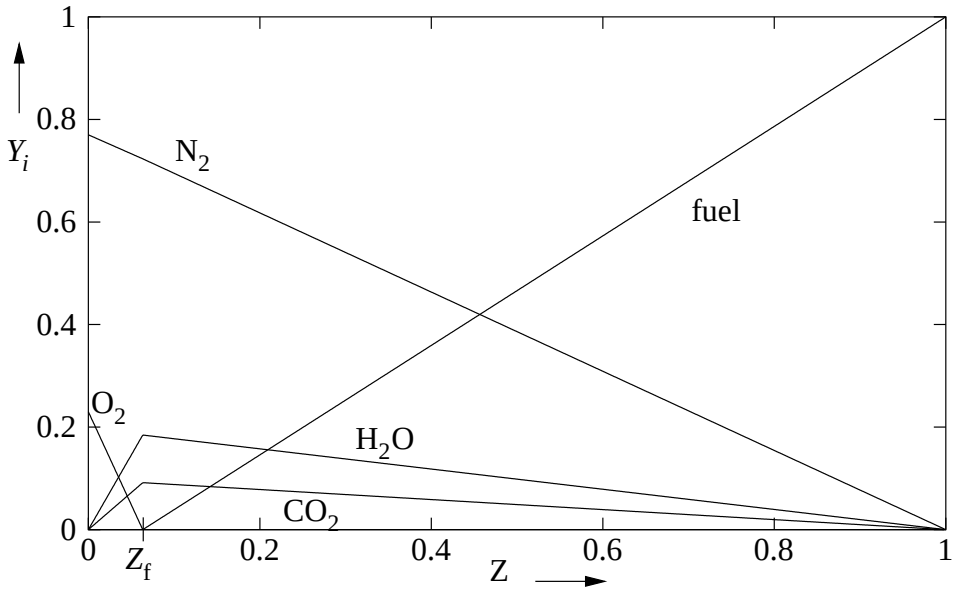

Figure 3.2: Mixture fraction of the combustion of n-heptane.

oxygen mass fraction Y_O can be computed as a function of the mixture fraction

$$Y_O = \begin{cases} Y_O^\infty(1 - Z/Z_f) & ; \quad Z < Z_f \\ 0 & ; \quad Z > Z_f \end{cases} \tag{3.12}$$

where Y_O^∞ is the ambient mass fraction of oxygen. Since the mixture fraction can be interpreted as one of the species both oxygen mass fraction and mixture fraction fulfill the conservation law for the conservation of species (3.7)

$$\rho\left(\frac{\partial Z}{\partial t} + \mathbf{u}\nabla Z\right) = \nabla \cdot \rho D \nabla Z, \tag{3.13}$$

$$\rho\left(\frac{\partial Y_O}{\partial t} + \mathbf{u}\nabla Y_O\right) = \nabla \cdot \rho D \nabla Y_O + \dot{m}_O'''. \tag{3.14}$$

From these two equations the following relation between the mass consumption rate of oxygen $\dot{m}_O'''$ and the mixture reaction can be obtained [19]

$$-\dot{m}_O''' = \nabla \cdot \rho D \frac{dY_O}{dZ} \nabla Z - \frac{dY_O}{dZ} \nabla \cdot \rho D \nabla Z. \tag{3.15}$$

The heat release rate can be written as

$$\dot{q}''' = \Delta H \cdot \dot{m}_O''', \tag{3.16}$$

with ΔH being the heat released per unit mass of oxygen consumed.
As mentioned before, the flame sheet is an infinite thin surface and the oxygen mass fraction

$Y_O(Z)$ has a discontinuity at $Z = Z_f$ (equation (3.12)), so the computational realization is made as follows. First the grid cells that are cut by the flame sheet are located, then the local heat release rate is calculated for these grid cells. So the two dimensional flame sheet is spread on the width of a grid cell and the grid must be fine enough to get suitable results.

3.3.2 Incomplete Combustion

During a complete combustion the fuel is decomposed into its complete oxidated products. Equation (3.17) shows the complete combustion of n-heptane.

$$C_7H_{16} \rightarrow 7CO_2 + 8H_2O \tag{3.17}$$

If a combustion is incomplete, which means that there is not enough oxygen provided to decompose the fuel into its products of complete combustion, additional combustion products emerge [21], e.g. CO and smoke. For the production of smoke the type of fuel is of importance. There are fuels which do not give smoke, while other fuels have a large smoke yield under the same condition [58]. The implementation of incomplete combustion into the mixture fraction combustion model is still a matter of research. In the FDS the incomplete combustion is considered by adjusting the mass fractions due to the emerge of products like smoke or CO [46, chap. 5.3.2], while the yields of soot and CO are defined before the simulation. In the calculations soot is treated in the same way as the other species that are produced during combustion. No difference between soot and smoke is made , so in the following the two denotations are used synonymically. The results for the simulation of species are given as the volume or the mass fraction of the whole amount of species produced during the fire. There is no reference to the material the smoke is built of or to the molecular or particulate properties of the smoke.

3.4 Performance of Fire Simulations

The FDS program has been chosen to realise the fire simulations for different reasons. First, detailed spatial information of the simulation results are mandatory. Therefore a field model was needed. One important advantage is that the combustion material and the combustion reaction can be defined in detail with the FDS. Furthermore, the FDS software as well as its source code are freely accessible, so that it is possible to make changes in the FDS software if necessary. Before a simulation with the FDS can be started, a number of parameters have to be set. These contain information about the fire environment, the definition of the combustion material and the definition of the computational grid. Most of the parameters are given by the environment and the fuel, but there are also parameters which are unknown or which depend on unknown properties. Normally the geometry of the environment is given

as well as different ambient values. The material properties like the density or the heat conductivity can be found in the literature [17]. But there are other parameters that can vary to a given degree like the maximum burning rate [46, chap 5.3.3], which limits the burning rate of the fire, or the soot yield, which defines the mass fraction of fuel that is converted into soot. Both depend among other things on the ventilation of the fire [58]. The number of grid cells is also a parameter which has to be chosen. A large number of cells gives more detailed simulation results because the grid structure defines the spatial discretisation of the computation. But with an increasing number of grid cells the duration of the simulation increases. If the cells are too small the stability criterion (equation (3.11)) for solving the conservation laws can not be maintained. Therefore a compromise has to be found between the accuracy and the duration of the calculation. In general a CFD model needs a uniform grid for the calculations, but with the FDS there is the opportunity to compress the grid in certain areas and uncompress it in other areas resulting in the fact that the total number of grid cells stays the same. This non-uniform grid is transformed into a uniform grid for calculation and the results are transformed back into the non-uniform grid. Thus it is possible to get a finer grid for example in the direct environment of the fire without increasing the number of cells.

In the following calculations the main interest lies in the smoke development and the smoke distribution during a fire. Therefore some parameters are examined in terms of their influence on the smoke development and the smoke distribution. A standardized EN54 [13] testfire is simulated for these purposes. The specific fire is a testfire TF5, an n-heptane fire, where the fire environment is the fire detection laboratory at the University Duisburg-Essen [40]. It is assumed that the laboratory is empty except for the socket the fire is burned on. The results give the conditions at a location under the ceiling in a radius of three meters around the fire, which is the measurement position for test fire experiments following the EN54 standard. The parameters which are examined are the maximum burning rate (mbr) and the soot yield (Y_s), both can be set to define the combustion. The maximum burning rate gives the mass loss of fuel per unit area and limits the conversion of fuel into its combustion products. The soot yield gives the amount of the burned fuel that is converted into soot and thus it determines the completeness of the combustion. In the fire experiment the n-heptane is burned in a metal tray wherefore it is also examined if the tray has any effect on the simulation results. The material properties of the n-heptane can be taken from the existing literature [17] or from a FDS database [12] developed by NIST or they can be acquired from the reaction equation for the complete combustion of n-heptane (C_7H_{16}), which is like follows

$$C_7H_{16} + 11O_2 = 7CO_2 + 8H_2O. \tag{3.18}$$

From this equation the stoichiometric coefficients can be obtained, which are needed for the parameters of the reaction.

The duration of a fire is determined mainly by the amount of fuel, the density of the fuel and the maximum burning rate. The density and the amount of fuel are known. In the following the maximum burning rate is varied to examine its influence on the smoke development. The lower the maximum burning rate is, the longer the fire burns, but with a lower heat release. This has an effect on the other simulation results which are of interest, i.e. smoke

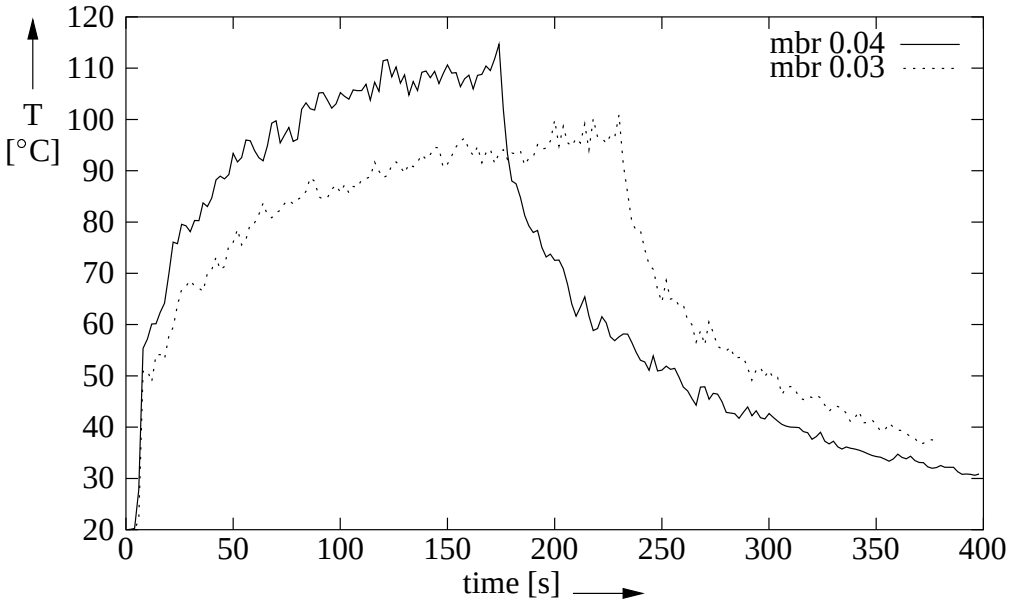

Figure 3.3: Simulated temperature with different maximum burning rates for a n-heptane fire.

mass density, temperature and flow velocity. Figures 3.3 and 3.4 show that the amplitude of the temperature and the smoke mass density are lower with a lower maximum burning rate and they decrease at a later point, because the fire burns longer. With a maximum burning rate of 0.03 the fire burns out at 220s, with a maximum burning rate of 0.04 at 170s. The reason for the sudden decrease of the particle mass density at 260s for a mbr= 0.04 cannot be given. But this decrease happens 90s after the fire burned out. At this point of time nearly no flowstream exists - just the ambient one - and the temperature has decreased to half of its maximum. The amplitude of the flow velocity shown in figure 3.5 is nearly independent of the maximum burning rate if the degree of change is not too high. But the flow continues to a later point of time also because of the longer duration of the fire. The maximum burning rate mainly affects the duration and the intensity of the fire.
By varying the smoke yield, a higher soot yield increases the smoke mass density as expected (figure 3.6). The short decrease of the smoke mass density at 310s happens 90s after the fire burned out. With regard to the flow velocity and the temperature a variation of the soot yield has no observable effect. With the FDS burning solids are simulated by defining an obstacle

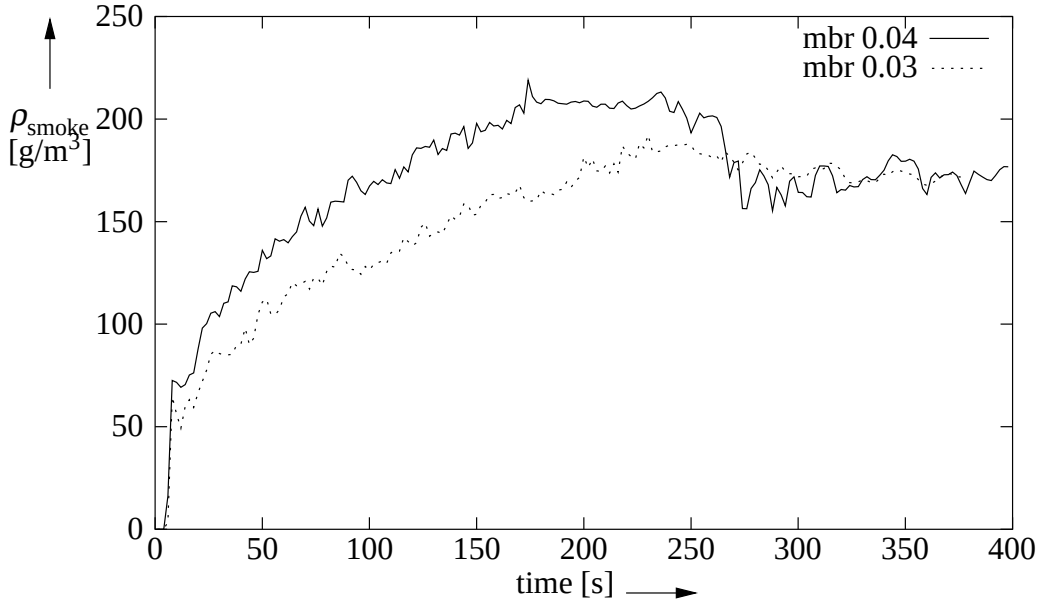

Figure 3.4: Simulated smoke mass density with different maximum burning rates.

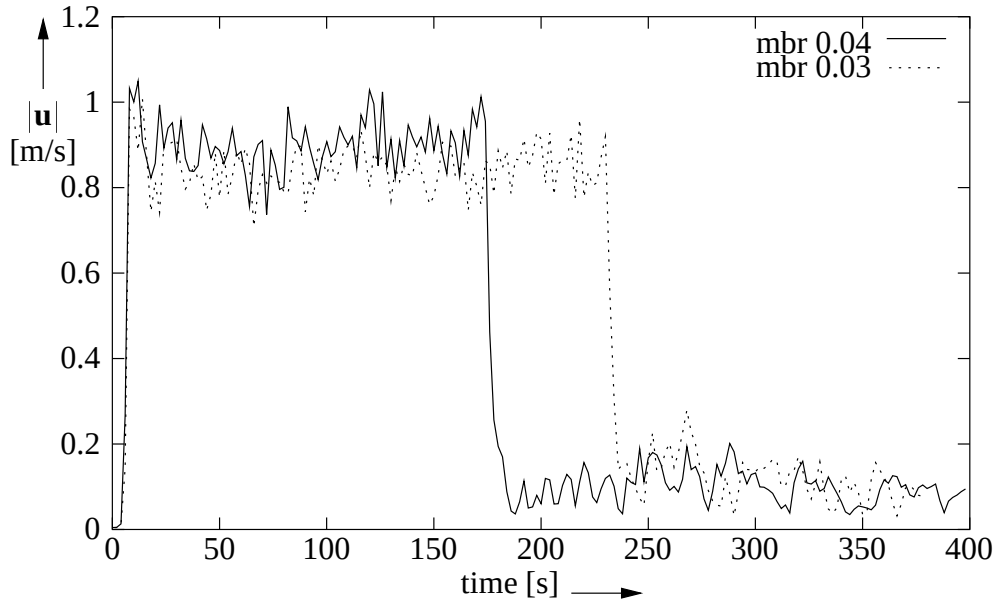

Figure 3.5: Magnitude of the simulated flow velocity with different maximum burning rates.

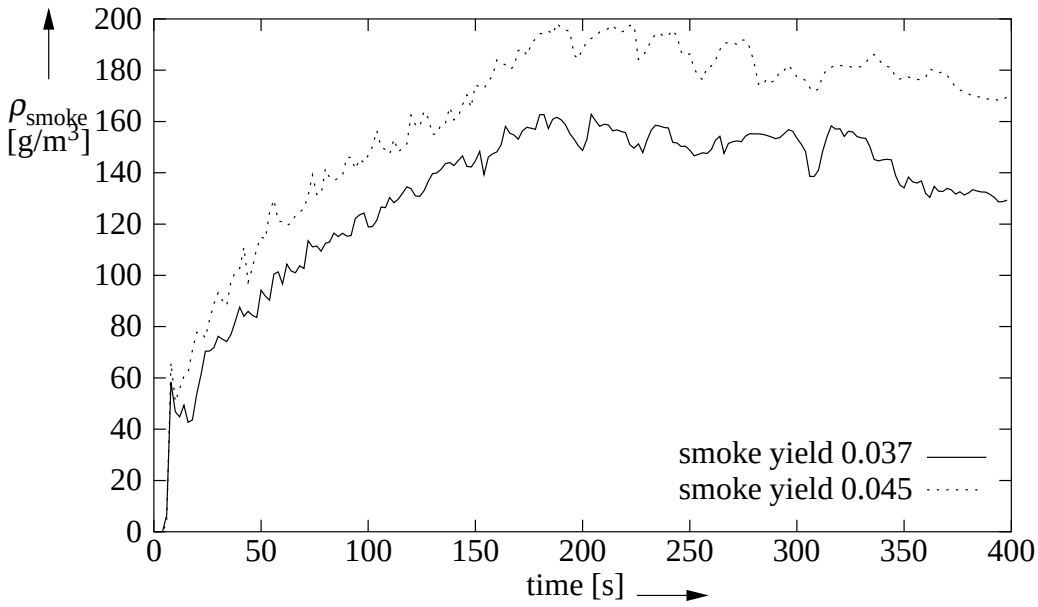

Figure 3.6: Simulated smoke mass density with different smoke yields.

which has one or more burning surfaces. For gases a vent is defined which represents the burning incoming gas flow. Burning liquids like n-heptane can be defined like burning solids with an additional parameter to define them as liquids. Therefore it is possible to define a burning liquid without any vessel. During the experiment the n-heptane is burned in a metal vessel. It is examined to what extent the tray and its material have an influence on the simulation results. The results have shown that the simulation with the tray results in a higher smoke mass density than without a tray, see figure 3.7. This can be explained by worse ventilation of the fire. The influence of the material of the tray on the smoke mass density shows when the fire has burned out. The smoke mass density decreases later when the n-heptane is burned in a metal tray (see figure 3.7). In the case of the metal tray it heats up during the fire and after the fire has burned out the tray releases the heat. Due to this there is still a small upward heat flow. By simulating the combustion in a tray the duration of the fire is about 10% longer than without the tray. The reason for this is the worse ventilation of the fire due to the vessel. This has to be considered in the simulation. The amplitudes of temperature and velocity (figures 3.8 and 3.9) are nearly the same for all three simulations. Only the longer duration has an effect as the decrease of the simulated values starts at a later point of time.

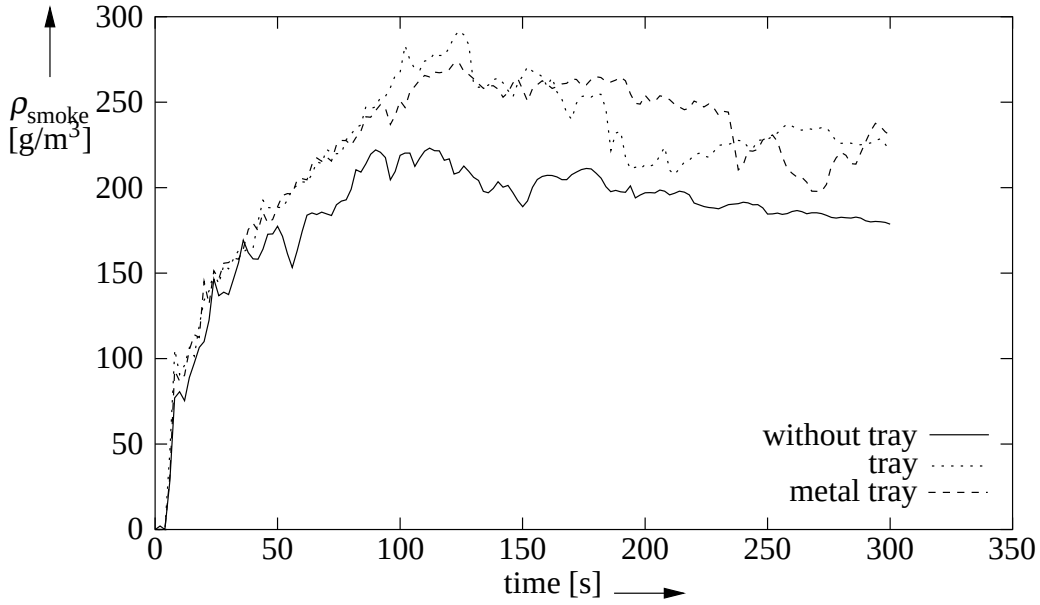

Figure 3.7: Smoke mass density simulated without a tray and with trays of non temperature conducting and temperature conducting (metall) materials.

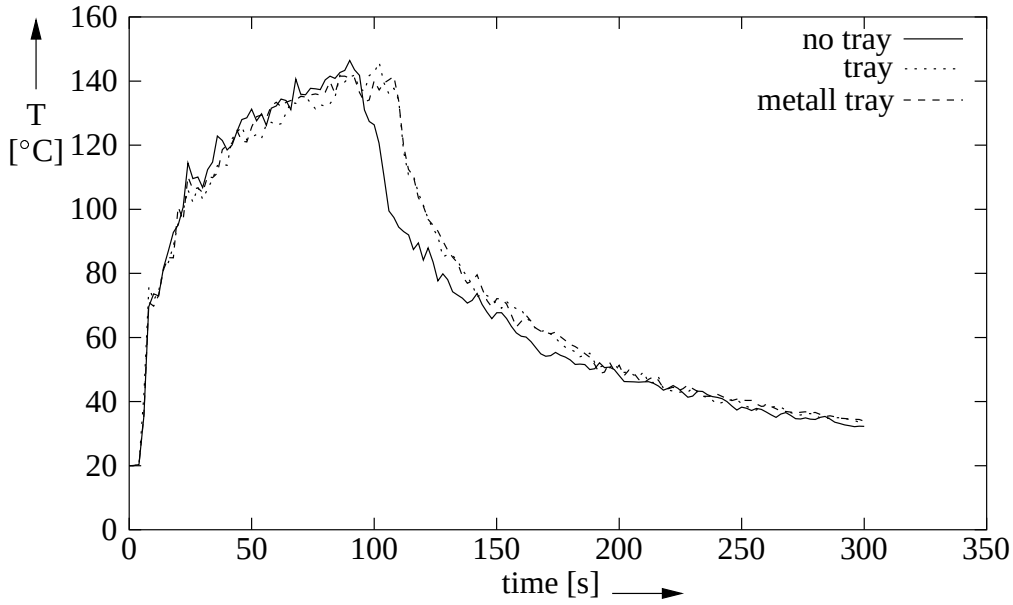

Figure 3.8: Temperature simulated without a tray and with trays of non temperature conducting and temperature conducting (metall) materials.

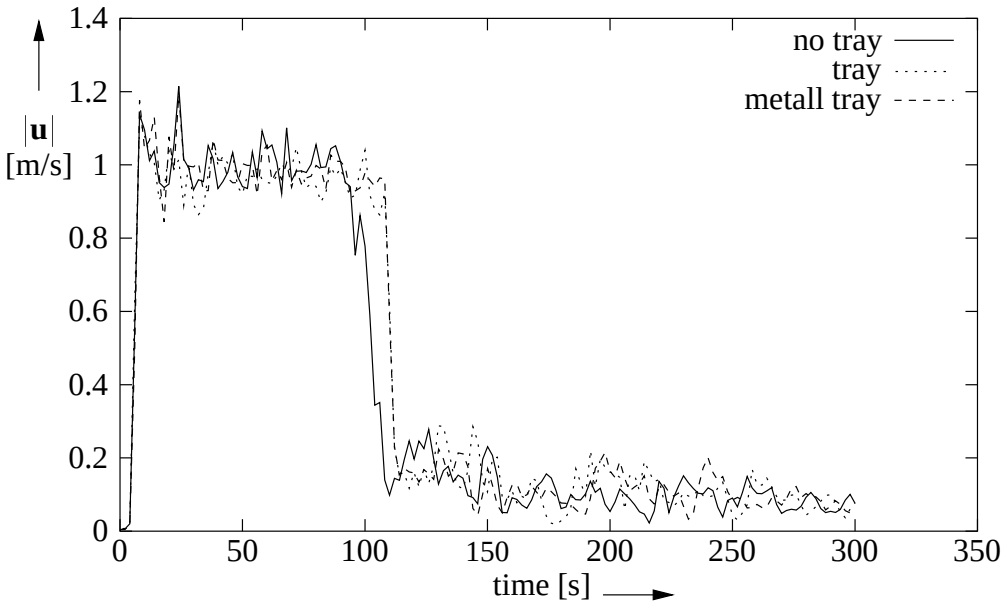

Figure 3.9: Velocity simulated without a tray and with trays of non temperature conducting and temperature conducting (metall) materials.

4 A Model for Simulating the Particulate Smoke Matter

The input parameters of the sensor model described in chapter 2.3 shall be simulated by the fire model as far as possible. Table 4.1 shows the output parameters of the fire model and the necessary input parameters for the sensor models. The flow velocity and the temperature can be simulated with the FDS program directly [46], but looking at the smoke properties the FDS only calculates the mass density as mass per volume. Therefore a model has to be developed to obtain the particulate smoke properties from the smoke mass density. Also processes which affect the particle size distribution but not the mass density of smoke and which are therefore not considered in the fire simulator have to be implemented. The carbon fraction of the smoke can not be simulated so far and has to be taken from other studies.

4.1 Particle Number Concentration

In a first step the particle number concentration shall be computed from the results given by the FDS. Again a log-normal size distribution of the particle sizes is assumed as in chapter 2.1. In the following the particle volume distribution for a well mixed medium is used [32]

$$n_{\mathrm{v}}(v,t) = \frac{N}{3\sqrt{2\pi}\cdot \ln(\sigma_{\mathrm{r}})v} \exp\left(\frac{\ln^2(v/v_{\mathrm{g}})}{18\ln^2\sigma_{\mathrm{r}}}\right). \tag{4.1}$$

where v_{g} is the geometric mean volume of the particles and $\ln\sigma_{\mathrm{r}}$ is the geometric standard deviation of the distribution, with σ_{r} the geometric deviation based on the particle radius,

fire model	**sensor model**
smoke mass density ρ_{smoke}	particle number concentration N geometric mean particle diameter d_{g} geometric standard deviation σ_{d}
flow velocity **u**	flow velocity **u**
temperature T	temperature T
-	fraction of carbon κ

Table 4.1: Input parameter of sensor model and results of the fire model

all these values are standardized. The relation between the particle diameter distribution and the particle volume distribution is given in appendix A. As shown in table 4.1 the FDS gives the smoke mass density as a result of the simulation. The smoke sensor model needs the particle number concentration, the geometric particle diameter and the standard deviation as input parameters. The particle number concentration can be computed from the smoke mass density using the first order moment of the distribution. The relation between the particle size distribution and the smoke mass density is given by

$$N_0 = \frac{\rho_{\text{smoke}}}{\rho_{\text{part}}} v_{\text{g}}^{-1} \exp\left(-\frac{9}{2}\ln^2 \sigma_{\text{r}}\right). \tag{4.2}$$

Where ρ_{smoke} is the smoke mass density and ρ_{part} is the specific density of the smoke particles, which is a material property. The derivation of equation (4.2) can be found in appendix B.

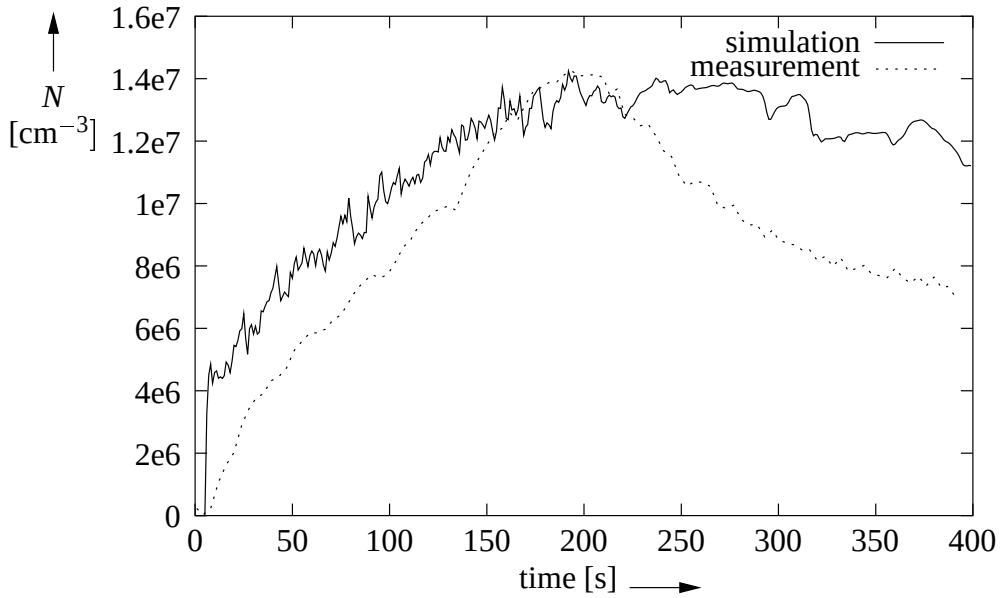

Figure 4.1: Particle number concentration

Figure 4.1 shows the simulated particle number concentration compared with measurement results. It can be seen that the amplitudes of the results are nearly the same, but after the fire burned out at 180s the measured particle number concentration decreases strongly, while the simulated one decreases very slowly [61]. Due to different mechanisms the size distribution of particles changes over the time. These mechanisms are coagulation, condensation, evaporation, removal of particles from the aerosol and nucleation. Figure 4.2 shows the principles for these mechanisms. The mechanisms have different effects on the smoke and its particular matter. With coagulation collisions between the particles in an aerosol occur due to the relative movement. These colliding particles adhere and from a new particle with a certain

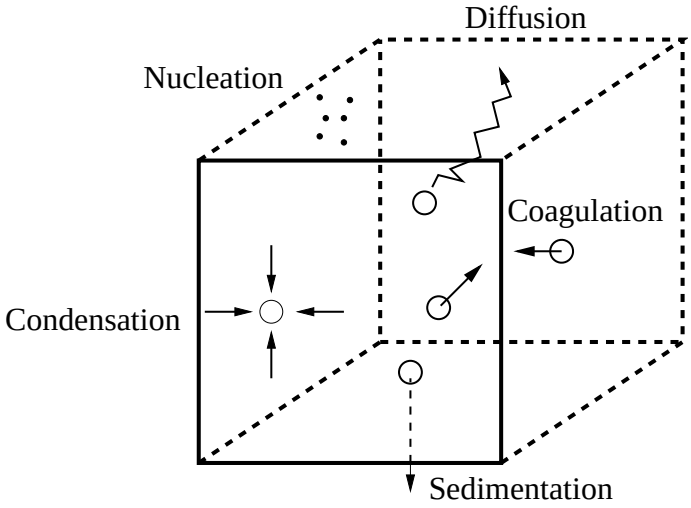

Figure 4.2: Mechanisms that influence the particle size distribution [20]

probability. The coagulation causes a decrease of the number of particles and an increase of the mean particle size. This type of coagulation is called Brownian coagulation. Due to this mechanism the particle number concentration decreases while the mass density of smoke stays the same.

In case of condensation diffusing gas molecules of the surrounding accumulate at the particle surface. With the opposite mechanisms the evaporation gas molecules emerge from the surface of the particles. So with condensation the mass density of smoke increases to a low degree, while the mass density decreases through evaporation. In general the particle number stays the same in both cases. However, they may disintegrate into their molecules, if they become very small due to evaporation.

The diffusion of the particles and the sedimentation shown in figure 4.2 and possible other effects that remove particles from the aerosol are summarized into the removal of particles. Removal of particles means that particles are removed from the aerosols by some chemical or physical processes. The particle number concentration as well as the mass density decrease due to these mechanisms. In case of nucleation gas molecules of a saturated gas build up new small particles, if these particles exceed a critical volume v_{cr} they do not disintegrate again. In table 4.2 the different mechanisms of particle aging and their effects on the particle number concentration and the smoke mass density are listed. The mechanisms with the strongest effects on the particle size distribution are the coagulation and the removal of particles, other effects can be neglected.

mechanism	particle number concentration	mass density
coagulation	decreases	constant
condensation	constant	increases
evaporation	constant (decreases)	decreases
removal	decreases	decreases
nucleation	increases	increases

Table 4.2: Influence of different mechanisms on smoke with regard to size distribution and smoke mass density

4.1.1 General Dynamic Equation

The evolution of the size distribution can be described by a general dynamic equation (GDE). The particle volume distribution satisfies the following GDE [50]

$$\frac{\partial}{\partial t}n(v,t)+\frac{\partial}{\partial v}[I(v,t)n(v,t)]+R(v,t)n(v,t)-L(v_{cr},t)\delta(v-v_{cr})=\left(\frac{\partial}{\partial t}n(v,t)\right)_{\text{coag}}. \quad (4.3)$$

The second term on the left hand side of equation (4.3) represents the condensation of gas molecules at the surface of particles or the evaporation of gas molecules from the surfaces of particles with the condensation/evaporation rate $I(v,t)$. The third term represents the removal of particles from the aerosol with the removal rate $R(v,t)$, the forth describes the nucleation of new condensation kernels, where $\delta(v)$ is Dirac's delta distribution and $L(v_{cr},t)$ the rate of nucleation. The term on the right hand side of the calculation represents the effect of coagulation of particles. In the relevant literature different numerical as well as analytical approaches can be found to solve this equation for combinations of different mechanisms [20], [71], [32], [33], [4]. In the following only the coagulation and the removal of particles from the aerosol are considered, so the GDE is reduced to [4]

$$\frac{\partial}{\partial t}n(v,t)+R(v,t)n(v,t)=\left(\frac{\partial}{\partial t}n(v,t)\right)_{\text{coag}}. \quad (4.4)$$

In the following chapters solutions for the GDE in its reduced form (4.4) are given. It is assumed that the coagulation is much faster than the removal of particles so that both mechanisms can be treated separately. In the first step only coagulation is considered.

4.2 Coagulation

With equation (4.2) the particle number concentration is calculated from the smoke mass density, assuming that the specific soot density, the geometric mean volume and the standard

deviation of the particle size distribution are known. As mentioned before the coagulation has no effect on the smoke mass density, therefore the coagulation can not be considered using this equation. In this chapter several approaches for implementing coagulation in the calculation of the particle number concentration N, the geometric mean volume v_g and the standard deviation of the size distribution $\ln \sigma_r$ by solving the GDE are introduced and compared.

The first one who gave an analytic solution for the change of the size distribution of particles undergoing coagulation was Smoluchowski [64]. Although Smoluchowski worked on collisions in hydrosols the principles stay the same for aerosols. Considering two particles with the radii r_1 and r_2 leads to the following equation for the time rate of change of the particle number concentration due to coagulation [71, chap 3.1]:

$$\frac{\mathrm{d}N}{\mathrm{d}t} = -4\pi(D_1 + D_2)(r_1 + r_2)\frac{N^2}{2}, \tag{4.5}$$

where D_i is the diffusion coefficient

$$D_i = \frac{kT}{6\pi\mu r_i},$$

where k is the Boltzmann constant and μ is the dynamic viscosity of the aerosol. Due to the coagulation the size of the particles depends on time, if two particles collide they form one large particle. But for the solution of equation (4.5) an initial mean particles radius r is assumed. Inserting the diffusion coefficient in equation (4.5) and replacing the particle radii r_1 and r_2 by r, one gets the following differential equation

$$\frac{\mathrm{d}N}{\mathrm{d}t} = -\frac{4kT}{3\mu}N^2, \tag{4.6}$$

which is independent of the particle size.

With the initial condition $N(0) = N_0$ the solution of this differential equation is

$$N(t) = \frac{N_0}{1 + 2K_c N_0 t}, \tag{4.7}$$

with $K_c = 2kT/(3\mu)$ the collision coefficient. The dynamic viscosity μ depends on the pressure and on the temperature. The higher the dynamic viscosity is the lower is the movability of the smoke particles and the lower is the probability that collisions take place.

Smoluchowski's solution is based on monodisperse particles, but the collision of particles depends upon their size. Despite the fact that Smoluchowski's assumption of monodisperse particles does not agree with measurements, his solution also gives reasonable results for the change of particle size distribution due to coagulation in later stages of the particle evolution [32].

In the following a solution for polydisperse particles is given. A continuous particle size distribution is considered, and it is assumed that the probability that two particles which collide coagulate to one particle is equal to 1. The probability that two particles of the volumes u and v collide is given by

$$\beta(u,v)n(u,t)n(v,t)\mathrm{d}v\mathrm{d}u,$$

where $\beta(u,v)$ is the so called coagulation kernel. The decay of the particles due to coagulation can be written as follows [32]

$$\frac{\partial}{\partial t}n(v,t)_{\mathrm{coag}} = \frac{1}{2}\int_0^v \beta(u,v-u)n(u,t)n(v-u,t)\mathrm{d}u - n(v,t)\int_0^\infty \beta(u,v)n(u,t)\mathrm{d}u. \qquad (4.8)$$

The first term on the right hand side of equation (4.8) gives the increase of particles of the size v due to coagulation between particles of the volume $u(u \leq v)$ and particles of the volume $v-u$. Because of the integration over all volumes and the symmetry of the coagulation kernel the particles are counted twice, therefore the factor 1/2 is introduced. The second term on the right hand side gives the decrease of particles with volume v due to coagulation between particles of volume v and particles of volume u. The coagulation kernel depends on the size of the particles. Due to the complexity of the governing equation for particles undergoing coagulation a general analytic solution of the problem is not known.

To solve equation (4.8) analytically, three regimes of particles sizes have to be considered separately. These regimes are determined by the Knudsen number Kn, which is the ratio of the mean free path λ of an atom in the gas and the radius of the particles. For a Knudsen number less than 0.1, which obtains for particles with a radius larger than 1μm and $\lambda = 0.065\mu$m for air at 20°C, the regime is called the continuum regime or the continuum flow [71, chap 4], [63, Kap.7]. A Knudsen number less than 0.1 means that the particles are large compared to the mean free path. For a Knudsen number larger than 10, which obtains for particle radii less than 6.5nm, one has the free molecular regime. In this regime the particles can be treated as molecules due to their small size, and they travel in free unlimited flight between two collisions. The regime between the continuum regime and the free molecule regime is called slip regime ($0.1 < Kn < 10$). Measurements have shown that Knudsen numbers of particles of smoke lie in the lower part of the slip regime close to the continuum regime. The approaches for the different regimes are based on different coagulation kernels β.

Continuum regime

In the continuum regime the coagulation kernel $\beta(u,v)$ in equation (4.8) is given as [20], [32]

$$\beta(u,v) = K_c(u^{1/3}+v^{1/3})\left(\frac{1}{u^{1/3}}+\frac{1}{v^{1/3}}\right) \tag{4.9}$$

with $K_c = 2kT/(3\mu)$.

Slip regime

In the slip regime the radii of the particles are in the dimension of the mean free path length of the gas atoms. To solve the GDE in this regime usually a coagulation kernel is used which is equal to the coagulation kernel of the continuum regime corrected by a correction factor C. The collision of small particles ($r < 1\mu$m) with gas atoms affects the movement of the particles. This interference is considered by the correction factor also called the Cunningham or slip factor. The Cunningham factor is given by [20, chap 3] [71, Chap 2.6]

$$C = 1 + A_1 Kn + A_2 Kn \exp\left(\frac{A_3}{Kn}\right)$$

and is dependent on the particle size due to the Knudsen number. A_i are experimental determined constants which are given in the literature as $A_1 = 1.257$, $A_2 = 0.4$ and $A_3 = 1.1$. For $Kn < 5$ the Cunningham factor can be approximated with [71, Chap 4.2.2]

$$C = 1 + AKn$$

with $A = 1.591$. The coagulation kernel for the slip regime is given as

$$\beta(u,v) = K_c(u^{1/3}+v^{1/3})\left(\frac{C(u)}{u^{1/3}}+\frac{C(v)}{v^{1/3}}\right). \tag{4.10}$$

The Cunningham factor C is a function of the particle volume because of the particle size dependent Knudsennumber in the definition of the Cunningham factor (4.2).

There exist different methods to solve this GDE for coagulation in the different regimes.

4.2.1 Analytic Solution of the GDE in the Continuum Regime

One method to solve the GDE is the moments method [32] [63]. In the following it is described how the GDE for coagulation can be expressed in terms of the moments of the particle size distribution. A more detailed solution of solving the GDE in the continuum regime using the moments method is given in the appendix C.

The k-th order moment of a volume distribution is given by

$$M_k = \int_0^\infty v^k n(v,t)\mathrm{d}v.$$

Some of the moments have physical meanings. The zeroth order moment

$$M_0 = \int_0^\infty n(v,t)\mathrm{d}v$$

gives the total number of particles at a given place and a given time. The first order Moment

$$M_1 = \int_0^\infty vn(v,t)\mathrm{d}v$$

gives the total volume of particles. The mean particle volume is given by the quotient of the first order moment M_1 and the zeroth order moment M_0. Some non whole-numbered moments also have physical meanings. The Quotient of the $1/3$-rd order moment and the zeroth order moment is proportional to the particle radius.
By multiplying equation (4.8) with v^k and integrating from $v = 0$ to $v = \infty$ we get the GDE for coagulation in its momentum form

$$\frac{\mathrm{d}}{\mathrm{d}t}M_k(t) = \frac{1}{2}\int_0^\infty \int_0^\infty [(u+w)^k - w^k - u^k]\beta(u,w)n(u,t)n(w,t)\mathrm{d}w\mathrm{d}u, \tag{4.11}$$

with $w = u - v$. For $k = 0$ and $k = 1$ equation (4.11) is reduced to

$$\frac{\mathrm{d}}{\mathrm{d}t}M_0(t) = -\frac{1}{2}\int_0^\infty \int_0^\infty \beta(u,w)n(u,t)n(w,t)\mathrm{d}w\mathrm{d}u \tag{4.12}$$

and

$$\frac{\mathrm{d}}{\mathrm{d}t}M_1(t) = \frac{1}{2}\int_0^\infty \int_0^\infty [u+w-w-u]\beta(u,w)n(u,t)n(w,t)\mathrm{d}w\mathrm{d}u = 0 \tag{4.13}$$

Equation (4.13) shows that there is no change in the total particle volume due to coagulation. This is obvious because the coagulation effects the size of the single particles but not the amount of material in the aerosol. For a solution in the continuum regime the coagulation kernel described in equation (4.9) is used. So equation (4.12) becomes

$$\frac{\mathrm{d}}{\mathrm{d}t}M_0(t) = -\frac{1}{2}K_\mathrm{c}\int_0^\infty \int_0^\infty (u^{1/3}+w^{1/3})\left(\frac{1}{u^{1/3}}+\frac{1}{w^{1/3}}\right)n(u,t)n(w,t)\mathrm{d}w\mathrm{d}u. \tag{4.14}$$

The moments of the log-normal distribution are

$$M_k = N_0 v_\mathrm{g}^k \exp\left(\frac{9}{2}\ln^2\sigma_\mathrm{r}\right). \tag{4.15}$$

With this equation and the assumptions that the particles sizes stay log-normally distributed during coagulation and $\ln(\sigma_\mathrm{r}(t)) \approx \ln(\sigma_\mathrm{r}(0))$ an analytical solution of the change of the particle number during coagulation can be derived [32]

$$\frac{N(t)}{N_0} = \frac{1}{1+[1+\exp(\ln^2\sigma_{\mathrm{r},0})]\cdot K_\mathrm{c}N_0 t}, \tag{4.16}$$

with the initial values $N(0) = N_0$ and $\ln \sigma_r(0) = \ln \sigma_{r,0}$. A comparison with Smoluchowski's solution (equation (4.7)) shows that this is a special case of the analytic solution in the continuum regime for a standard deviation of zero.
Furthermore, Lee gives a solution for the change of the geometric mean particle volume [32]

$$\frac{v_g(t)}{v_{g,0}} = \frac{\exp(9\ln^2(\sigma_{r,0})/2) \cdot [1 + \{1 + \exp(\ln^2 \sigma_{r,0})\} K_c N_0 t]^{3/2}}{[2 \cdot (1 + \{1 + \exp(\ln^2 \sigma_{r,0})\} K_c N_0 t) + \exp(9\ln^2 \sigma_{r,0}) - 2]^{(1/2)}}, \tag{4.17}$$

with $v_{g,0} = v(0)$ the initial geometric mean particle volume for the lognormal distribution. It is assumed that the particles stay log-normally distributed but the geometric standard deviation of the size distribution changes due to coagulation. Lee also gave a solution for the geometric standard deviation

$$\ln \sigma_r(t) = \frac{1}{9} \ln \left(2 + \frac{\exp(9\ln^2 \sigma_{r,0}) - 2}{1 + [1 + \exp(\ln^2 \sigma_{r,0})] K_c N_0 t} \right). \tag{4.18}$$

In can be seen that the extent of coagulation depends on the standard deviation of the distribution. The greater the polydispersity of the aerosol, the higher is the decrease of particles due to coagulation.

4.2.2 Similarity Solution of the GDE in the Continuum Regime

Another solution for the GDE in the continuum regime is given by Friedlander [20, chap 11]. The similarity solution supposes that the volume distribution reaches a form which is independent of the initial distribution after a sufficiently long period of time. This is known as the so called self-preserving distribution. After an adequate while the time rate of change of the volume distribution can be written as

$$\frac{dN(t)}{dt} = -K_c(1 + ab)N(t)^2. \tag{4.19}$$

The solution of this equation is given by

$$N(t) = \frac{N_0}{1 + abK_c N_0 t}. \tag{4.20}$$

For the product *ab* Friedlander gives a value of 1.05. For $ab = 2$ Friedlander's solution would be the same Smoluchowski's (4.7). Due to the fact that the product *ab* is a constant the decrease of the number of particles does not depends on the deviation of the distribution as seen in the moments method before. The time to reach the self preserving distribution in the continuum regime can be calculated as follows [20, chap 7]

$$\tau_{spd} = 13(K_c N_0)^{-1}. \tag{4.21}$$

4.2.3 Analytical Solution of the GDE in Slip Regime

The moments method can also be used in the slip regime to solve the GDE for coagulation. The detailed solution is given in appendix C.
In the slip regime the momentum form of the GDE for $k = 0$ is given as [33]

$$\frac{\mathrm{d}}{\mathrm{d}t}M_0(t) = -\frac{1}{2}K_\mathrm{c}\int_0^\infty\int_0^\infty (u^{1/3}+w^{1/3})\left(\frac{C(v)}{u^{1/3}}+\frac{C(w)}{w^{1/3}}\right)n(u,t)n(w,t)\mathrm{d}w\mathrm{d}u, \tag{4.22}$$

with the coagulation kernel for the slip regime (4.10) and the cunningham factor in its approximated form (4.2). The solution for the change in the particle size distribution can only be given in an intrinsic from [33].
A dimensionless time $t^{'}$ is introduced which depends on the relation between the particle number concentration before and after coagulation.

$$\begin{aligned} t^{'} = K_\mathrm{c}N_0 t &= \frac{3}{a}\left[\frac{1}{3}\left\{\left(\frac{N}{N_0}\right)^{-1}-1\right\}-\left(\frac{b}{2a}\right)\left\{\left(\frac{N}{N_0}\right)^{(-2/3)}-1\right\}\right. \\ &+ \left(\frac{b}{a}\right)^2\left\{\left(\frac{N}{N_0}\right)^{(-1/3)}-1\right\} \\ &- \left.\left(\frac{b}{a}\right)^3\ln\left\{\frac{1+(b/a)(\frac{N}{N_0})^{(1/3)}}{(1+(b/a))(\frac{N}{N_0})^{(1/3)}}\right\}\right] \end{aligned} \tag{4.23}$$

$$\begin{aligned} a &= 1+\exp(\ln^2\sigma_{\mathrm{r},0}) \\ b &= AKn_0\left\{\exp\left(\frac{1}{2}\ln^2\sigma_{\mathrm{r},0}\right)+\exp\left(\frac{5}{2}\ln^2\sigma_{\mathrm{r},0}\right)\right\} \\ c &= \frac{a+b\exp(-3\ln^2\sigma_{\mathrm{r},0})(N/N_0)^{1/3}}{a+b(N/N_0)^{1/3}} \end{aligned}$$

where Kn_0 is the initial Knudsen number. The time $t^{'}$ gives a measure for the duration of a decrease of the particle number concentration due to coagulation. Also the geometric standard deviation and the geometric mean particle volume are given as a function of the ratio of the particle number concentrations. The time dependent geometric standard deviation is given as

$$\ln^2\sigma = \frac{1}{9}\ln\left[2c+\left(\frac{N}{N_0}\right)\{\exp(9\ln^2\sigma_{\mathrm{r},0})-2c\}\right]. \tag{4.24}$$

The geometric mean particle volume can be obtained as follows

$$\frac{v_\mathrm{g}}{v_{\mathrm{g},0}} = \frac{\exp((9/2)\ln^2\sigma_{\mathrm{r},0})(N/N_0)^{-1}}{[2c+(N/N_0)\{\exp(9\ln^2\sigma_{\mathrm{r},0})-2c\}]^{1/2}}. \tag{4.25}$$

With the solutions of Lee [32], [33] and Friedlander [20] the influence of the coagulation on the particle size distribution can be calculated for particles in the low Knudsen number regime, where N_0, $v_{g,0}$ and $\ln\sigma_{r,0}$ are the initial values for the particle number concentration, the geometric mean particle volume and the geometric standard deviation. The effect of coagulation for large Knudsen numbers is not of interest for the following simulations. Therefore the solution of the GDE for this regime is not mentioned here. However, a derivation can be found in the literature [71], [63].

4.2.4 Results of Particle Simulation with the Different Methods

To compare the described methods of solving the GDE for coagulation and to find out which one is suitable for the intended application, the solution in the slip regime and the two solutions for the continuum regime are implemented in the coagulation of the particulate smoke parameters. For all three methods the geometric mean particle volumes and the standard deviations can be calculated directly. For the two methods in the continuum regime the particle number concentration can also be calculated directly, while for the solution in the slip regime the particle number concentration is only given in an intrinsic way. In this case the time t' has first to be calculated for different relations of the particle number concentrations (see equation (4.24)). Then the time t' has to be compared with the fire simulation results to get the value of the particle number concentration.
The rate of coagulation depends apart from other parameters on the temperature and the number of particles. The coagulation will mainly occur in the area near the fire, but the results of the fire simulation are computed for a place at a distance from the fire, according to the EN54 standard. Therefore a factor for the coagulation rate is introduced which shall adjust these differences due to the simulation position. The value of the factor depends on the distance and the type of fire experiment that is simulated. The probability that a particle has collided with another particle also depends on the age of the particles. The longer a particle exists the higher is the probability that it has collided with other particles [18]. Therefore a modification of the fire model had to be made, and due to this modification it is possible to simulate the age of a particle assuming that it has arisen from the surface of the flame and that it is transported by the thermal flow stream. The simulation shows that the calculation of the particle number concentration using the method for the slip regime with a value of $A = 1.591$, taken from the literature [33], is too low by a factor of $2 \cdot 10^2$. When the value for A is reduced by the factor of 10 to $A = 0.1591$ the results for the calculation in the slip regime and in the continuum regime are nearly the same. Figure 4.3 shows the particle number concentration calculated with the three methods, the moments method in the slip regime, the moments method in the continuum regime and the similarity solution of the GDE. The initial particle number concentration without coagulation is also shown. It can be seen that

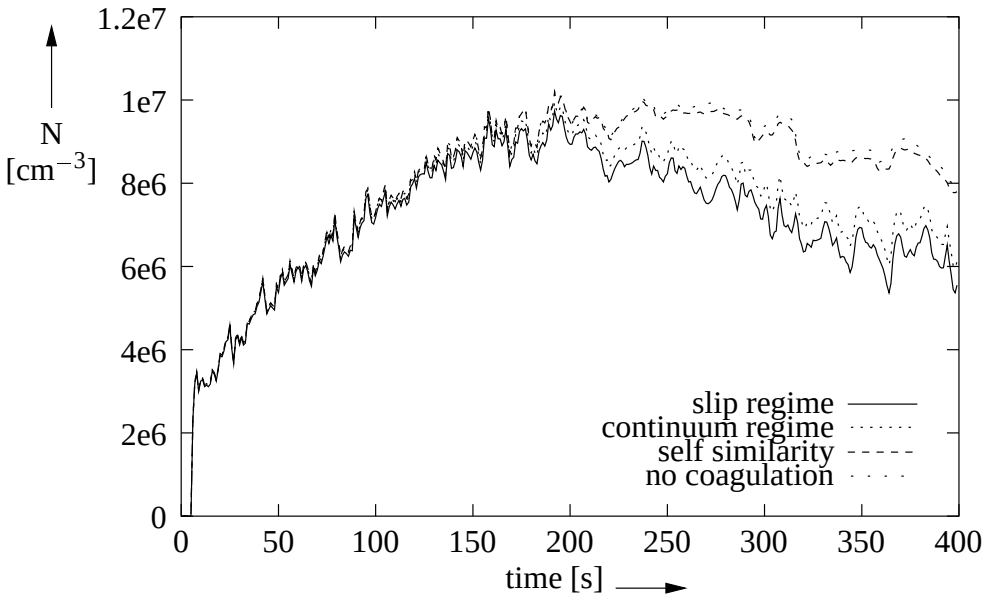

Figure 4.3: Simulated particle number concentration considering the effect of coagulation

the results for the moments method in the slip regime (with $A = 0.1591$) and in the continuum regime are nearly the same. Due to the coagulation the number of particles decreases after the fire burned out after 180s. Using the similarity solution to calculate the particle number concentration the coagulation has nearly no effect compared to the initial particle number concentration. With the self similarity solution a constant coagulation kernel is used. With this kernel the rate of coagulation is constant and is not affected by the temperature nor the particle size distribution as in the moments method and has thus not such a large influence on the results.

Similar results can be achieved for the geometric mean particle diameter (figure 4.4). The results of the calculations following the moments methods are very similar whereas the increase of the diameter due to the coagulation is higher by the calculation for the slip regime ($A = 0.1591$). For the self similarity solution the diameter is nearly constant. For the following simulations the analytic solution of the GDE in the continuum regime has been chosen.

4.3 Removal of Particles from the Aerosol

In the following it is assumed that only the removal operates on the particles of an aerosol. There are different effects that can remove particles from the aerosol [20], e.g. gravitational settling, Coulomb forces and van der Waals forces. The physical reason for the removal is not determined in detail in this case, it is only assumed that the removal depends on the size of the particles. In this case the GDE (4.3) can be solved analytically and the size distribution

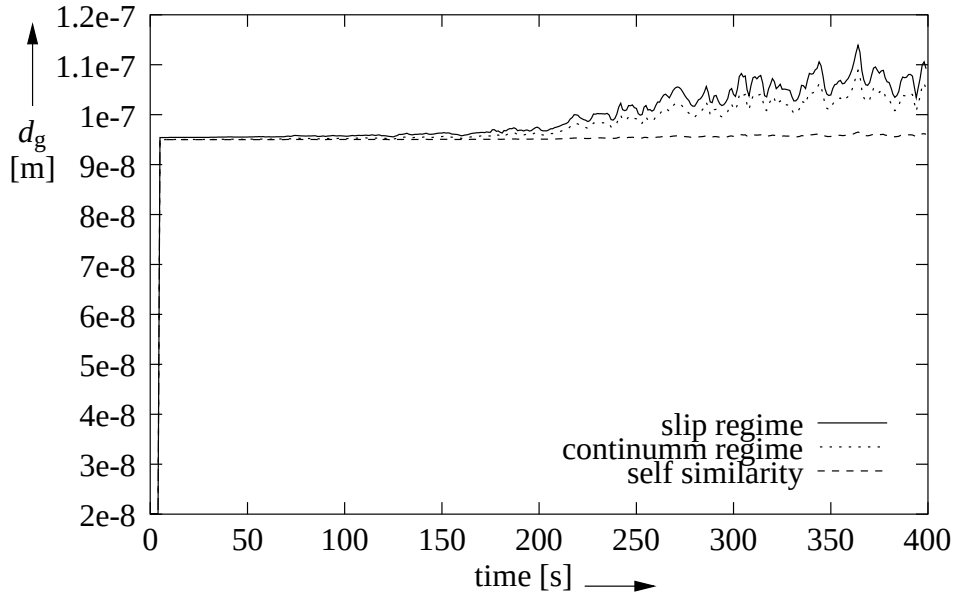

Figure 4.4: Simulated geometric mean diameter considering the effect of coagulation

is given by the following equation [4]

$$n(v,t) = n_0(v,t) \cdot \exp(R(v,t) \cdot t),$$

with $R(v,t) = R_m(t) \cdot v^m$ the removal rate. The numerical value for m depends on the mechanisms of removal. For gravitational settling m is equal to $2/3$.
The moments of this modified size distribution are given by

$$\begin{aligned} M_k &= \int_0^\infty v^k n_0(v,t) \exp(R(v,t) \cdot t) \mathrm{d}v \\ &= \int_0^\infty v^k n_0(v,t) \exp(R_m v^m t) \mathrm{d}v. \end{aligned} \tag{4.26}$$

To obtain the particle number concentration after the removal of particles from the aerosol the zeroth order moment has to be solved

$$M_0 = \int_0^\infty n_0(v,t) \exp(R_m v^m t) \mathrm{d}v. \tag{4.27}$$

$n_0(v,t)$ is the initial size distribution before the removal of particles occur

$$n_0(v,t) = \frac{N_0}{3\sqrt{2\pi} \cdot \ln(\sigma_r) v} \exp\left(\frac{\ln^2(v/v_{g,0})}{18 \ln^2 \sigma_r}\right)$$

So equation (4.27) becomes

$$M_0 = \frac{N_0}{3\sqrt{2\pi} \cdot \ln(\sigma_r)} \int_0^\infty \frac{1}{v} \exp\left(\frac{\ln^2(v/v_g)}{18 \ln^2 \sigma_r}\right) \exp(R_m v^m t) \mathrm{d}v. \tag{4.28}$$

The integral in equation (4.28) can be evaluated numerically by quadrature. The zeroth moment corresponds the total volume of the particles, which is the basis for calculating the particle number concentration.

4.4 Results of Smoke Simulation

To verify the results of the smoke simulation the simulated particle number concentration and geometric mean diameter are compared with measured values. Two standardized testfires [13] were chosen for the comparison, an n-heptane testfire (TF5) as an example for open flame fires and a smoldering cotton wick fire (TF3) as an example for smoldering fires. A description of these fires can be found in appendix D. For the simulation of the cotton wick fire with the FDS program an approximation has to be made. Following the setup procedure for testfire TF3, 90 cotton wicks are mounted on a bracket and are ignited in a way that they smolder without open flames. Of course it is not possible to model every single cotton wick with the FDS, the grid cells would be far too small, so for simulation purposes the cotton wicks are replaced by an obstacle which builds a chimney as the cotton wicks do. The material and combustion properties of this chimney are adjusted to the cotton wicks [70]. The measurement results of the particle number concentration and the geometric mean diameter were taken at the fire detection laboratory at the University Duisburg-Essen [40], using the Electrical Aerosol Spectrometer [65] of Tartu University. The environmental parameters for the simulation of both testfires where chosen with respect to the parameters of the fire detection laboratory experiments.

4.4.1 Simulation Results of the Particle Number Concentration

First the simulation results of the particle number concentration need to be verified. For the simulation only the coagulation is implemented, not the removal of particles from the aerosol. To compare the results not only qualitatively but also quantitatively two quality criteria are introduced. The first criterion q_1 appraises the absolute magnitude of the signals, it is the relative difference between the maximum amplitudes related to one of the maxima

$$q_1 = \frac{|\max(S_1(t)) - \max(S_2(t))|}{\max(S_1(t))}, \tag{4.29}$$

where $S_1(t)$ and $S_2(t)$ are the compared signals. For an early fire detection the beginning phase of the fire is of interest. Therefore the second criterion q_2 appraises the beginning phase of the signal by giving the mean gradient of the signal. For the particle number concentration this value gives the change of the particle number concentration per unit time. Figure 4.5 shows the simulated and the measured particle number concentration for an n-

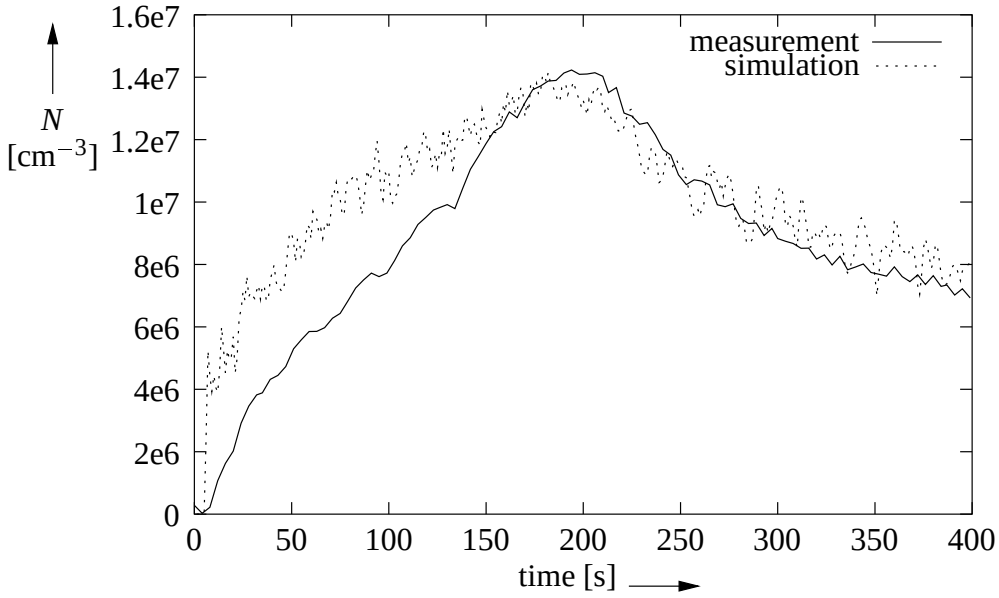

Figure 4.5: Simulated and measured particle number concentration for an n-heptane fire

heptane fire. It can be seen that the amplitude can be simulated very exactly ($q1 = 0.03$). Comparing particle number concentrations measured during two n-heptane fire experiments, the value for the relative difference is $q_{1,\mathrm{m}} = 0.23$ (figure 4.6).

The simulated particle number concentration has a sudden increase at the beginning of the fire but reaches the maximum at the same time as the measured one does. Due to this increase of the signal the mean gradient of the simulated particle number concentration $q_{2,\mathrm{s}} = 371\mathrm{cm}^{-3}\mathrm{s}^{-1}$ is smaller than the mean gradient of the measured one $q_{2,\mathrm{m}} = 1421\mathrm{cm}^{-3}\mathrm{s}^{-1}$. The relation between the two gradients is $\Delta q_2 = 0.26$, where a value of 1 would be the optimum case. This shows that the simulation of the beginning phase of the fire is not very exact. The comparison of two measured particle number concentrations (see figure 4.6) gives a relation of $\Delta q_2 = 0.97$ for the mean gradients.

The sudden increase can be explained by the fact that in the case of liquid fires, like n-heptane, the whole surface starts burning at the moment the liquid is ignited. This means that the generation of smoke and heat starts very quickly and also the thermal flow velocity increases rapidly. Therefore the smoke suddenly arises in form of a cloud which reaches the measurement position after a short delay of time. The slower decrease of the measured particle number concentration is assumed to be caused by the measuring procedure. At the measurement the smoke is sucked through a tube, diluted by clean air and then supplied to the measurement apparatus [66]. During this process a certain amount of particles will deposit in the tube and there also may be other effects that influence the measurement results. In this way the measurement apparatus acts like a lowpass filter on the particle size

distribution like the housing of a sensor does [22]. In the simulation of the fire the smoke mass density, from which the particle number concentration is calculated, is computed at a chosen position inside the enclosure. No effect of any measurement equipment or housing is considered. All influences of the sensor housing are considered later by the sensor model. Comparing the simulated and the measured particle number concentration with a visual observation of an n-heptane fire experiment the simulated signal seems to correspond better to the experiment than the measured one. A similar effect can be observed for other simulation and measurement results, e.g. the temperature.

Figure 4.7 shows the simulation and measurement results for a cotton wick fire. For this fire

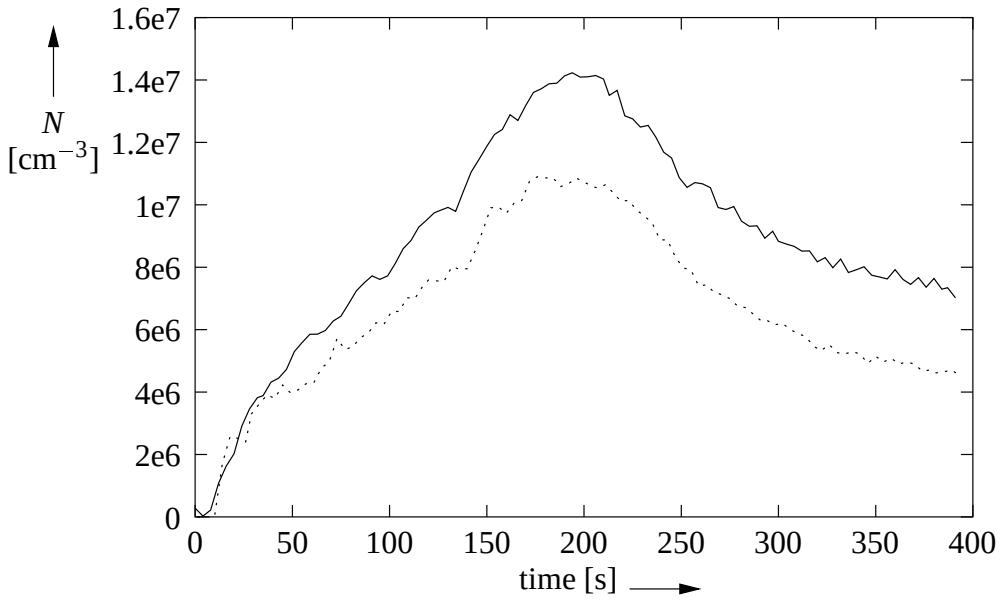

Figure 4.6: Particle number concentrations measured at two n-heptane fire experiments

the gradient of the simulated particle number concentration is given by $q_{2,\mathrm{s}} = 13.67\mathrm{cm}^{-3}\mathrm{s}^{-1}$ and by $q_{2,\mathrm{m}} = 61.42\mathrm{cm}^{-3}\mathrm{s}^{-1}$ for the measured one. The relation between the gradient is given by $\Delta q_2 = 0.34$. Due to the lower thermal flow and the slower rising of smoke there is no sudden increase at the beginning of the simulation. It can also be seen that the amount of produced smoke is smaller than for the n-heptane fire. Because of the long duration of the smoldering fire and the steady increase of the smoke density there is no explicit maximum of the particle number concentration during the measuring period. The relation of the mean gradient of two measured particle number concentrations gives a value of $\Delta q_2 = 0.69$. This shows that the repeatability of a cotton wick fire is worse than the one of an n-heptane fire. Due to low thermal flow the smoke plume of this fire can easily be deviated by an ambient flow stream in the laboratory. In addition the amount of produced smoke strongly depends on the humidity of the cotton wicks, which also effects the measurement results.

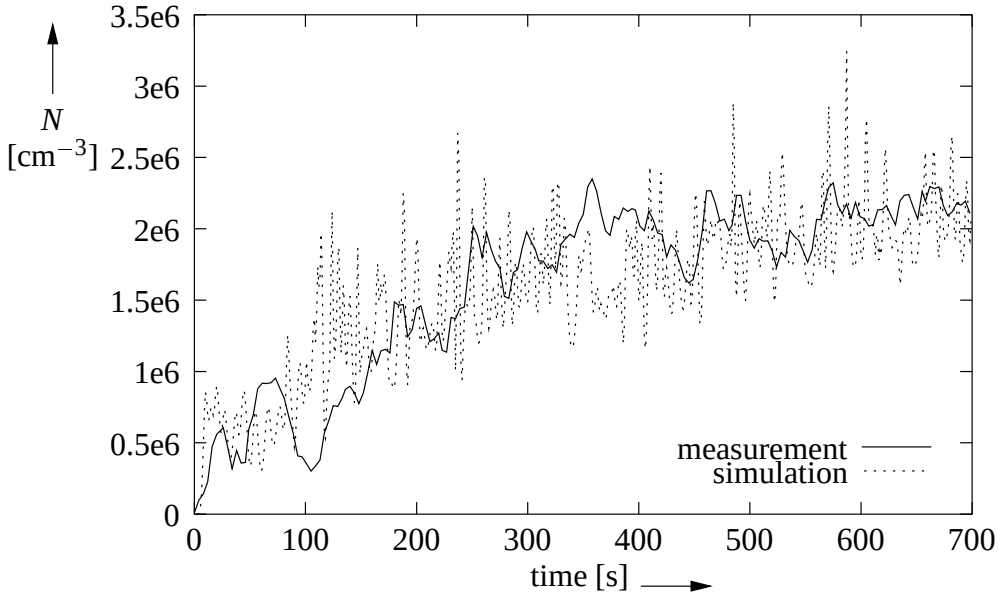

Figure 4.7: Simulated and measured particle number concentration for a cotton wick fire

4.4.2 Simulation Results of the Geometric Mean Diameter

Figure 4.8 shows that the simulation of the geometric mean diameter for n-heptane fires gives reasonable results. For the measured as well as for the simulated geometric mean particle diameter there is a sudden increase at the beginning of the fire. After the fire burned out both diameters start to increase. This is caused by the fact that the particles become larger due to coagulation, but no new smaller smoke particles are produced. In the case of the cotton wick fire (figure 4.9) the measured diameter increases slowly while the simulated diameter has a sudden increase, but after this starting phase the simulation gives reasonable results. The comparison of results of the simulations as well as of the measurements shows, that the effect of coagulation on the particle diameter is slightly stronger for the n-heptane fire than for the cotton wick fire. This is justified by the higher temperature and the higher particle number produced by the n-heptane fire.

4.5 Evaluation of the Simulation Method

The results presented in this chapter show, that the simulation method gives the opportunity to simulate the evolution of the number concentration and the geometric mean diameter of smoke particles during a fire, whereby the simulation is not influenced by any kind of measurement equipment. The simulation takes coagulation into account. Comparing the two fire experiments chosen for the verification of the method, it can be seen that the magnitude of an n-heptane fire can be simulated in good correlation to measurement results. With a cotton

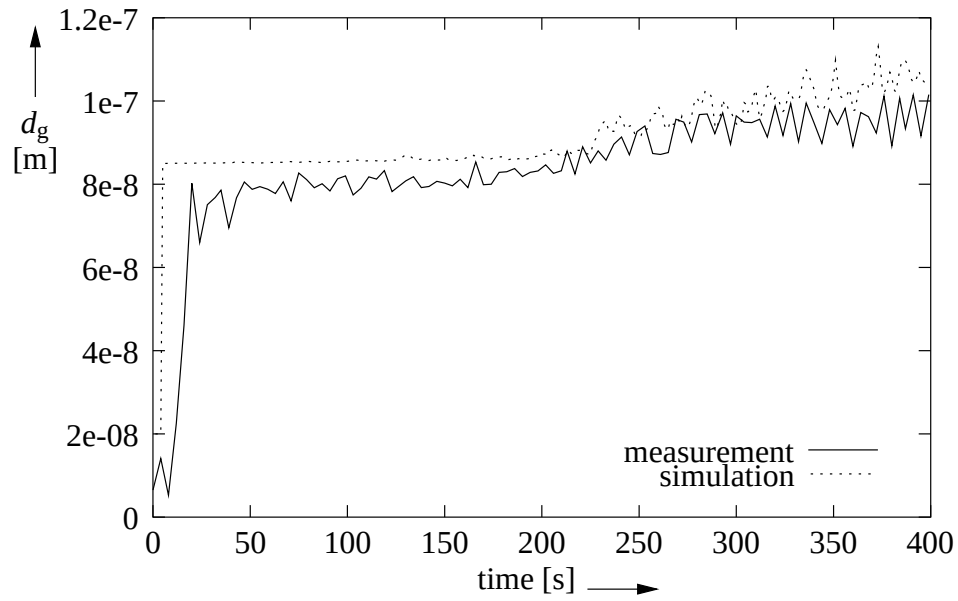

Figure 4.8: Simulated and measured geometric mean particle diameter for an n-heptane fire

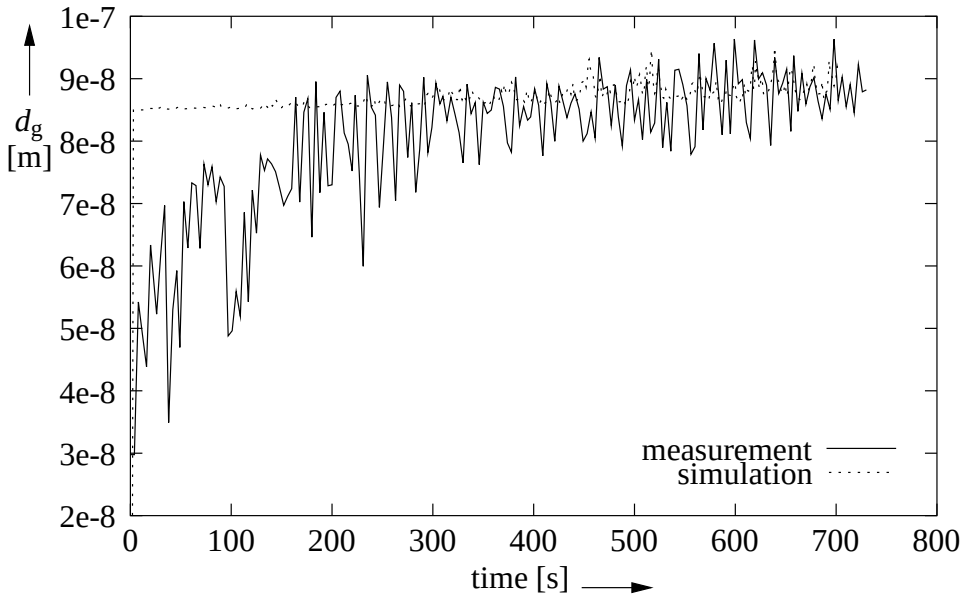

Figure 4.9: Simulated and measured geometric mean particle diameter for a cotton wick fire

wick fire the increase of the particle number concentration can be simulated more exactly than in the case of the n-heptane fire. A disadvantage of the described simulation method is that the geometric mean diameter cannot be derived from the fire simulation. Equation (4.2) shows that for calculating the initial particle number concentration the geometric mean volume and thus the geometric mean diameter have to be known. Merely the evolution of the geometric mean diameter due to the coagulation of smoke particles can be simulated.

5 The Interface between Fire Model and Sensor Model

As mentioned before the input parameters for the smoke sensor model are to be taken from the results of the fire simulation. In the following signals of an extinction light sensor, a scattered light sensor and an ionization chamber are simulated and investigated. Table 4.1 on page 29 shows the input parameters for the sensor models, of which the fraction of carbon in the smoke is only necessary for the two optical sensors. The fraction of carbon cannot be simulated so far, but the other parameters can be received from the fire simulation combined with the simulation of the coagulation of the smoke described in chapter 4. Again the n-heptane fire and the cotton wick fire are used for the verification of the simulation results. For the discussion of the simulation results three types of sensor signals are compared.

- measured sensor signals S_m
  These signals are measured during fire experiments in the fire detection laboratory at the University Duisburg-Essen.
- sensor simulated signals S_s
  The signals are simulated with the described sensor model, using measured input signals from the same fire experiments.
- over-all simulated signals S_o
  The signals are also simulated with the described sensor model. The input signals for the sensor model are simulated as far as possible, i.e. particle number concentration, geometric mean particle diameter, standard deviation of the particle size distribution, the flow velocity and the temperature.

The indices (m, s, o) for the measured signals, the sensor simulated signals and the over-all simulated signals are used for all the following evaluations. These three signals are chosen to verify which properties of the simulated signals come from the sensor model and which from the fire model.
Before the verification of the model, it has to be pointed out, that different parameters of the sensor model can not be measured or taken from existing literature. These values have been ascertained by Gockel by comparing simulation results with measured signals. Therefore the sensor model is adjusted to some extent to the measured signals Gockel has used. For the fire and the sensor simulations a number of parameters have to be chosen. It is important that

these parameters are defined carefully and in the best possible conformity with the existing chemical and physical parameters of the fire experiment.

5.1 Extinction Light Sensor

The measured extinction coefficients are taken from measurements in the fire detection laboratory, the extinction coefficient is measured with the Mirex [14], an extinction light sensor used for reference measurements during the test fire experiments. During the same experiments the input values for the sensor simulation were measured. To compare the fire measurements with the simulation results a constant factor is introduced. This factor represents the gain of the electronic circuits and the sensitivity of the photo diode. Such a correction factor has already been used by Gockel [22] for the verification of the simulation results. The factor stays the same for all test fires.

n-heptane fire:

Figure 5.1 shows the extinction coefficient $\hat{\sigma}_{ext}$ (see equation(2.7)) which is a measure for the extinction of light due to smoke and thereby the smoke concentration. It can be seen that when the fire starts the over-all simulated extinction coefficient $\hat{\sigma}_{ext,o}$ is higher than the one from the sensor simulation $\hat{\sigma}_{ext,s}$ and the measured one $\hat{\sigma}_{ext,m}$. But at about 180s they have reached the same value. This can be explained by the fact, that the extinction coefficient depends strongly on the particle number concentration. Comparing figure 5.1 and figure 4.5 it can be maintained that the simulated extinction coefficient $\hat{\sigma}_{ext,s}$ has nearly the same progression as the particle number concentration. The reason for the differences between the measured and simulated particle number concentration has already been explained in chapter 4.4. It is based on the fact that influences caused by the apparatus for measuring the particle number concentration are not taken into account in the simulation. This is also noticeable in the simulation results of the extinction light sensor, due to the strong dependence of the extinction coefficient on the particle number concentration. However, it shows in the results that the measured extinction coefficient $\hat{\sigma}_{ext,m}$ increases with a higher gradient in the starting phase of the fire than the sensor simulated extinction coefficient $\hat{\sigma}_{ext,s}$, but not as strong as the over all simulated one $\hat{\sigma}_{ext,o}$. After the fire burned out (200s) the extinction coefficients decrease for all three signals. In contrast to the investigated smoldering fire liquid fires go out more quickly. From this moment on no smoke is produced and the thermal flow stream stops off suddenly. Different measurements in the fire detection laboratory have shown that the measuring results for the extinction coefficient using the Mirex show a high reproducibility.

cotton wick fire:

The dependence of the extinction coefficient on the particle number concentration is the

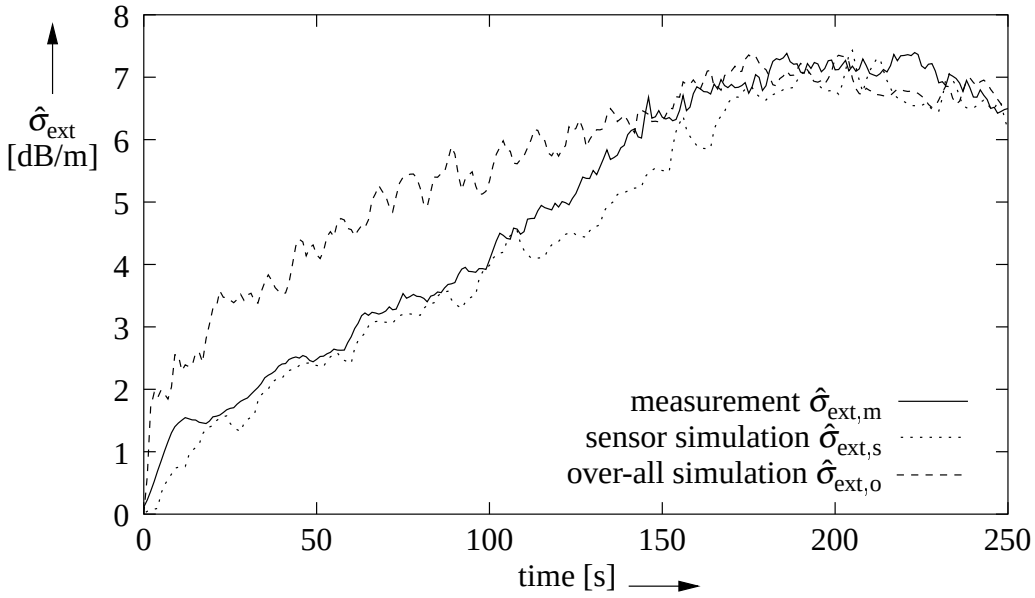

Figure 5.1: Assessed extinction coefficient n-heptane fire

same as in the case of the cotton wick fire (see figure 5.2 and figure 4.7). All three signals in figure 5.2 show a strong fluctuation. Due to the low thermal flow there is no constant smoke stream as with the n-heptane fire. During the monitored time period the measured extinction coefficient $\hat{\sigma}_{ext,m}$ is smaller than the simulated one ($\hat{\sigma}_{ext,o}$, $\hat{\sigma}_{ext,s}$). Gockel also mentions problems with simulating the signals of smoldering fires [22, Kap. 5.5]. He assumes the complex refractive index and the dilution of the aerosol during the measurements to be possible reasons for that. At the start of the fire the difference between the values of the sensor simulated extinction coefficient $\hat{\sigma}_{ext,s}$ and the over-all simulated extinction coefficient $\hat{\sigma}_{ext,o}$ is larger than at the end of the observed time period. At the time when the values approach each other the smoke starts to build a layer of high density close to the ceiling.

5.2 Scattered Light Sensor

The scattered light sensor is more sensitive to small changes in the input parameters than the extinction light sensor, for it measures the intensity of the light that is scattered in a defined direction, which is a very small part of the incoming light. This way even small changes in the particle number or size have strong effects on the sensor signal. On the other hand the extinction light sensor measures the light that passes through the smoke. Only a small part of the emitted light is absorbed or scattered. The measured scattered light signals were obtained with a sensor, which is installed directly under the ceiling of the fire detection laboratory [67, pp. A1-A4]. Inside the housing of this sensor the smoke moves through an optical labyrinth,

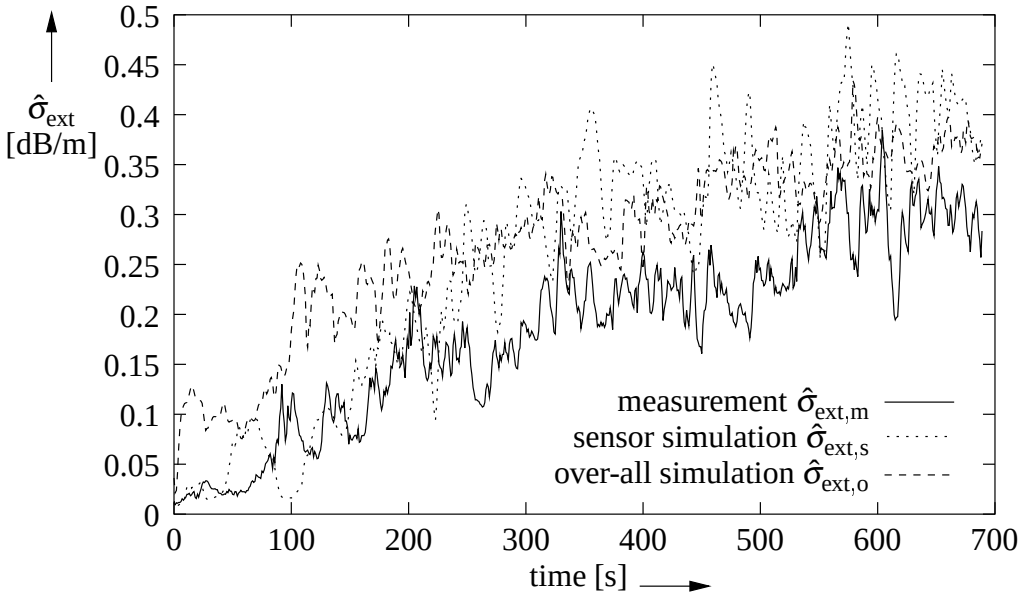

Figure 5.2: Assessed extinction coefficient cotton wick fire

to avoid light from the outside disturbing the measurement. Then the smoke gets into the measurement chamber where an infrared diode emits light in the near infrared region. The light intensity $\hat{I}_s$ scattered under a discrete angle is measured as a value for the amount of smoke inside the measurement chamber. The analog signal of the simulated scattered light sensor is not the intensity of the scattered light. It is a signal, that is proportional to the inverse intensity, therefore the sensor signal has to be converted first. In the following figures the scattered intensity is always related to the intensity of the light that is emitted into the measurement chamber. Therefore, there is no unit given for the scattered intensity.

n-heptane:

Figure 5.3 shows a correlation between the measured intensity $\hat{I}_{s,m}$ and the intensity from the over-all simulation $\hat{I}_{s,o}$ at the very beginning of the fire. Both signals show a sudden increase in the beginning, while the signal of the sensor simulation increases more smoothly. But after a short period of time the over-all simulated intensity $\hat{I}_{s,o}$ starts to increase at a higher degree than the measured one. The difference between the over-all simulated intensity $\hat{I}_{s,o}$ and the sensor simulation $\hat{I}_{s,s}$ can be explained by the measuring procedure for the particle number concentration. At about 180s all signals reach nearly the same value which corresponds to the extinction coefficient. The results show that after the fire burned out (200s) the scattered intensities decrease also and all three signals show good correlations.

cotton wick fire:

The scattered light intensity shows a strong fluctuation, this is also true for the extinction coefficient. At the beginning $\hat{I}_{s,m}$ and the over-all simulated intensity $\hat{I}_{s,o}$ show a good corre-

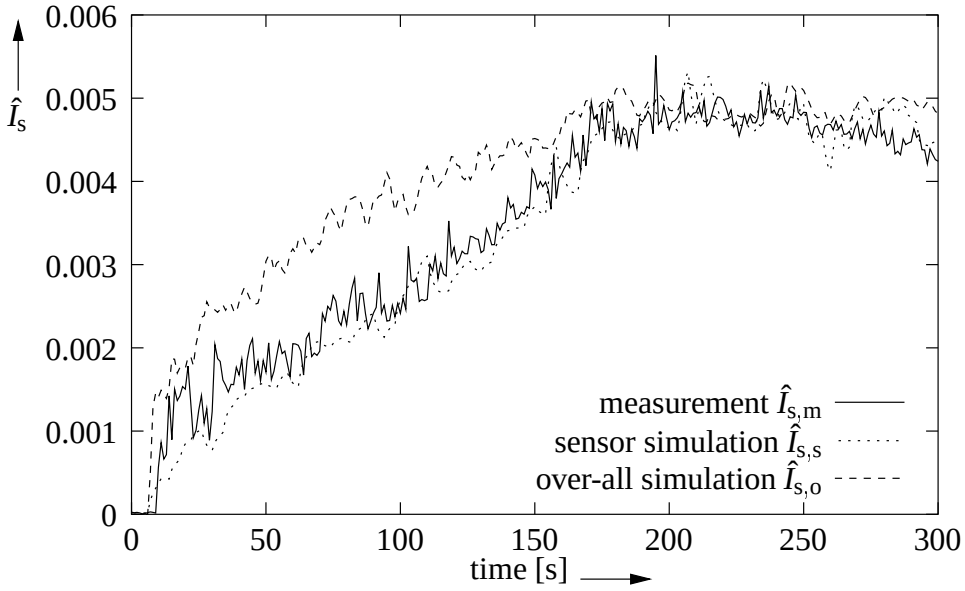

Figure 5.3: Assessed scattered intensity for n-heptane fire

lation, with the passing of time the sensor simulated intensity $\hat{I}_{s,s}$ and the over-all simulated intensity $\hat{I}_{s,o}$ approach each other.

5.3 Ionization Chamber

In addition to the two optical smoke sensor types signals of a smoke sensor using the ionization chamber principle are simulated. The measurement ionization chamber (MIC) [15] used for this task gives the dimensionless smoke density y (equation (2.9)) as a result. By knowing the initial current i_0 the chamber current can be calculated with the characteristic chamber equation (2.8).

n-heptane:

The simulation of the chamber current of a MIC monitoring an n-heptane fire (figure 5.5) gives good results compared to measurements. Especially in the starting phase of the fire. At the beginning of the fire the measured chamber current $\hat{i}_{c,m}$ as well as the over-all simulated chamber current $\hat{i}_{c,o}$ show a sudden increase, while the sensor simulated chamber current $\hat{i}_{c,s}$ decreases more slowly. From the beginning of the fire up to 200 seconds the measured chamber current $\hat{i}_{c,m}$ and the over-all simulated chamber current $\hat{i}_{c,o}$ have nearly the same progression. During this period the over-all simulation gives better results than the sensor simulation. When the fire burns out (200s) the over-all simulated current $\hat{i}_{c,o}$ and the simulated one $\hat{i}_{c,s}$ start to increase, while the measured one stays nearly the same. This could be caused by the measurement procedure of the MIC.

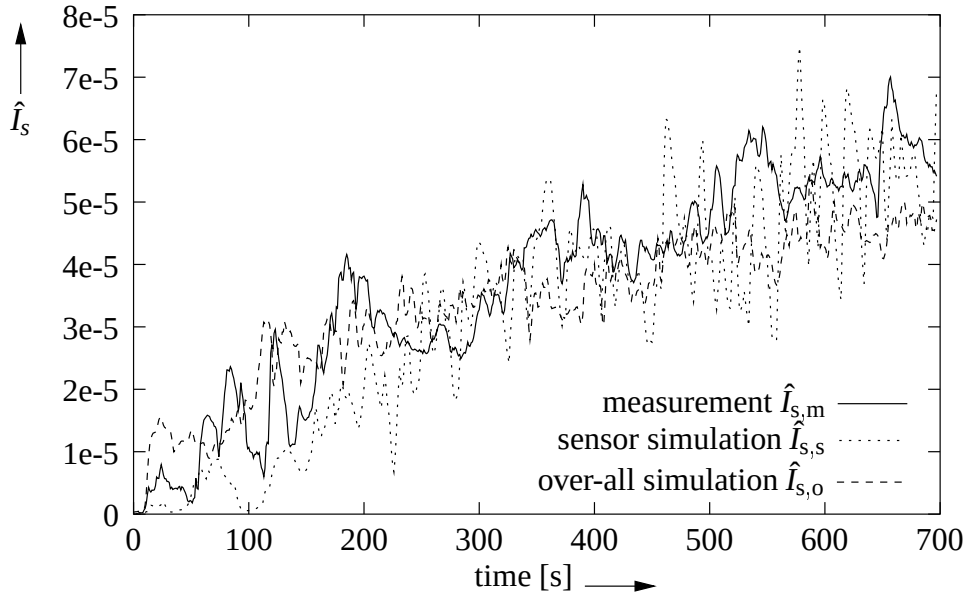

Figure 5.4: Assessed scattered intensity for cotton wick fire

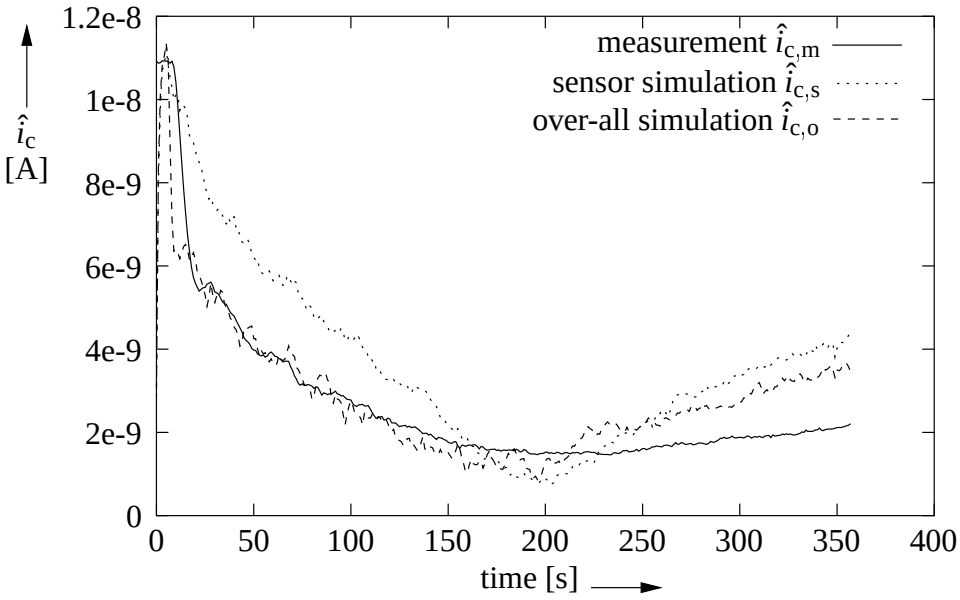

Figure 5.5: Chamber current for n-heptane fire

cotton wick fire:
At the start of the fire the progression of all three signals shown in figure 5.6 is nearly the same. But after about 200s the measured chamber current $\hat{i}_{c,m}$ decreases stronger than the simulated ones ($\hat{i}_{c,s}$, $\hat{i}_{c,o}$). The fluctuation of the measured signal is also stronger than that of the other signals. Measurement results show that the reproducibility of smoke measurements with the MIC during a cotton wick fire experiment is not good. The measuring procedure is very sensitive to changes in the humidity and the temperature of the environment and thus the MIC is more suitable for small particles, while the cotton wick fire produces large particles.

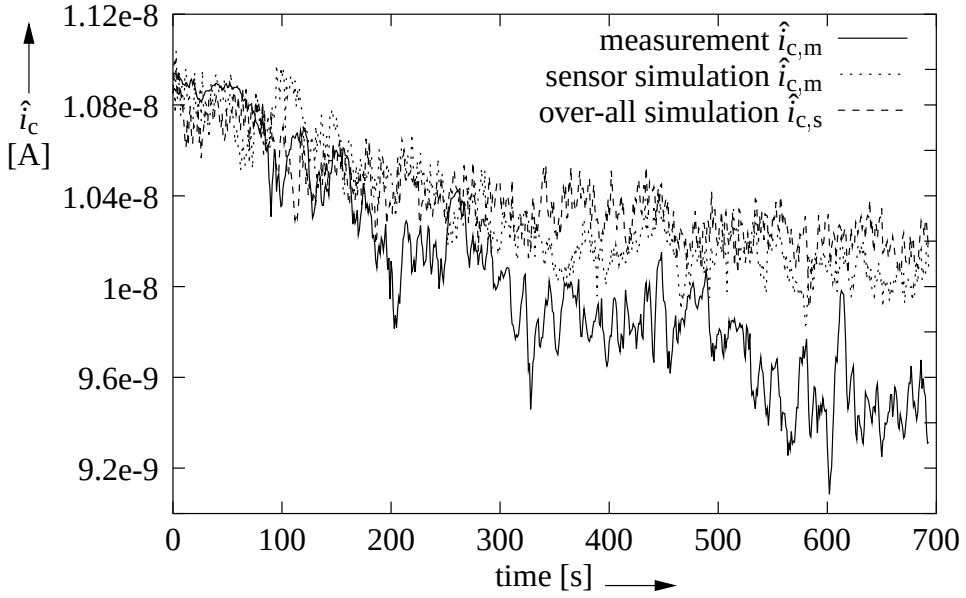

Figure 5.6: Chamber current for cotton wick fire

5.4 Evaluation of the Simulation Results

The simulation results presented in this chapter indicate that it is possible to simulate the smoke evolution during a fire experiment from the fire up to the output signal of a smoke sensor. Using the introduced model the development of the smoke density can be simulated from the fire up to the output signal of different kinds of smoke sensors. The simulations of the three investigated smoke sensors are of different quality. For the simulation of the extinction light sensor the extinction coefficient strongly depends on the particle number concentration. As a consequence one can establish differences in particle number concentrations in the results of the sensor simulation. In the beginning phase of the investigated fires the overall simulated scattered intensity complies with the measurement result more than the simulated extinction coefficient does. The best simulation result is received with the ioniza-

tion chamber. The overall simulated chamber current resembles the measured current more than the sensor simulated one does. The simulation results of the scattered intensity and the chamber current support the assumption that the simulated particle number concentration suits the fire experiment more than the measured one, in case of n-heptane fires. The measured as well as the over-all simulated sensor signals show a sudden increase at the beginning of the fire, and same applies to the simulated particle number concentration.
The comparison of an open flame liquid fire (n-heptane) and a smoldering solid fire (cotton wick fire) has shown that the simulation of the liquid fire is easier to execute and gives better results. The difference between the simulation of the two fires has its origin in the fire simulation part of the model. When the liquid is ignited the whole surface starts to burn at once and when the fire goes out the fire burns out totally in a very short period of time. When using a fuel like n-heptane, a large amount of heat is released and therefore a large thermal flow emerges which transports the smoke continuously. In the case of a smoldering fire the emerge of smoke starts slowly and increases over the time. Due to the low temperature there is only a small thermal flow which can be interfered easily by ambient air streams. The smoke of a smoldering fire consists of highly volatile materials [35], [36]. In the special case of the cotton wick fire an approximation had to be made due to the geometry of the cotton wicks, which are far too small to be modelled separately. Problems with simulating a smoldering fire by means of the sensor model are also mentioned by Gockel [22]. One possible reason for these problems is the complex refractive index of the smoke. A modification of the model [22, chap. 5.5] could solve this problem. But the modification would lead to another variable which is unknown so far and which would have to be determined by further investigations. Another possible reason is the dilution of the aerosol for the measurement. Due to the mentioned highly volatile materials in the smoke a dilution of the smoke with compressed air could lead to smaller particles, which affect the measurement. To confirm these theories further investigations are necessary. But despite these problems the introduced model gives suitable results. Further investigation of the different sensor signals can be found in the following chapter. The good correspondence between some sensor simulated and measured signals may be based on the fact that these measured signals have been used during the development of the sensor model.

6 A Signal Model for Fire Signals

The following chapter presents an application of the developed model. To analyze the signals of a fire sensor the signal model introduced by Klose [30] is used. It is assumed that the sensor signal is a sample function $\{y(n)\}$ of a random process $Y(n)$, which consists of a deterministic lowpass signal $y_{\mathrm{d}}(n)$ and an additive superimposed random process $X(n)$. Thus the fire signal can be described as follows [30], [60]

$$Y(n) = X(n) + y_{\mathrm{d}}(n). \tag{6.1}$$

In the following chapters the signal model is examined using measured and simulated sensor signals from optical smoke sensors. Again the measured signals S_{m} are compared with sensor simulations S_{s} with measured input signals and with over-all simulated signals S_{o}. The deterministic signal part is referred to as deterministic signal, the statistic signal part is referred to as statistic signal. Despite the fact that the fire model as well as the sensor model are deterministic models, Klose's signal model is also used to describe the simulated signals . These are also separated into deterministic signals and statistic signals. The deterministic signal describes the smoke evolution in principle. In case of identical environmental conditions, which are impossible to realize during different fire experiments in the fire detection laboratory, the deterministic signals of different measurements would be the same. The origin of the statistic signal is not clarified. The introduced combined fire and sensor model is used to get information whether the statistic signals have their origin in the fire or in the smoke sensor or in both. The investigation of the statistic signal can give additional information for an early fire detection and thus help to avoid false alarms.

6.1 Extinction Light Sensor

For the investigation of the extinction light sensor, measurements and simulations of the same n-heptane fire, as investigated in chapter 5, are used. Figure 6.1 shows the deterministic extinction coefficient. The deterministic signals are received by lowpass filtering the signal of the extinction light sensor shown in figure 5.1 in chapter 5.1 with a filter of second order. The signals confirm that the sensor simulated extinction coefficient $\hat{\sigma}_{\mathrm{ext,s}}$ yields good results compared to the measured one, while the values of the over-all simulated extinction coefficient $\hat{\sigma}_{\mathrm{ext,o}}$ are higher until the fire burns out. In figure 6.2 the statistic extinction coefficient is shown. It can be seen that the amplitudes of the simulated extinction coeffi-

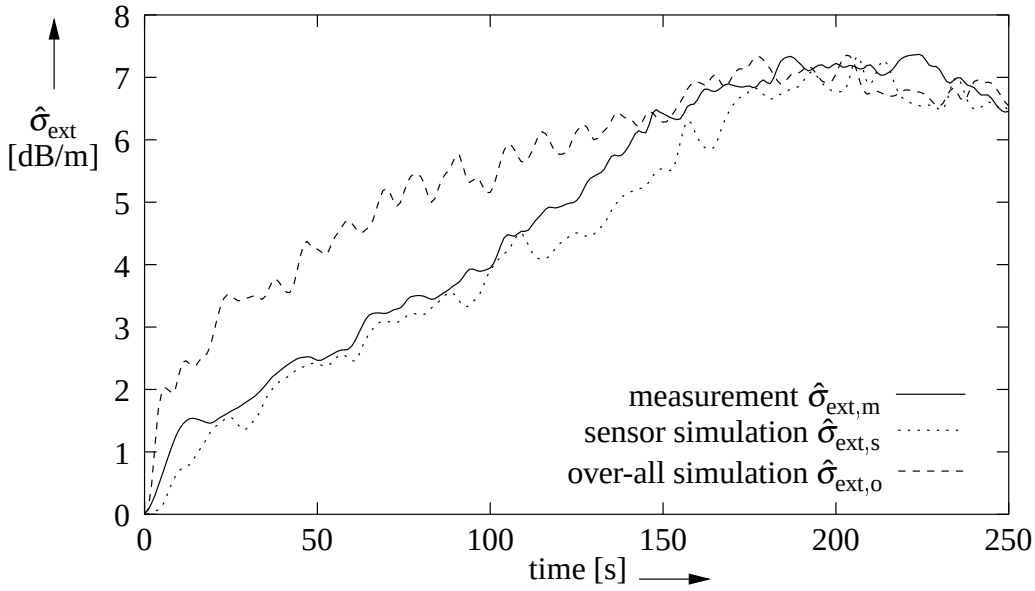

Figure 6.1: Deterministic extinction light sensor for an n-heptane fire

cients, especially of the over-all simulated one $\hat{\sigma}_{ext,o}$, are higher than the one of the measured extinction coefficient. This is also confirmed by figure 6.3, which shows the amplitude distribution of the statistic extinction coefficients. To compare the statistic extinction coefficients quantitatively a variation coefficient is employed, which is defined as follows

$$V = \frac{\sigma^2(X)}{E(X)} \tag{6.2}$$

where $\sigma^2(X)$ is the variance of the statistic signal X and $E(X)$ the expectation value. For the statistic extinction coefficient the variation coefficient of the measurement $V_m = 0.2506$ is the smallest. This can be explained as follows. The determination of the extinction coefficient with the sensor model follows another proceeding than the measurement. In the measurement the intensity of light that has passed through the smoke is measured. With a known travel length and a known emitted light intensity the extinction coefficient can be calculated using equation (2.6) chapter 2.2.1. For the measurement the effects of all particles which enter the light beam are added up, whereby every particle scatters and/or absorbs only a very small part of the light. The measurement is a method that integrates over the travel length of the light and the different particles. In case of the Mirex the emitted light is reflected back to the emitter after a travellength of 1 meter then the intensity is measured. With the sensor model the extinction coefficient is calculated using equation (2.7), that is why it just integrates over the particle sizes. Looking at the variation coefficients the over-all simulated one $V_o = 0.8916$ is larger than the sensor simulated one $V_s = 0.3929$. Considering the fact that the simulated extinction coefficient depends strongly on the particle number concentration

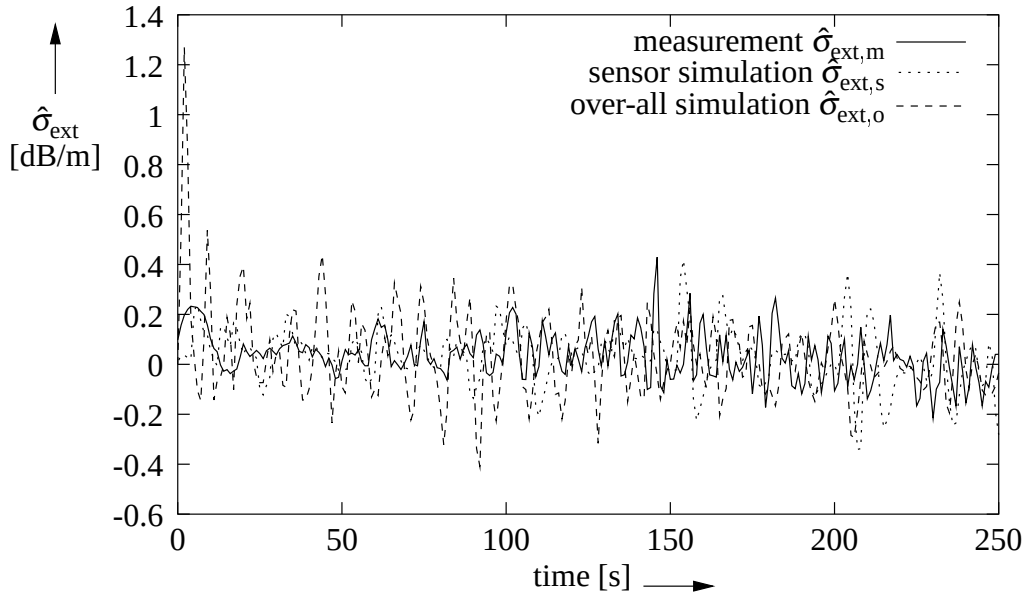

Figure 6.2: Statistic extinction light sensor for an n-heptane fire

and the geometric mean particle diameter, this means that the simulated particle number concentration and geometric mean particle diameter have a larger variance than the measured one in case of an n-heptane fire. These differences in the variances show that the fluctuation of the simulated input parameters for the over-all simulation is larger than the fluctuation of the measured input parameters for the sensor simulation.

6.2 Scattered Light Sensor

Klose's signal model shall also be examined using signals of scattered light sensors. Figure 6.4 shows the deterministic scattered intensities. In this figure it can again be seen that the measured intensity $\hat{I}_{s,m}$ as well as the over-all simulated one $\hat{I}_{s,o}$ have a sudden increase at the beginning of the fire, while the sensor simulated one $\hat{I}_{s,s}$ increases more slowly. Shortly before the fire burns out (200s) the three signals have nearly the same values. Comparing the deterministic extinction coefficients in figure 6.1 and the deterministic intensities it can be ascertained that the sensor simulated signals ($\hat{\sigma}_{ext,s}$,$\hat{I}_{s,s}$) and the over-all simulated ones ($\hat{\sigma}_{ext,o}$,$\hat{I}_{s,o}$) follow the same progression. This shows again the strong dependency of the simulation of optical sensors on the particle size and number again. Figure 6.5 shows the statistic scattered intensities. During the fire the amplitudes of the measured intensity are higher than after the fire has burned out (200s). This cannot be observed for the simulated intensities. Figure 6.6 shows the amplitude distribution of the scattered intensities. Opposite to the extinction coefficient the variation coefficient of the measured intensity is the largest

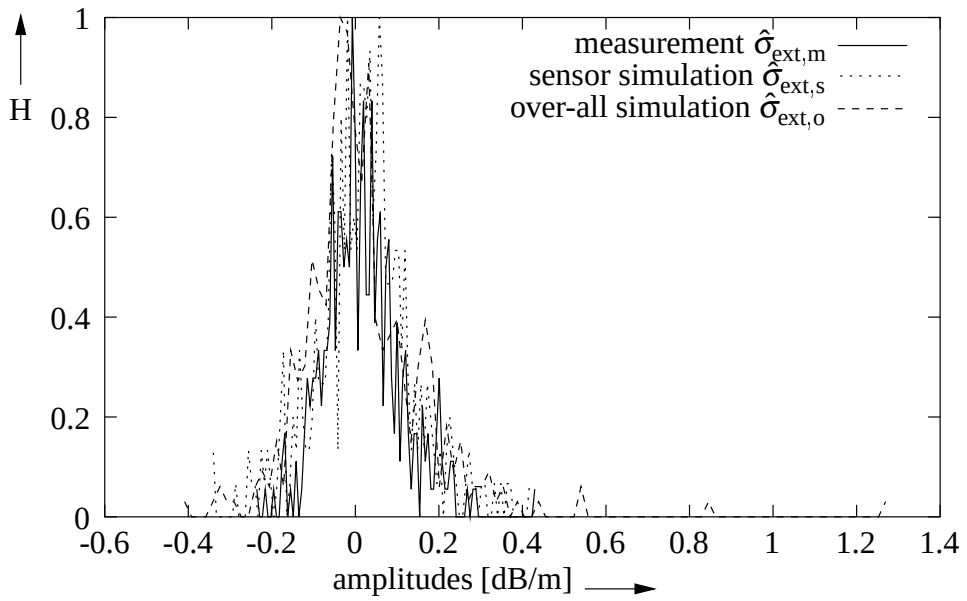

Figure 6.3: Amplitude distribution of the statistic extinction coefficient for an n-heptane fire

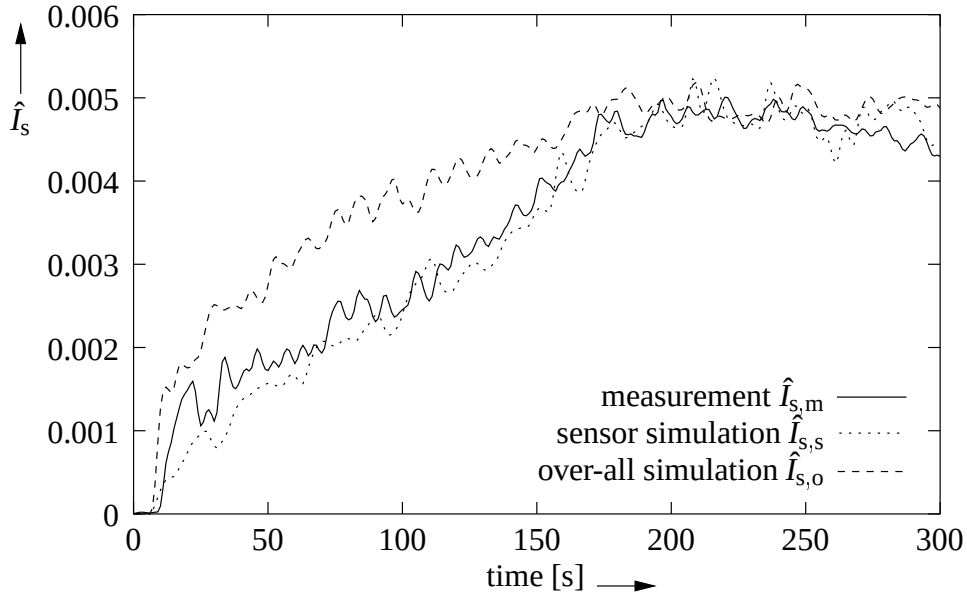

Figure 6.4: Deterministic scattered intensities of an n-heptane fire

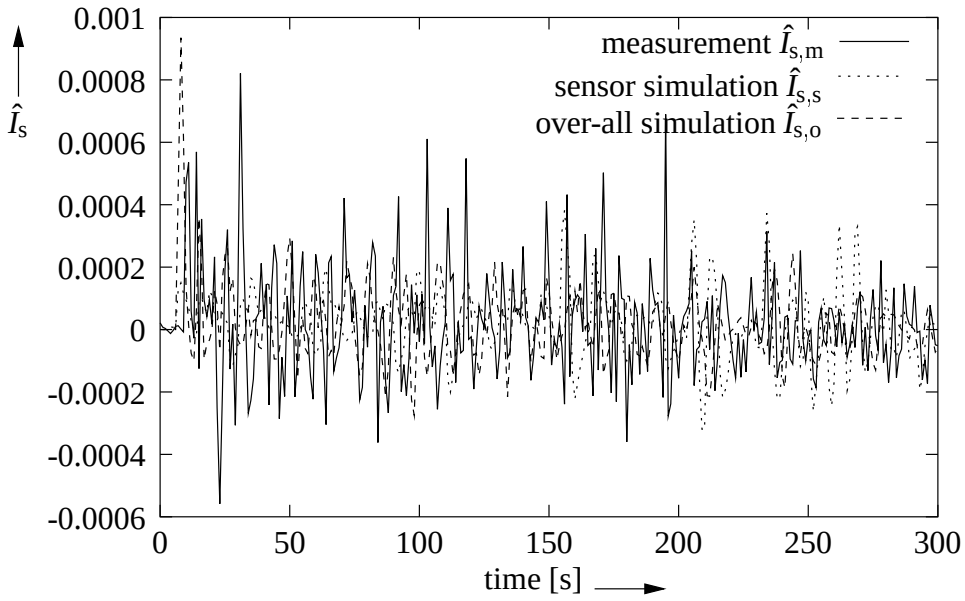

Figure 6.5: Statistic scattered light intensities of an n-heptane fire

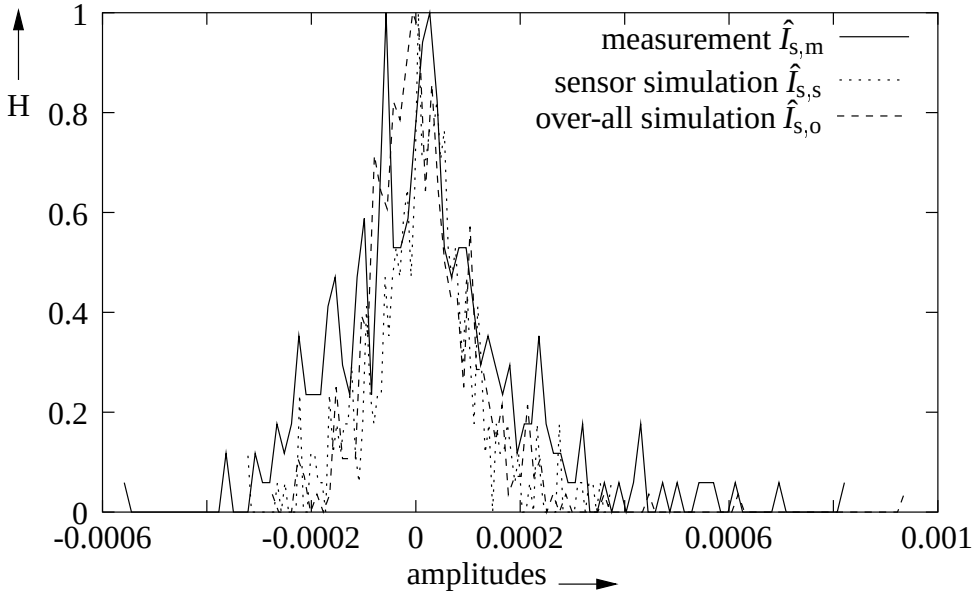

Figure 6.6: Amplitude distribution of the scattered light intensities of an n-heptane fire

$V_m = 0.0011$, while the ones of the simulated extinction coefficients have nearly the same value ($V_s = 0.0005$, $V_o = 0.0006$).
With the scattered light sensor light is emitted into a measurement chamber (figure 2.2) and the intensity of light scattered by particles inside this chamber is measured under a discrete angle. This scattered intensity is a very small part of the incoming light intensity. Due to this small measured signal the scattered light sensor is more sensitive to changes of the particle number and size than the extinction light sensor. Simulations have shown that small changes in the particle size cause large changes in the intensity of the scattered light. In addition to that, signals of scattered light sensors often contain high signal peaks at one sample time. These peaks will be treated in more detail in chapter 6.4.

6.3 Comparison of an n-Heptane Fire and a Cotton Wick Fire

The same investigations of the signals are carried out for the cotton wick fire. For the cotton wick fire the variation coefficient of the measured and the sensor simulated extinction coefficients (see figure 6.7) are very close to each other ($V_m = 0.3548$, $V_s = 0.3321$), while the one of the over-all simulated extinction coefficient is smaller ($V_0 = 0.1977$). The result is also confirmed by the amplitude distribution of the statistic extinction coefficient (see figure 6.8). This is the opposite result of the observance during an n-heptane fire experiment.

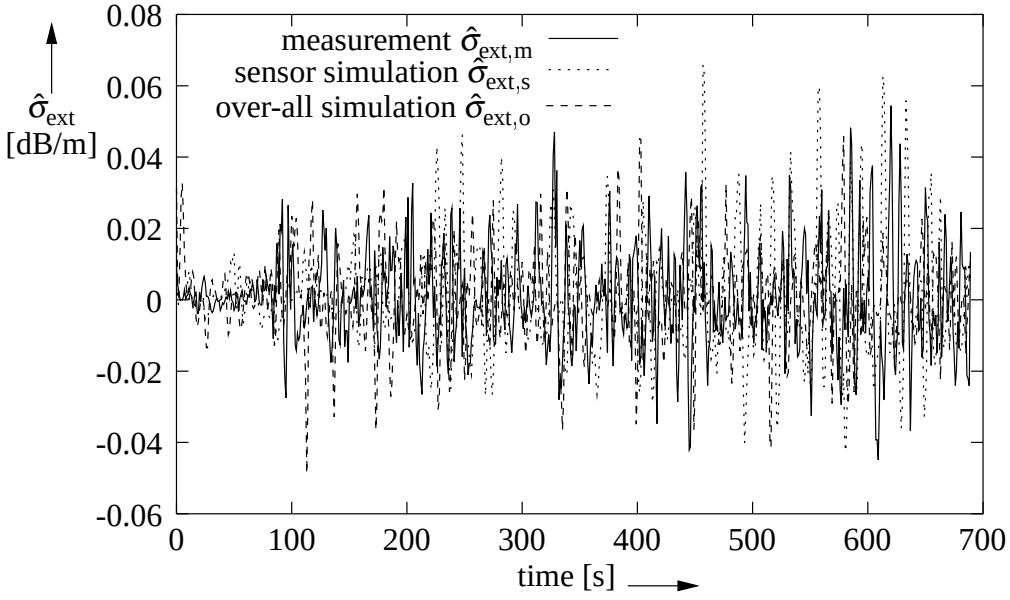

Figure 6.7: Statistic signal part from the extinction light detector for a cotton wick fire

The over-all simulated smoke distribution is more uniform than the one caused by a real fire

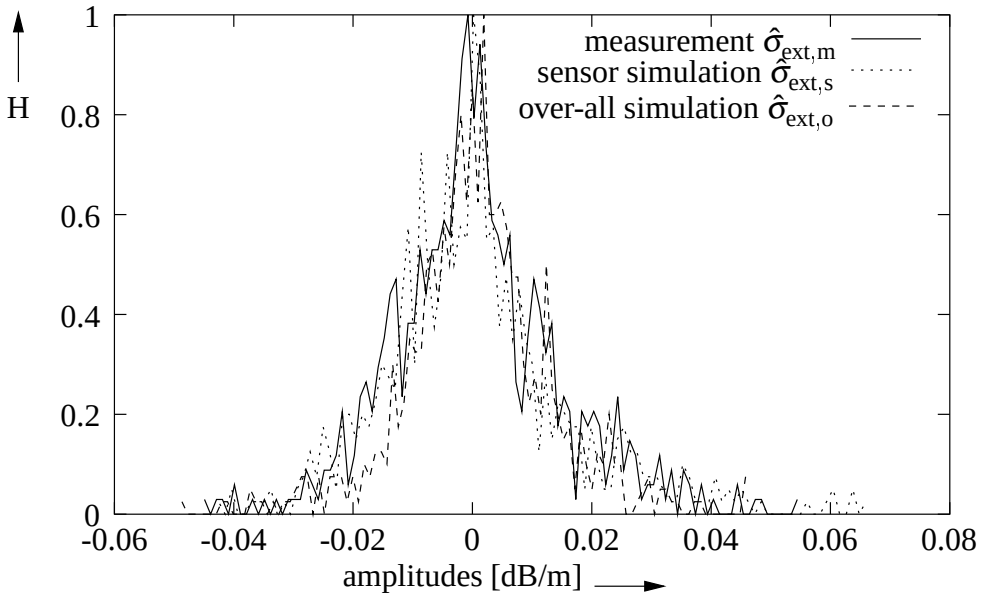

Figure 6.8: Amplitude distribution of the random signal part from the extinction light detector for a cotton wick fire

experiment. During cotton wick fire experiments the thermal flow is very small and can be disturbed easily, e.g. by an air stream due to different wall temperatures in the fire laboratory. This ambient flow has been considered in an additional simulation. The variation coefficient of the extinction coefficient, $V_{s,T_w} = 0.3561$, simulated with different wall temperatures is in the same order of size as the measured and sensor simulated ones. These data show that the results of a cotton wick fire experiment can be influenced by small changes of the environmental conditions. The difference of just 4°C between the walls of the laboratory leads to the described results. This temperature difference can easily occur, if there are external and internal walls. During some cotton wick fires it can be observed, that the smoke plume does not rise vertically, it meets the ceiling up to 1m away from the point perpendicular over the fire place.

For the scattered intensities, shown in figure 6.9, the sensor simulated variation coefficient $V_s = 0.8090 * 10^{-4}$ is the largest one, it is 3 to 4 times larger than the measured one $V_m = 0.2012 * 10^{-4}$ and the over-all simulated one $V_o = 0.252 * 10^{-4}$. The amplitude distribution (figure 6.10) shows that the negative as well as the positive amplitudes of the sensor simulated scattered intensity are larger. Figure 4.9 shows that the measured mean particle diameter is much more variant than the simulated one. The higher variance of the particle diameter combined with the higher variation coefficient of the sensor simulation allows the conclusion that the scattered light sensor model depends stronger on the particle diameter than on the extinction coefficient.

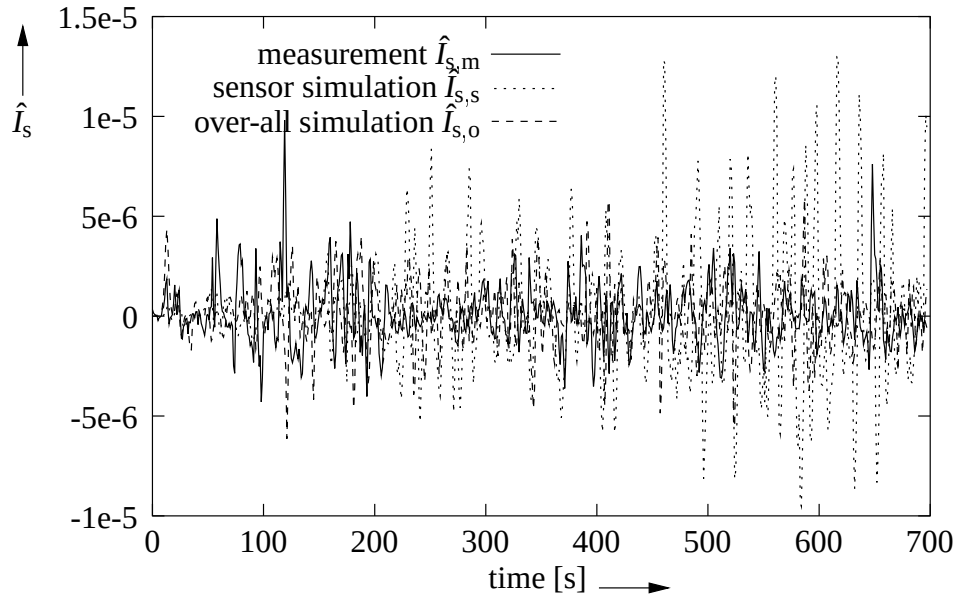

Figure 6.9: Statistic signal part from the scattered light detector for a cotton wick fire

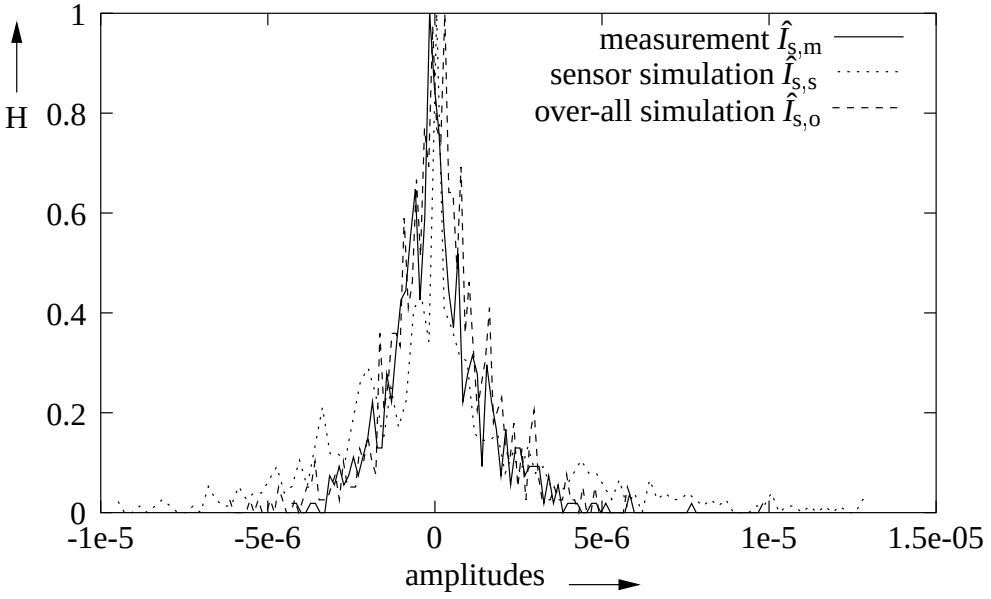

Figure 6.10: Amplitude distribution of the random signal part from the scattered light detector for a cotton wick fire

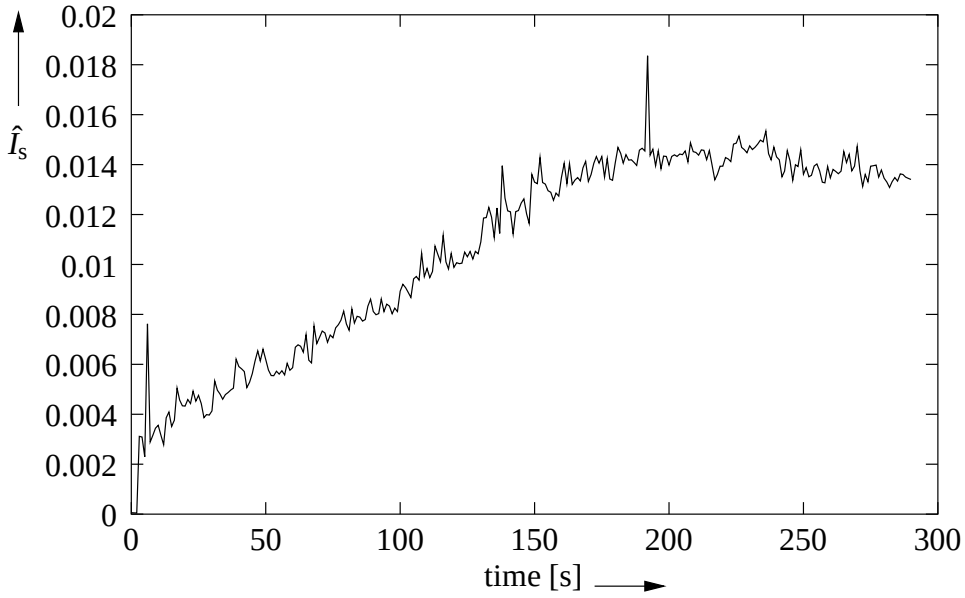

Figure 6.11: Scattered intensity measured during n-heptane fire

6.4 Special Properties of Signals from Scattered Light Sensors

As mentioned in chapter 6.2 signals of scattered light sensors contain peaks with an amplitude much higher than the mean amplitude of the signal [49], [60]. Figure 6.11 shows the scattered intensity measured during the n-heptane fire experiment, that has been evaluated before, being measured with another scattered light sensor of the same type. Figure 6.12 shows the corresponding statistic signal. It can be seen that there are two signal peaks one at 7 seconds and one at 193 seconds. The origin of these peaks is unknown so far. Investigations of the scattered intensities measured during four different types of test fire experiments have shown that the peaks do not occur during all these experiments. A description of the investigated fire experiments can be found in appendix D. The measured intensities of the smoldering test fires experiments, which are the smoldering cotton wick fire (TF3) and the smoldering wood fire (TF2), show no signal peaks. On the other hand nearly all scattered light signals measured during n-heptane fire experiments contain signal peaks. For the open wood fire (TF1) all measured intensities show these signal peaks. These results make it clear that the peaks are caused by the smoke properties and that they are not random noise of the sensor electronic. The smoke of the open flame fires (TF1, TF5) and the smoldering fires (TF2, TF3) has different properties [35], [36]. The open fires produce a large amount of smoke with a high particle number concentration ($N \sim 10^7/\mathrm{cm}^3$) and small particles ($< 100$ nm). They also produce a high thermal flow and a lot of heat. Smoldering fires produce less

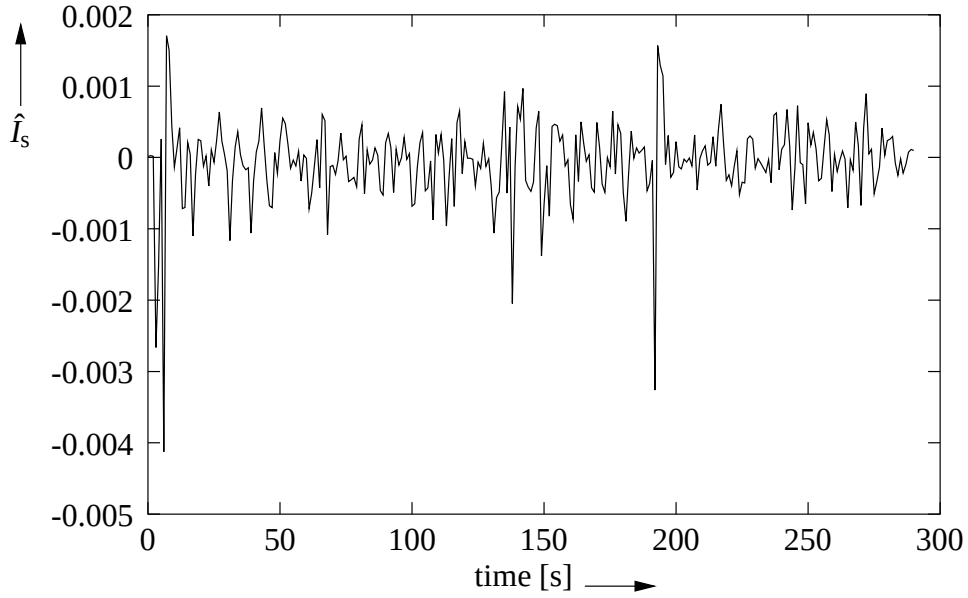

Figure 6.12: Statistic scattered intensity measured during n-heptane fire

smoke with a lower particle number concentration ($N \sim 10^6/\mathrm{cm}^3$) but larger particles ($> 100$ nm). These smoke properties are of special interest, because the intensity of the scattered light depends strongly on the particle number concentration and the particle sizes. Furthermore the smoldering fires produce only a small thermal flow. In the following investigations the results of sensor simulations with modified input signals are discussed to find possible reasons for the peaks and to discover if this effects can be simulated with the described model. Figure 6.13 show the simulation of a scattered light sensor with a modified input signal. At 150 seconds the value of the geometric mean particle diameter has been varied. The sensor simulation with this modified diameter gives a peak at the output signal which is spread over several samples due to filter properties of the sensor model. So a larger particle size could be a reason for the peak. But the sensor simulation has shown that this peak also appears for the simulated extinction coefficient and for the simulated chamber current. And the simulation results do not explain the fact that peaks only appear during open flame fires - especially the open wood fire. Open flame fires produce weakly scattering smoke particles while the smoldering fires produce strongly scattering particles [35]. Figure 6.14 shows the simulation results with a modified carbon fraction index κ. The simulated scattered intensity contains a peak, while the modification has no effect on the simulated extinction coefficient. Due to the fact that just an optical property of the smoke has been varied the simulation of the ionization chamber is not influenced. The optical properties of the smoke are not simulated so far but they were taken from existing literature, therefore this effect on the sensor signal can only be simulated by modifying the carbon fraction index. A modification of the

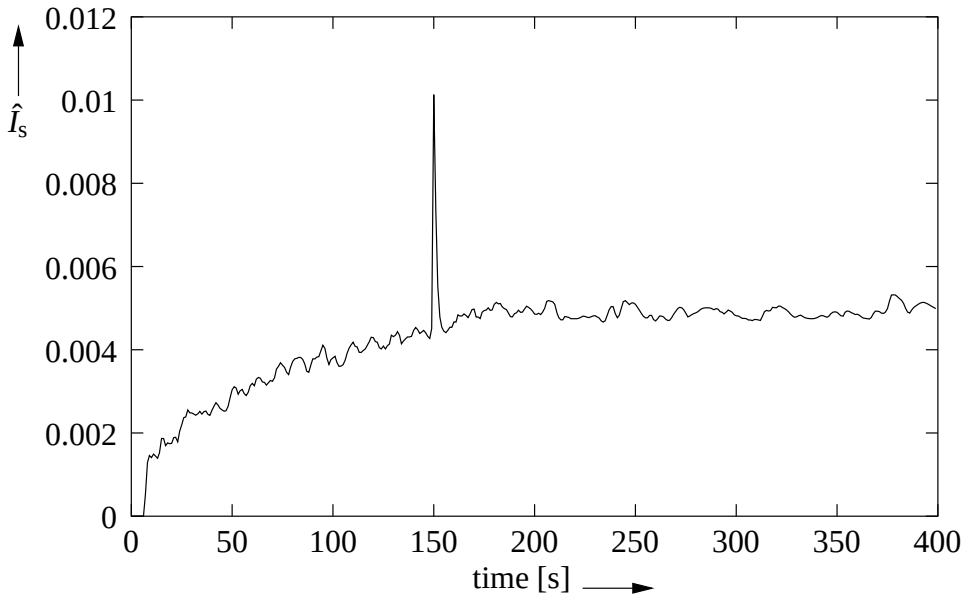

Figure 6.13: Simulated scattered intensity for n-heptane fire

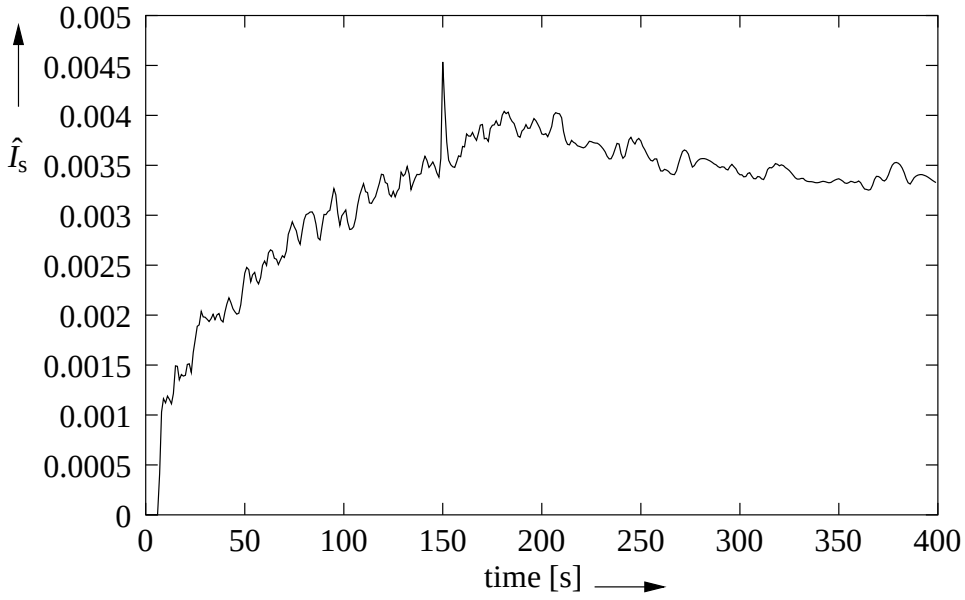

Figure 6.14: Simulated scattered intensity for n-heptane fire with modified carbon fraction index

particle number concentration at a discrete point of time has shown no visible effect on the simulation results.

6.5 Summary of the Statistic Investigation of the Model

The statistical investigation of the signals of optical smoke sensors has shown that the separation of the sensor signal into a deterministic signal and a statistic signal, following Klose's signal model, is also suitable for the simulated signals. The separation of the sensor signal provides different results for the two investigated sensor types. For the extinction light sensor the statistic signal of the extinction coefficient measured during an n-heptane fire experiment has the lowest variance, whereas the variances of the two simulated signals vary strongly. The comparisons of the simulated and the measured results of a cotton wick fire have shown that the measurement is strongly influenced by the environmental conditions of the experiment. For the scattered light sensor the measured signal has the largest variance, while the simulated signals have nearly the same variance. For the simulation of the scattered intensities , the variances of the input signal do not have such a strong effect as they have for the extinction coefficient. The comparison of the simulation and measurement results leads to the conclusion that the origin of the statistic signal lies mainly in the fire itself. A possible reason for the peak in the signal of the scattered light sensor could be found by varying the carbon fraction of the smoke, but this effect can not be simulated with the combined fire and sensor model so far.

7 A Simulation of Non-fire Situations

False alarms are a large problem in the field of automatic fire detection. They produce unnecessary costs, e.g. the fire brigade marching out for no reason, and in case of frequent false alarms people start to ignore the alarms. As a consequence the risk for their life increases, should they not leave the endangered area in case of a real fire. Thus non-fire situations which may cause false alarms are an important object of investigation. In the following an example is given for the simulation of a non fire experiment with the described model. In this experiment dust [53] is emitted into the fire detection laboratory by means of a dust generator [51]. The dust is transported by a forced flow stream and reaches the smoke sensors under the ceiling after a while. During the experiment the particle number concentration and the particle sizes are measured. These values are used for sensor simulations with measured input parameters. Although there is no fire the FDS software can be used for the simulation of the experiment. In this case the source species are not produced by a combustion process, but the scenario is implemented by an open vent through which the dust is transported into the laboratory. For the simulation the dust is only defined by its molecular weight. For the dust simulation not the mass density , which is needed for further simulations is calculated, but the mass fraction of dust Y_{d}. With the assumption that there is only dust and air, the dust mass density ρ_{dust} can be calculated as follows

$$\rho_{\mathrm{dust}} = Y_{\mathrm{d}}((1-Y_{\mathrm{d}})\rho_{\mathrm{a}} + \rho_{\mathrm{d}}), \tag{7.1}$$

where ρ_{a} is the density of the surrounding air and ρ_{d} is the specific density of the dust. Afterwards the dust mass density is treated in the same way as the smoke mass density. Figure 7.1 shows the simulated and the measured particle number concentration of the dust. The simulation gives reasonable results. The flow stream caused by the flow inlet has a low velocity, so there is as high a fluctuation in the particle number concentration as for the cotton wick fire (figure 4.7). Due to the fact that no coagulation is assumed the geometric mean particle diameter keeps its initial value for the whole simulation. The measured and simulated values are used as input values for the simulation of optical smoke sensors. The results are then compared to measurement results in the same way as in chapter 5. One problem arises at the simulation of the response of an optical smoke sensor to intruding dust. The smoke model used for the fire simulation is developed for particles which mainly consist of carbon, while the dust particles mainly consist of silicon oxide (SiO_2), which has a different complex refractive index. The usage of the smoke model for the dust simulation

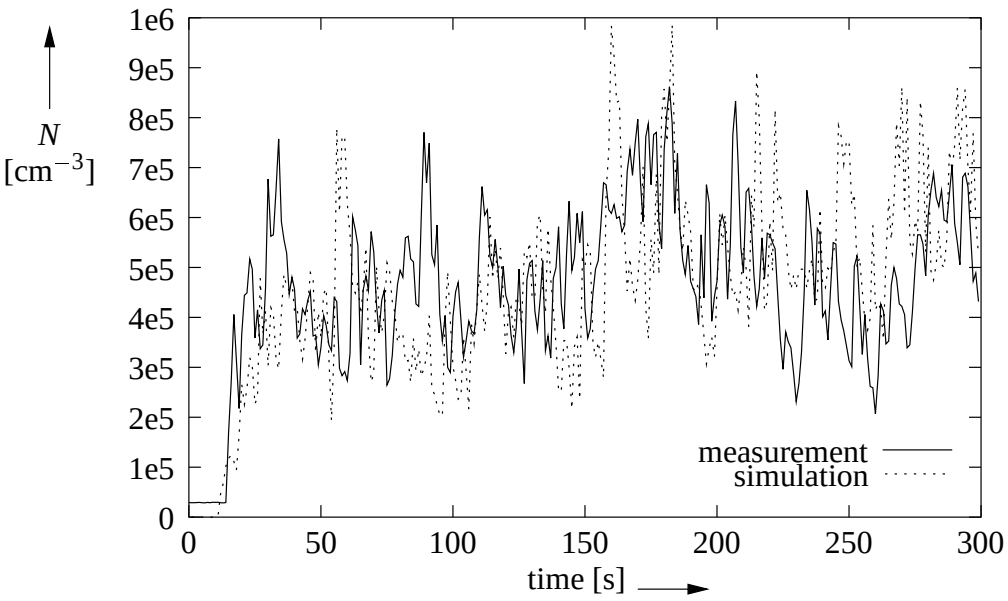

Figure 7.1: Particle number concentration of dust experiment

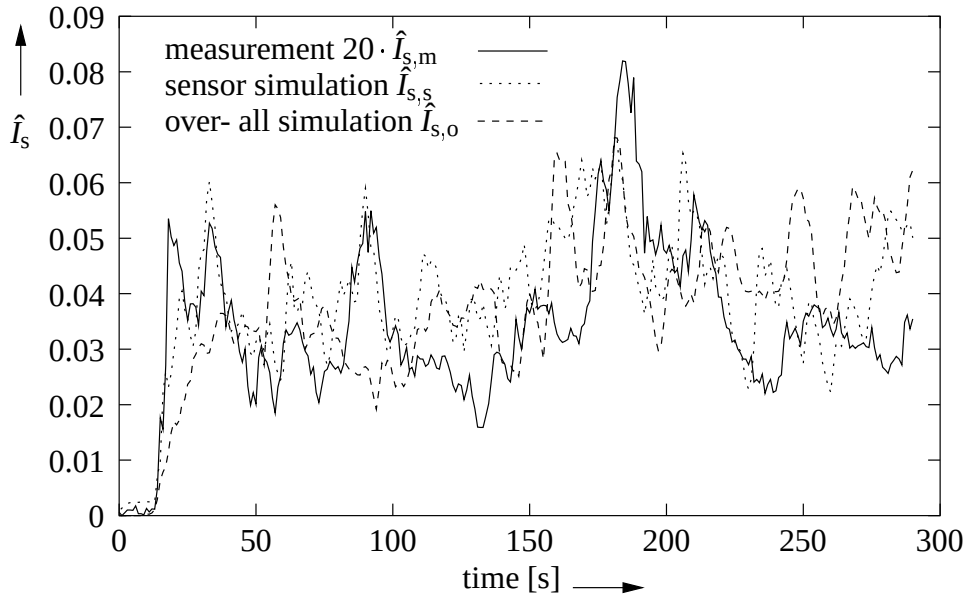

Figure 7.2: Scattered intensity of dust experiment

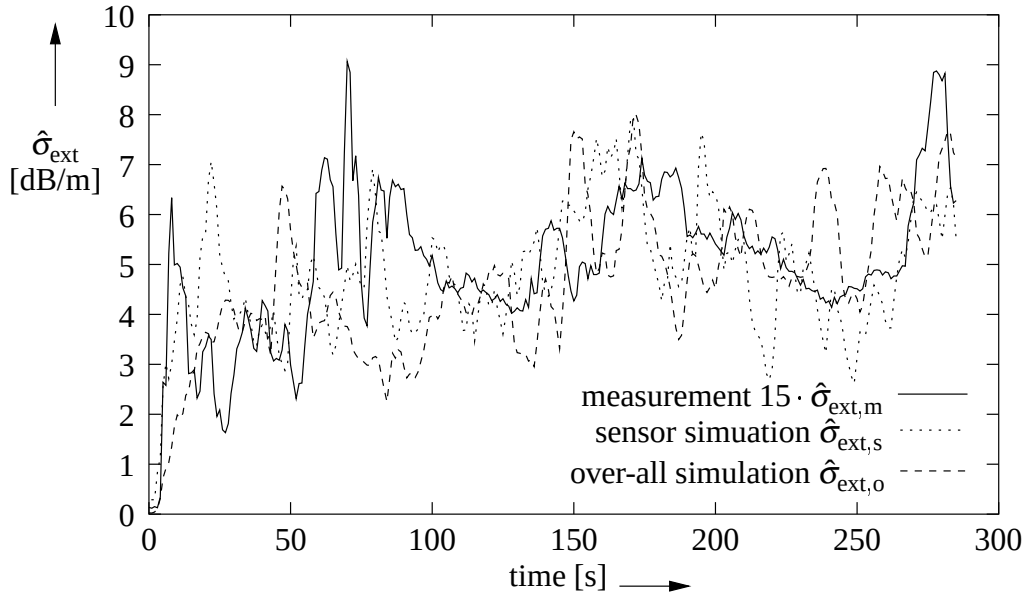

Figure 7.3: Scattered light intensity of dust experiment

results in signals which are too high. Figure 7.2 shows the extinction coefficients. The measured one $\hat{\sigma}_{ext,m}$ is smaller by a factor of about 20 than the simulated ones ($\hat{\sigma}_{ext,s}$, $\hat{\sigma}_{ext,o}$). The same results are achieved for the scattered intensities (figure 7.3), where the measured scattered intensity $\hat{I}_m$ is smaller by a factor of about 15. So carbon scatters and absorbs light more strongly than SiO_2 in the near infrared region. This problem can be relieved by using the complex refractive index of the dust instead of the smoke model for the sensor simulation. Beside this effect, both simulations give reasonable results compared to the measurements. The results show that the introduced model is also suitable for the simulation of non-fire experiments, with some small modifications to be made.

8 Conclusion

An interface between a fire model and a smoke sensor model has been developed and thus a part of an over-all model for the automatic fire detection has been build up. For the fire simulation part of the over-all model the Fire Dynamics Simulator (FDS) of the National Institute of Standards and Technology has been used, a field model for fire simulations in enclosures and open environments. The smoke sensor models used in this work have been developed by Frank Gockel at the Institute of Communication Systems of University Duisburg-Essen. To realize the interface the simulation results of the FDS had to be converted into the input signals of the smoke sensor models. The fire model gives the smoke mass density as a result of the simulation of smoke development during a fire. But the smoke sensor models need the information about the size distribution of the smoke particles, i.e. the particle number concentration, the geometric mean particle diameter and the geometric standard deviation. Simulation results have shown that the mechanism of coagulation and the removal of particles had also to be implemented in the model. To implement the coagulation a solution of the general dynamic equation (GDE) has been employed. Different approaches to solve the GDE have been implemented and the suitable approach has been chosen by comparing simulation results. For the implementation of the removal of particles the GDE has also been used. The developed model for fire and smoke sensor simulation has been evaluated by two EN54 test fire experiments. The n-heptane fire has been chosen as an example of open flame fires, the cotton wick fire as an example of smoldering fires. It has been shown that the model is also suitable for the simulation of non-fire experiments.

For the evaluation of the model three smoke sensor types, two optical sensors (a scattered light sensor and an extinction light sensor) and an ionization chamberhave been simulated. The comparison of simulated and measured signals has made clear that the developed model is suitable to simulate fire experiments and that the simulations yield suitable results. The quality of the results depend on the simulated sensor type and on the simulated fire experiment.

An application of Klose's signal model to the simulation results has shown that the model can be used to simulate special properties of smoke sensor signals. Although the model is deterministic the statistic signal part of Klose's model could be verified in the simulated signals. With this results possible origins for the statistic signal could be found. A special property of the signals of scattered light sensors has also been investigated. Reasons for the signal peaks on measured scattered intensity were given.

The comparisons of measured and simulated results have shown, that the model is suitable for simulations of different fire experiments. It gives the opportunity to change environmental parameters of a fire experiment easily, even parameters which are impossible to control during a laboratory experiment. Thus the influence of the properties on the signal of smoke sensors can be verified without a large number of fire experiments. The model can be used to investigate which property of a sensor signal arises from the sensor and which from the fire itself, in order to explore new approaches on smoke sensors.

A Logarithmic Normal Size Distribution

Aerosols have a non symmetric size distribution because the number of larger particles outbalances the smaller particles. In addition the particle sizes vary over a wide range and no negative sizes appear. For this reasons the widely used normal distribution is not suitable to describe the particle size distribution of an aerosol. In general the logarithmic normal distribution is used [24, chap 4.4]
Different forms of the particles size distribution are used in the relevant studies. Gockel [22] employs the particle diameter distribution

$$n_{\mathrm{d}}(d) = \frac{1}{\sqrt{2\pi}\sigma_{\mathrm{d}} d} \exp\left(-\frac{1}{2}\frac{\ln^2(\frac{d}{d_{\mathrm{g}}})}{\sigma_{\mathrm{d}}^2}\right) \tag{A.1}$$

for the derivation of his sensor model, where d_{g} is the geometric mean particle diameter and σ_{d} is the geometric standard deviation.
Lee [32] [33] uses the particle volume distribution

$$n(v) = \frac{1}{3\sqrt{2\pi}\ln(\sigma_{\mathrm{r}})v} \exp\left(-\frac{\ln^2(\frac{v}{v_{\mathrm{g}}})}{18\ln^2\sigma_{\mathrm{r}}}\right). \tag{A.2}$$

v_{g} represents the geometric mean volume of the particles

$$\ln v_{\mathrm{g}}(t) = \int_0^\infty \ln(v) n(v,t) \mathrm{d}v.$$

The geometric mean volume is the median particle volume in case of log-normally distributed volumes [63], $\ln(\sigma_{\mathrm{r}})$ is the geometric standard deviation of the particle size distribution, while σ_{r} is the standard deviation based on the particle radius [63]. The two forms of the size distribution can be transformed into each other by use of transformation for nonlinear systems [38]. The transformation equation for a non linear system with stochastic input parameters is

$$p_y(y) = \sum_{i=1}^{n} \frac{p_x(x_i(y))}{|g'(x_i)|},$$

$$g'(x_i) = \frac{\mathrm{d}g(x_i)}{\mathrm{d}x_i}$$

In this case $p_x(x)$ is the particle diameter distribution $p_d(d)$ and $p_y(y)$ is the particle volume distribution $p_v(v)$.

The function $g(x)$ is the relation between the diameter and the volume of a sphere in this particular case, with

$$g(x) = g(d) = v = \frac{1}{6}\pi d^3 \Rightarrow g'(d) = \frac{1}{2}\pi d^2$$

and

$$d = \left(\frac{6v}{\pi}\right)^{1/3}$$

With this we get

$$p_v(v) = \frac{p_d(d(v))}{|g'(d)|} \tag{A.3}$$

With:

$$p_d(d) = \frac{1}{\sqrt{2\pi}\sigma_{\mathrm{d}} d} \exp\left(-\frac{1}{2}\cdot\frac{\ln^2(\frac{d}{d_{\mathrm{g}}})}{\sigma_{\mathrm{d}}^2}\right),$$

replacing d by v in (A.3)

$$\begin{aligned} p_v(v) &= \frac{p_d(d(v))}{g'(d)} \\ &= \frac{2}{\pi(6v/\pi)^{2/3}} \cdot \frac{1}{\sqrt{2\pi}\cdot\sigma_{\mathrm{d}}(6v/\pi)^{1/3}} \exp\left(-\frac{1}{2}\frac{\ln^2(\frac{(6v/\pi)^{1/3}}{d_{\mathrm{g}}})}{\sigma_{\mathrm{d}}^2}\right) \\ &= \frac{2}{\pi\sqrt{2\pi}\cdot\sigma_{\mathrm{d}}(6v/\pi)} \exp\left(-\frac{1}{2}\frac{\frac{1}{9}\ln^2(\frac{6v/\pi}{d_{\mathrm{g}}^3})}{\sigma_{\mathrm{d}}^2}\right) \\ &= \frac{1}{3}\frac{1}{\sqrt{2\pi}\cdot\sigma_{\mathrm{d}} v} \exp\left(-\frac{1}{18}\frac{\ln^2(v/v_{\mathrm{g}})}{\sigma_{\mathrm{d}}^2}\right) \end{aligned} \tag{A.4}$$

Equation (A.4) corresponds to the size distribution used by Lee (A.2). A comparison of equations (A.4) and (A.2) gives the relations between the geometric mean diameter and the geometric mean volume

$$v_{\mathrm{g}} = \frac{1}{6}\pi d_{\mathrm{g}}^3$$

and the geometric standard deviations

$$\ln(\sigma_{\mathrm{r}}) = \sigma_{\mathrm{d}}.$$

B Initial Particle Number Concentration

To derive the initial concentration of smoke particles it is assumed that the smoke particles have a spherical shape and the particle size is log-normally distributed

$$n(v) = N_0 \frac{1}{3 \cdot \sqrt{2\pi} \cdot \ln(\sigma_r) v} \exp\left(-\frac{\ln^2(\frac{v}{v_g})}{18 \ln^2 \sigma_r}\right).$$

Where v_g is the geometric mean particle volume and $\ln \sigma_r$ the geometric standard deviation of the particle size distribution.
The moments of particle size distribution are defined in the following way

$$M_k = \int_{v=0}^{\infty} v^k \cdot n(v) \mathrm{d}v = N_0 v_g^k \exp\left(\frac{9}{2} \ln^2 \sigma_r\right)$$

The first order moment M_1 gives the dimensionless total volume of particles per unit volume [32], [63]

$$M_1 = V_{\text{part}} = \int_{v=0}^{\infty} v \mathrm{d}N(v) \tag{B.1}$$

$$= N_0 v_g \exp\left(\frac{9}{2} \ln^2 \sigma_r\right). \tag{B.2}$$

The total volume of the particles equals the ratio of the smoke mass density ρ_{smoke} and the specific smoke density ρ_{part}

$$V_{\text{part}} = \frac{\rho_{\text{smoke}}}{\rho_{\text{part}}}. \tag{B.3}$$

The smoke mass density is the amount of smoke produced during a fire while the specific smoke density is a constant material property of the smoke. Combining equation (B.3) and equation (B.2) we get

$$V_{\text{part}} = \frac{\rho_{\text{smoke}}}{\rho_{\text{part}}} = N_0 v_g \exp\left(\frac{9}{2} \ln^2 \sigma_r\right)$$

Consequently the initial particle number concentration can be written as a function of the smoke mass density

$$N_0 = \frac{\rho_{\text{smoke}}}{\rho_{\text{part}}} v_g^{-1} \exp\left(-\frac{9}{2} \ln^2 \sigma_r\right).$$

C Derivation of the Solution of the GDE with the Moments Method

Continuum regime

The GDE for pure coagulation in the continuum regime is given as

$$\frac{\partial}{\partial t}n(v,t)_{\mathrm{coag}} = \frac{1}{2}\int_0^v \beta(u,v-u)n(u,t)n(v-u,t)\mathrm{d}u - n(v,t)\int_0^\infty \beta(u,v)n(u,t)\mathrm{d}u. \quad \text{(C.1)}$$

with

$$\beta = (u,v) = K_{\mathrm{c}}(u^{1/3}+v^{1/3})\left(\frac{1}{u^{1/3}}+\frac{1}{v^{1/3}}\right) \quad \text{(C.2)}$$

By multiplying equation(C.1) with v^k and integrating from 0 to ∞ we get the GDE for coagulation in its momentum form [63, App. A].

$$\begin{aligned}\frac{\mathrm{d}}{\mathrm{d}t}M_k(t) &= \frac{1}{2}\int_0^\infty\int_0^\infty (u+w)^k n(v,t)\beta(u,w)\cdot n(w,t)\mathrm{d}v\mathrm{d}w \\ &\quad -\frac{1}{2}\int_0^\infty\int_0^\infty u^k n(u,t)\cdot\beta(u,v)n(v,t)\mathrm{d}v\mathrm{d}u, \end{aligned} \quad \text{(C.3)}$$

with $w = u - v$. Because of the symmetries of β concerning u and v, u^k can be written as $(v^k+u^k)/2$, and we get

$$\frac{\mathrm{d}}{\mathrm{d}t}M_k(t) = \frac{1}{2}\int_0^\infty\int_0^\infty [(u+w)^k - w^k - u^k]\beta(u,w)n(u,t)n(w,t)\mathrm{d}w\mathrm{d}u. \quad \text{(C.4)}$$

The integral at the right hand side of the equation (C.4) can be written as moments of the distribution

$$M_k(t) = \int_0^\infty v^k n(v,t)\mathrm{d}v.$$

So with equation (C.2) and for k=0,1,2 we obtain

$$\begin{aligned}\frac{\mathrm{d}}{\mathrm{d}t}M_0(t) &= -\frac{1}{2}K_{\mathrm{c}}\int_0^\infty\int_0^\infty \left[(u^{1/3}+w^{1/3})\left(\frac{1}{u^{1/3}}+\frac{1}{w^{1/3}}\right)\right] n(u,t)n(w,t)\mathrm{d}w\mathrm{d}u \\ &= -\frac{1}{2}K_{\mathrm{c}}\int_0^\infty\int_0^\infty \left[2+\left(\frac{u}{w}\right)^{1/3}+\left(\frac{w}{u}\right)^{1/3}\right] n(u,t)n(w,t)\mathrm{d}w\mathrm{d}u \\ &= -K_{\mathrm{c}}[M_0^2 + M_{1/3}M_{-1/3}] \end{aligned} \quad \text{(C.5)}$$

$$\frac{\mathrm{d}}{\mathrm{d}t}M_1(t) = -\frac{1}{2}K_{\mathrm{c}}\int_0^\infty\int_0^\infty (u+w-w-u)n(u,t)n(w,t)\mathrm{d}w\mathrm{d}u = 0 \quad \text{(C.6)}$$

$$\begin{aligned}\frac{\mathrm{d}}{\mathrm{d}t}M_2(t) &= -\frac{1}{2}K_\mathrm{c}\int_0^\infty\int_0^\infty[(u+w)^2+u^2+w^2]\\ &\cdot\quad\left[2+\left(\frac{u}{w}\right)^{1/3}+\left(\frac{w}{u}\right)^{1/3}\right]n(u,t)n(w,t)\mathrm{d}w\mathrm{d}u\\ &= -\frac{1}{2}K_\mathrm{c}\int_0^\infty\int_0^\infty 2uw\left[2+\left(\frac{u}{w}\right)^{1/3}+\left(\frac{w}{u}\right)^{1/3}\right]n(u,t)n(w,t)\mathrm{d}w\mathrm{d}u\\ &= 2K_\mathrm{c}[M_1^2+M_{4/3}M_{2/3}] \qquad \text{(C.7)}\end{aligned}$$

These equations are now first-order ordinary differential equations, where M_0 is the total particle number concentration and M_1 is the total volume of particles. For pure coagulation the change of the total volume of particle is zero as expected. The moments of the log-normal distribution can be expressed in terms of the zeroth oder moment

$$M_k = M_0 v_\mathrm{g}^k \exp\left(\frac{9}{2}k^2\ln^2\sigma_\mathrm{r}\right) \qquad \text{(C.8)}$$

or the first order moment

$$M_k = M_1 v_\mathrm{g}^{k-1}\exp\left(\frac{9}{2}(k^2-1)\ln^2\sigma_\mathrm{r}\right). \qquad \text{(C.9)}$$

To take advantage of the property $M_1 = const$ the moments are written in terms of M_1

$$M_0 = M_1 v_\mathrm{g}^{-1}\exp\left(-\frac{9}{2}\ln^2\sigma_\mathrm{r}\right), \qquad \text{(C.10)}$$

$$M_2 = M_1 v_\mathrm{g}\exp\left(\frac{27}{2}\ln^2\sigma_\mathrm{r}\right), \qquad \text{(C.11)}$$

$$M_{1/3}M_{-1/3} = M_1^2 v_\mathrm{g}^{-2}\exp(-8\ln^2\sigma_\mathrm{r}), \qquad \text{(C.12)}$$

$$M_{4/3}M_{2/3} = M_1^2\exp(\ln^2\sigma_\mathrm{r}). \qquad \text{(C.13)}$$

By differentiating (C.10) and (C.11) and inserting (C.6) we get

$$\frac{\mathrm{d}}{\mathrm{d}t}M_0(t) = -M_1 v_\mathrm{g}^{-1}\exp\left(-\frac{9}{2}\ln^2\sigma_\mathrm{r}\right)\cdot\left[\frac{\mathrm{d}(\ln v_\mathrm{g})}{\mathrm{d}t}+\frac{9}{2}\frac{\mathrm{d}(\ln^2\sigma_\mathrm{r})}{\mathrm{d}t}\right], \qquad \text{(C.14)}$$

and

$$\frac{\mathrm{d}}{\mathrm{d}t}M_2(t) = M_1 v_\mathrm{g}\exp\left(\frac{27}{2}\ln^2\sigma_\mathrm{r}\right)\cdot\left[\frac{\mathrm{d}(\ln v_\mathrm{g})}{\mathrm{d}t}+\frac{27}{2}\frac{\mathrm{d}(\ln^2\sigma_\mathrm{r})}{\mathrm{d}t}\right]. \qquad \text{(C.15)}$$

Inserting (C.10) to (C.15) in (C.5) and (C.7) we get

$$\exp\left(\frac{9}{2}\ln^2\sigma_r\right)\left[\mathrm{d}(\ln v_g)+\frac{9}{2}\mathrm{d}(\ln^2\sigma_r)\right]=KM_1v_g^{-1}[1+\exp(\ln^2\sigma_r)]\mathrm{d}t \tag{C.16}$$

and

$$\frac{1}{2}\exp\left(\frac{27}{2}\ln^2\sigma_r\right)\left[\mathrm{d}(\ln v_g)+\frac{27}{2}\mathrm{d}(\ln^2\sigma_r)\right]=KM_1v_g^{-1}[1+\exp(\ln^2\sigma_r)]\mathrm{d}t \tag{C.17}$$

By subtracting(C.14) and (C.15) dt can be eliminated and we get

$$\mathrm{d}(\ln v_g)=\frac{9\left[1-\frac{3}{2}\exp(9\ln^2\sigma_r)\right]}{\exp(9\ln^2\sigma_r)-2}\mathrm{d}(\ln^2\sigma_r) \tag{C.18}$$

Integrating both sides results in

$$v_g=v_{g,0}\frac{\exp(9\ln^2\sigma_{r,0})-2}{\exp(9\ln^2\sigma_r)-2}\cdot\exp\left[\frac{9}{2}(\ln^2\sigma_{r,0}-\ln^2\sigma_r)\right] \tag{C.19}$$

a relation between v_g and σ_r, where $v_{g,0}$ and $\sigma_{r,0}$ are the initial values of v_g and σ_r at the time $t=t_0$. By inserting (C.18) and (C.19) in (C.16) and using (C.10) we obtain

$$\frac{-9[\exp(9\ln^2\sigma_{r,0})-2]\exp(9\ln^2\sigma_r)}{[\exp(9\ln^2\sigma_{r,0})-2]^2[1+\exp(\ln^2\sigma_r)]}d(\ln^2\sigma)=KN_0dt, \tag{C.20}$$

where N_0 is the initial value of M_0.

To solve the equation (C.20) we assume that $[1+\exp(\ln^2\sigma_r)]\simeq[1+\exp(\ln^2\sigma_{r,0})]$, which means that the variance of the distribution does not change significantly due to coagulation. By integrating equation (C.20) we get

$$\ln\sigma_r(t)=\frac{1}{9}\ln\left(2+\frac{\exp(9\ln^2\sigma_{r,0})-2}{1+[1+\exp(\ln^2\sigma_{r,0})]K_cN_0t}\right). \tag{C.21}$$

Setting (C.21) in (C.19) we get for the particle volume

$$\frac{v_g(t)}{v_{g,0}}=\frac{\exp(9\ln^2(\sigma_{r,0})/2)\cdot[1+\{1+\exp(\ln^2\sigma_{r,0})\}K_cN_0t]^{3/2}}{[2\cdot(1+\{1+\exp(\ln^2\sigma_{r,0})\}K_cN_0t)+\exp(9\ln^2\sigma)-2]^{(1/2)}}. \tag{C.22}$$

Using (C.16) and (C.22) we get

$$\frac{N(t)}{N_0}=\frac{1}{1+[1+\exp(\ln^2\sigma_{r,0})]\cdot K_cN_0t} \tag{C.23}$$

Slip Regime

The coagulation kernel in the slip regime is given as

$$\beta(u,v)=K_c(u^{1/3}+v^{1/3})\left(\frac{C_u}{u^{1/3}}+\frac{C_v}{v^{1/3}}\right) \tag{C.24}$$

Therefore derivating the zeroth to second moments in the slip regime and writing them in terms of other moments gives

$$\frac{\mathrm{d}M_0}{\mathrm{d}t} = -K_\mathrm{c}\left[M_0^2 + M_{1/3}M_{-1/3} + A\lambda\left(\frac{4}{3}\pi\right)^{1/3}\cdot\left(M_0M_{-1/3} + M_{1/3}M_{-2/3}\right)\right] \tag{C.25}$$

$$\frac{\mathrm{d}M_1}{\mathrm{d}t} = 0 \tag{C.26}$$

$$\frac{\mathrm{d}M_2}{\mathrm{d}t} = 2K_\mathrm{c}\left[M_1^2 + M - 4/3M_{2/3} + A\lambda\left(\frac{4}{3}\pi\right)^{1/3}\cdot\left(M_1M_{2/3} + M_{4/3}M_{1/3}\right)\right] \tag{C.27}$$

Again the moments can be expressed in the following ways

$$M_k = M_0 v_\mathrm{g}^k \exp\left(\frac{9}{2}k^2\ln^2\sigma\right) \tag{C.28}$$

or

$$M_k = M_1 v_\mathrm{g}^{k-1} \exp\left(\frac{9}{2}(k^2-1)\ln^2\sigma\right) \tag{C.29}$$

Differentiating (C.28) with respect to t for $k = 0$ and $k = 2$ results in

$$\frac{\mathrm{d}M_0}{\mathrm{d}t} = -M_0\left[\frac{d(\ln v_\mathrm{g})}{\mathrm{d}t} + \frac{9}{2}\frac{\mathrm{d}Z}{\mathrm{d}t}\right] \tag{C.30}$$

and

$$\frac{\mathrm{d}M_2}{\mathrm{d}t} = v_\mathrm{g}^2\exp(18Z)\left[\frac{d(\ln v_\mathrm{g})}{\mathrm{d}t} + \frac{27}{2}\frac{\mathrm{d}Z}{\mathrm{d}t}\right], \tag{C.31}$$

with $Z = \ln^2\sigma$. Expressing all moments in terms of $M_0 = N$ (C.25) and (C.27) can be written as

$$\frac{\mathrm{d}M_0}{\mathrm{d}t} = \frac{\mathrm{d}N}{\mathrm{d}t} = -K_\mathrm{c}N^2\left[1 + \exp(Z) + A\cdot Kn\left(\exp\left(\frac{Z}{2}\right) + \exp\left(\frac{5}{2}Z\right)\right)\right] \tag{C.32}$$

$$\frac{\mathrm{d}M_2}{\mathrm{d}t} = 2KN^2v_\mathrm{g}^2\exp(9Z)\left[1 + \exp(Z) + A\cdot Kn\left(\exp\left(-\frac{5}{2}Z\right) + \exp\left(-\frac{Z}{2}\right)\right)\right] \tag{C.33}$$

As well as in the continuum regime the following approximation is made $Z = \ln^2\sigma \simeq \ln^2\sigma_{r,0} = Z_0$, except for the term $\exp(9Z)$ in equation (C.33). This can be done because the standard deviation σ changes to a much lesser extend than N and v_g [33]. It is also assumed that the Knudsen number Kn can be expressed in terms of the initial Knudsen number Kn_0 with the following expression $Kn = Kn_0(N/N_0)^{1/3}$. Then we get for (C.32)

$$\frac{\mathrm{d}N}{\mathrm{d}t} = -K_\mathrm{c}N^2\left[a + b\left(\frac{N}{N_0}\right)^{1/3}\right] \tag{C.34}$$

with

$$a = 1 + \exp(Z_0)$$

and

$$b = AKn_0 \left[\exp\left(\frac{Z_0}{2}\right) + \exp\left(\frac{5}{2}Z_0\right) \right]$$

Integrating (C.34) results in

$$\int_0^{N/N_0} \frac{\mathrm{d}(N/N_0)}{(N/N_0)^2[1+(b/a)(N/N_0)^{1/3}]} = -a \int_0^t KN_0 \mathrm{d}t. \tag{C.35}$$

From (C.35) we get the expression for the dimensionless time t' in terms of (N/N_0)

$$\begin{aligned} t' = K_c N_0 t \;=\; & \frac{3}{a}\left[\frac{1}{3}\left\{\left(\frac{N}{N_0}\right)^{-1} - 1\right\} - \left(\frac{b}{2a}\right)\left\{\left(\frac{N}{N_0}\right)^{(-2/3)} - 1\right\}\right. \\ & + \left(\frac{b}{a}\right)^2\left\{\left(\frac{N}{N_0}\right)^{(-1/3)} - 1\right\} \\ & - \left.\left(\frac{b}{a}\right)^3 \ln\left\{\frac{1+(b/a)(\frac{N}{N_0})^{(1/3)}}{(1+(b/a))(\frac{N}{N_0})^{(1/3)}}\right\}\right] \end{aligned} \tag{C.36}$$

From (C.30), (C.31), (C.32) and (C.33) we get

$$\mathrm{d}(\ln v_g) = \frac{9c - (27/2)\exp(9Z)}{\exp(9Z) - 2c}\mathrm{d}Z \tag{C.37}$$

and

$$\mathrm{d}(\ln N) = \frac{\mathrm{d}[\exp(9Z)]}{\exp(9Z) - 2c} \tag{C.38}$$

with

$$c = \frac{a + b\exp(-3Z_0)(N/N_0)^{1/3}}{a + b(N/N_0)^{1/3}}$$

integrating (C.37) gives

$$\frac{N}{N_0} = \frac{\exp(9Z) - 2c}{\exp 9z_0) - 2c}. \tag{C.39}$$

from this we get for Z

$$Z = \ln^2 \sigma = \frac{1}{9}\ln\left[2c + \frac{N}{N_0}[\exp(9Z_0) - 2c]\right]. \tag{C.40}$$

For the particle volume we get

$$\frac{v_g}{v_{g,0}} = \frac{\exp((9/2)\ln^2 \sigma_{r,0})(N/N_0)^{-1}}{[2c + (N/N_0)\{\exp(9\ln^2 \sigma_{r,0}) - 2c\}]^{1/2}}. \tag{C.41}$$

D Testfires

All the measurement results used in this work were obtained during measurements at the fire detection laboratory of the University Duisburg-Essen following the European norm EN54 part9 [13]. For the extinction light sensor and the ionization chamber measurement results of the MIREX [14] and the MIC [15] were taken which are used for reference measurements following EN54. The two measurement apparatuses were mounted at a 3m radius around the fire place under the ceiling of the laboratory. For the scattering light signal a scattering light sensor [55] was used. Thereby a sensor is used which is also mounted at the 3m radius around the place of the fire. Moreover the particle number concentration and the particle diameter were measured at a 3m radius by means of the electrical aerosol spectrometer of Tartu University [66]. During all measurements the ceiling of the laboratory was adjusted at a height of 4m. These geometric properties of the measurement where modelled with the FDS.

For the verification of the model two testfires were chosen. The testfire TF3 [13], a smoldering cotton wick fire, as an example for smoldering fires and the testfire TF5 [13], an n-heptane fire, as an example for open fires. For the smoldering cotton wick fire 90 cotton wicks were fixed on a mounting in shape of ring, with a diameter of 10 cm. The wicks were ignited in a way that they smoldered without open flames. The cotton wicks build a chimney which led the smoke. For the n-heptane fire 650g of n-heptane was burned in a tray with a base area of 1100 cm^2 build of 2mm thick steel sheet metal. Table D.1 shows some important properties of the fires [22]. The testfires TF1, an open flaming wood fire, and TF2, a smoldering wood fire, were used to verify the properties of the signals of scattered light sensors. The test fire TF1 is an open wood fire in which 70 small beechwood bricks ($1 * 2 * 25 cm^3$) are burned. The testfire TF2 is a smoldering wood fire. During this fire experiment 24 birchwood bricks were smoldered on a hot plate. Open flame fires like TF1 and TF5 produce larger quantities of pure carbon particles which agglomerate to chains, while smoldering (TF2, TF3) fires produce strongly scattering liquid droplets due to the high content of only partly burned material.

open wood fire TF1	dark smoke small smoke particles high thermal flow high temperature weak scattering in near infrared region
smoldering wood fire TF2	bright smoke large smoke partiles less thermal flow no open flame strong scattering in near infrared region
cotton wick fire TF3	bright smoke medium size smoke particles less thermal flow no open flame strong scattering in near infrared region
n-heptane fire TF5	dark smoke small smoke particles high thermal flow high temperature (the hottest testfire) weak scattering in near infrared region

Table D.1: Properties of testfires TF1, TF2, TF3 and TF5 [36] [22]

Bibliography

[1] Aggarwal S., Motevalli V., *Investigation of an Approach to Fuel Identification for Non-flaming Source Using Light-scattering and Ionization Smoke Detector Response*, Fire Safety Journal 29:99-112, 1997

[2] Ahonen A.I., Pauli A.S., *A Run-in Test Series of a Smoke Test Room - Tests according to the proposal prEN54-9*, Research Report, Technical Research Center of Finland, 1983

[3] Atkinson G., *Smoke Movement Driven by a Fire Under a Ceiling*, Fire Safety Journal 25:261-275, 1995

[4] Barrett J.C., Jheeta J.S., *Improving the Accuracy of the Method for Solving the Aerosol General Dynamic Equation*, Journal of Aerosol Science Vol.27 8:1135-1142, 1996

[5] Barrett J.C., Webb N.A., *A Comparison of some Approximate Methods for Solving the Aerosol General Dynamic Equation*, Journal of Aerosol Science Vol.29 1/2:31-39, 1998

[6] Beichelt F., *Stochastik für Ingenieure*, B.G. Teubner Stuttgart, 1995

[7] Bernigau N.G., Luck H., *The Principle of the Ionization Chamber in Aerosol Measurement Techniques*, Journal of Aerosol Science Vol.17 3:511-515, 1986

[8] Bohren C.F., Huffman D. R., *Absorption and Scattering of Light by Small Particles*, John Wiley & Sons, USA, 1983

[9] Chung I-P., Dunn-Rankin D., *In Situ Light Scattering Measurements of Mainstream and Sidestream Cigarette Smoke*, Aerosol Science and Technology 24:85-101, 1996

[10] Colbeck I., Atkinson B., Johar Y., *The Morphology and Optical Properties of Soot Produced by Different Fuels*, Journal of Aerosol Science Vol.28 5:715-723, 1997

[11] Covelli B. *Fachgerechte Anwendung von computergestützten Berechnungsmodellen im Brandschutz*, VDS-Fachtagung: Ingenieurmäßige Verfahren im Brandschutz(8) - Rauchausbreitung und Rauchfreihaltung, 26 Juni 2003, Köln, Deutschland

[12] *Database for Simulations with FDS 3*, ftp://ftp.nist.gov/pub/bfrl/mcgratta/FDS3/DATABASE/

[13] CEN - The European Committee for Standardization: EN54 part9, Bestandteile automatischer Brandmeldeanlagen, Erprobungstest, 1984

[14] CERBERUS LTD.: *Extinktionsmessgerät MIREX*, Technische Beschreibung, CERBERUS LTD. , Männedorf, 1991

[15] CERBERUS LTD.: *Messionisationskammer MIC*, Technische Beschreibung, CERBERUS LTD. , Männedorf, 1991

[16] *Beschreibung der Messionisationskammer*, CERBERUS, 1976

[17] DiNenno et al. (Editors), *SFPE Handbook of Fire Protection Engineering*, Second Edition, National Fire Protection Association, USA, 1995

[18] Farouk B., Mulholland G.W., McGrattan K.B., *Simulation of Smoke Transport and Coagulation for a Standart Test Fire*, Proceedings AUBE'01, Gaithersburg, USA, 2001

[19] Floyd J.E., Baum H.R., McGrattan K.B., *A Mixture Fraction Combustion Model for Fire Simulation Using CFD*, Proceedings of Conference on Engineering Fire Protection Design, June 11 - June 15 2001, San Francisco, USA

[20] Friedlander S.K., *Smoke, Dust and Haze - Fundamentals of Aerosol Behavior*, John Wiley and Sons, 1977

[21] Goertz R., *Systematisierung der Inhaltsstoffe des Brandrauchs*, Jubiläumsfachtagung 2000 493-507, vfdb, Stuttgart, Oktober 2000

[22] Gockel F., *Ein allgemeines Modell für Brandsensoren im Gehäuse* PhD Thesis, Fachgebiet Nachrichtentechnische Systeme, Universität Duisburg-Essen, Germany, 2001

[23] He Y., *Strömungsmessungen in der unmittelbaren Umgebung eines Branddetektors bei Testbränden*, internal report, department for communication systems, Universität Duisburg-Essen, Germany, 1998

[24] Hinds W.C., *Aerosol Technology- Properties, Behavior, and Measurement of Airborne Particles*, John Wiley & Sons, 1999 Second Edition

[25] Hölemann H.,*Vorlesung zum Brand- und Explosionsschutz, Fachbereich Sicherheitstechnik*, Bergische Universität GH Wuppertal, Germany, bis 2000

[26] Hosemann J.P., *Messkammer nach dem Kleinionenanlagerungsprinzip eines lernfähigen Detektorsystems in der automatischen Brandentdeckung zum quantitativen Nachweis von Aerosolpartikeln*, Forschungsbericht des Landes Nordrhein-Westfalen Nr. 2336, Westdeutscher Verlag Opladen, 1973

[27] Hottel H.C., *Simulation of Fire Research in the United States After 1940*, Combustion Science and Technology 39:1-10, 1984

[28] Jones W.W., Forney G.P., Peacock R.D., Reneke P.A., *A Technical Reference for CFAST: An Engineering Tool for Estimating Fire and Smoke Transport*, National Institute of Standards and Technology, Gaithersburg, USA 2000

[29] Kerker M., *The Scattering of Light*, Academic Press, New York, 1969

[30] Klose J., *Ermittlung der Eigenschaften von Signaldetektoren durch Analyse und Simulation von Zufallsprozessen mit einer Anwendung in der automatischen Brandentdeckung*, PhD Thesis, Fachgebiet Nachrichtentechnische Systeme, Universität Duisburg-Essen, Germany, 1992

[31] Klote J.H., *Method of Predicting Smoke Movement in Atria with Application to Smoke Management*, NISTIR 5516, NIST, Gaithersburg, USA, 1994

[32] Lee K.W., *Change of Particle Size Distribution during Brownian Coagulation*, Journal of Colloid and Interface Science 92:315-325, 1983

[33] Lee K.W., Lee Y.J., Han D.S., *The Log-Normal Size Distribution for Brownian Coagulation in the Low Knudsen Number Regime*, Journal of Colloid and Interface Science 188:486-492, 1997

[34] Park S.H., Xiang R., Lee K.W., *Brownian Coagulation of Fractal Agglomerates: Analytical Solution Using the Log-Normal Size Distribution Assumption*, Journal of Colloid and Interface Science 231:129-135, 2000

[35] Loepfe M., Ryser P. *Optische Eigenschaften von Brand- und Nichtbrandaerosolen*, Proceedings AUBE'95, Universität Duisburg-Essen, Germany, 1995

[36] Loepfe M., Ryser P., Tompkin C., Wieser D., *Optical Properties of Fire and Non-fire Aerosols*, Fire Safety Journal, 29:185-194, 1997

[37] Luck H.,*Remarks in the State of the Art in Automatic Fire Detection*, Fire Safety Journal 29:77-85, 1997

[38] Luck H., *Theoretische Grundlagen der Nachrichtentechnik*, Vorlesungsskript, Fachbereich Elektrotechnik, Universität Duisburg-Essen, Germany, 1998

[39] Luck H., Sievert U., *Does an Over-All Modeling Make any Sense in Automatic Fire Detection*, Proceedings AUBE'99, Universität Duisburg-Essen, Germany 1999

[40] Luck H., Kruell W., *The Duisburg Fire Detection Laboratory*, Universität Duisburg-Essen, 1991 , http://nts.uni-duisburg.de

[41] Mahalingham S., Thevenin D., Candel S., Veyante D., *Analysis and Numerical Simulation of a Nonpremixed Flame in a Corner*, Combustion and Flame 118:221-232, 1999

[42] McGrattan K.B., Baum H., Rehm R., Forney G., Prasad K, *The Future of Fire Simulation at NIST*, Fire Protection Engineering 13, Society of Fire Protection Engineering, 2002

[43] Nelson H.E.,*From Phlogiston to Computational Fluid Dynamics*, Fire Protection Engineering 13, Society of Fire Protection Engineering, 2002

[44] McGrattan K.B. et al., *Fire Dynamics Simulator (Version 2) - Technical Reference Guide*, NISTIR 6783, NIST, Gaithersburg, USA, 2002

[45] McGrattan K.B. et al., *Fire Dynamics Simulator (Version 3) - Technical Reference Guide*, NISTIR 6783, NIST, Gaithersburg, USA, 2002

[46] McGrattan K.B. et al., *Fire Dynamics Simulator (Version 3) - User's Guide*, NISTIR 6788, NIST, Gaithersburg, USA, 2002

[47] Mell W.E., McGrattan K.B., Baum R.B., *Numerical Simulation of Combustion in Fire Plumes*, 26th Symposium on Combustion/The Combustion Institute, pp1523-1530 ,1996

[48] Mie G., *Beiträge zur Optik über Medien, speziell kolloidaler Metallösungen*, Annalen der Physik, Band 25 Folge 4 Nr.3 377-445,1908

[49] Oppelt U., *Measuring Results of a Combined Optical, Thermal and CO Detector in Real Sites and Classifying Signals*, Proceedings AUBE Conference 2001, Maryland, USA

[50] Otto E., *Modellierung Brownscher und elektrischer Koagulation submikroner Partikel*, PhD Thesis, Fachgebiet Prozess- und Aerosolmesstechnik, Universität Duisburg-Essen, Germany, 1997

[51] Datenblatt: *Feststoff/Trockendispergierer Serie RBG*, Palas GMBH Partikel- und Lasermesstechnik, Karslruhe, Germany

[52] Park S.H., Lee K.W., Otto E., Fissan H., *The Log-normal Size Distribution Theory of Brownian Agglomeration for the Entire Particle Size Range*, Journal of Aerosol Science Vol.28 Suppl. 1:22-23, 1997

[53] *Certificate of Conformance Standard Test Dust ISO 12103 Pt1 A1 Ultrafine*, Particle Technology LTD, Derbyshire, United Kingdom, 2002

[54] Quintiere J.G., *Compartment Fire Modeling* The SFPE Handbook of Fire Protection Engineering 3:125-133, National Fire Protection Association, Quincy 1995

[55] Siemens AG: BR82 Rauchmelder, Thilo P., Post O., Luck H., Siebel R., Klose J., *Schlußbericht zum Forschungsprojekt 'Aufnahme und Analyse unterschiedlicher Brandkenngrößenverläufe mit dem Ziel, durch angepaßte Detektionsalgorithmen die Eigenschaften automatischer Brandmeldeanlagen zu verbessern'* A4-A6 , Gemeinschaftliches Projekt der Siemens AG München und der Universität-Gesamthochschule-Duisburg, Germany, 1989

[56] Kielkewicz M., *Accuracy of the Moments Method*, Ann. Nucl. Energy, Vol.21 3:189-193, 1994

[57] Mulholland G.W., *Smoke Production and Properties* The SFPE Handbook of Fire Protection Engineering 2:217-227, National Fire Protection Association, Quincy, 1995

[58] Rasbash D.J., Drysdale D.D., *Fundamentals of Smoke Production*, Fire Safety Journal 5:77-86, 1982

[59] Reist P.C., *Introduction to Aerosol Science*, Macmillan Publishing, USA, 1984

[60] Rexfort C., Kaiser Th., *A General Approach for Simulating Signals of Scattered Light Detectors*, Proceedings AUBE Conference 2001, Maryland, USA

[61] Rexfort C., *Smoke Distribution in Enclosures including Coagulation Effects, Modeling and Simulation*, EUSAS Newsletter no.16, December 2002

[62] Rexfort C., *Simulation der Lichtstreuung in einem Streulicht-Brandsensor*, Studienarbeit, Universität Duisburg-Essen, Germany, 1997

[63] Schwientek U., *Lösung der General Dynamic Equation durch eine Polynomapproximation der Momente der Partikelgrößenverteilungsdichte*, Diplomarbeit, Universität Duisburg-Essen, Germany, 1997

[64] Smoluchowski M., *Drei Vorträge über Diffusion, Brownsche Molekularbewegung und Koagulation von Kolloidteilchen*, Phys. Zeitschrift 17:577 , 1916

[65] Tamm E., Mirme A., Sievert U., Franken D., *Aerosol Particle Concentration and Size Distribution Measurements of Test-Fires as Background for Fire Detection Modelling*, Proceedings AUBE'99, Universität Duisburg-Essen, Germany, 1999

[66] Tammet H., Mirme A., Tamm E., *Electrical Aerosol Spectrometer of Tartu University*, Department of Environmental Physics, Tartu University, Estonia

[67] Thilo P., Post O., Luck H., Siebel R., Klose J., *Schlußbericht zum Forschungsprojekt 'Aufnahme und Analyse unterschiedlicher Brandkenngrößenverläufe mit dem Ziel, durch angepaßte Detektionsalgorithmen die Eigenschaften automatischer Brandmeldeanlagen zu verbessern'*, Gemeinschaftliches Projekt der Siemens AG München und der Universität-Gesamthochschule-Duisburg, Germany, 1989

[68] Truckbrodt E., *Lehrbuch der angewandten Fluidmechanik*, Springer Verlag, 1988

[69] Wendt J.F., *Computational Fluid Dynamics*, Springer Verlag, 1996

[70] Westermeier F., *Modellierung von Gefährdungsbränden*, Diplomarbeit, Universität Duisburg-Essen, 2002

[71] Williams M.M.R., Layolka S.K., *Aerosol Science- Theory and Practice*, Pergamon Press, 1991